

2017 MOUNTJOY CARBONATE RESEARCH CONFERENCE

Carbonate Pore Systems Abstracts



Canada's
Energy
Geoscientists



June 25-29, 2017
Austin, Texas USA

Pore system heterogeneity: Impact on reservoir modeling and field development

Hisham Alqassab*, Shawn Fullmer, Manal Alharbi, PJ Moore, and Brian Kelly

*ExxonMobil, 22777 Springwoods Village, Spring, TX, 77389, USA

e-mail: Hisham.m.alqassab@exxonmobil.com

Pore system heterogeneity has a profound influence on hydrocarbon displacement, water movement and ultimate recovery. Understanding the relationship between pore type distribution and its influence on both static (porosity and permeability) and dynamic (capillary pressure and relative permeability) properties is critical to understanding reservoir performance. The results of this study demonstrate the benefits of an integrated approach to pore system characterization, dynamic integration, and reservoir modeling that led to an improved match to historical water movement with implications for field development. The ratio of micro-pore space to interparticle pore space in a given unit of rock is a fundamental control on fluid flow. Rocks with a higher proportion of microporosity (>80%—micro-pore dominated) have systematically lower negative capillary pressure (P_c) and lower relative permeability (K_r) to water at a given water saturation than rocks with a lower proportion of microporosity (50–80%—mixed pore system). This translates to more favorable water movement in mixed pore system rocks that are already preferential pathways for water due to higher absolute permeability.

Two dynamic rock types were identified based on these observations replacing the 15 rock types utilized in previous modeling efforts. Mixed and micro-pore dominated rock types were identified at wells using core data and PLT calibration and distributed between wells using standard geostatistical techniques. Permeability was modeled using transforms from core data by rock type. The magnitude and distribution of permeability for mixed pore system rock types closely resembles permeability derived from pressure build-up tests at multiple wells providing dynamic validation of the distribution. A special core analysis (SCAL) framework was developed based on the relationship between percent fraction microporosity and P_c , K_r behavior. The resulting reservoir model was simulated to test a variety of scenarios to evaluate the performance differences between the pore system based characterization with mixed and micro-pore rock types presented here and the previous history-matched reservoir model. Water movement in the pore system based model is dramatically different than the previous model and results in a better match to historical water cut data. This study has implications for improved reservoir characterization, modeling and field development.

Pore network characterization of a tight carbonate reservoir from the Middle East using dynamic and static methods

Mohammad E. Alsuwaidi* and J. Frederick Sarg

*The Petroleum Institute, Sas Al Nakhal, Abu Dhabi, Abu Dhabi, P.O. Box 2533,
United Arab Emirates

e-mail: malsuwaidi@pi.ac.ae

This study aims to understand the pore architecture of a tight carbonate reservoir that has high porosity (up to 25%) but very low permeability (up to 1–3 mD) using integrated techniques at different scales. These techniques include core description, petrography, scanning electron microscopy (SEM), QEMSCAN[®] (Quantitative Evaluation of Minerals and Porosity by Scanning Electron Microscopy), CMS 300[®] (Core Measurement System), Mercury Porosimetry, Nitrogen Gas Adsorption–Desorption, and Stable isotope analysis. Results show that interparticle porosity between micrite particles is the main interconnected porosity, while high storage is accounted for by the 5–10 μm sized intraparticle pores within coccoliths and foraminifera. These microfossils were not compacted due to early cementation of the host mudstones and wackestones that held their morphology intact. Stylolite formation created vertical fluid-flow barriers as a result of dissolution of micrite and re-precipitation into diffused cement above and below clay-rich seams in lower porosity zones. Dynamic methods (conventional and special core analyses) were more diagnostic than static microscopic methods due to the small size of pores. SEM visualization provided key information on identification of preserved intraparticle porosity. Stable isotope data indicate early timing of cementation that supported microfossils from being compacted. Hence, this integrated study provides important clues to the origin and preservation of micropores in tight limestone reservoirs

Confocal and transmitted light petrography of cementation and grain types in a high-energy upper shoreface to foreshore carbonate strand line, Pleistocene (MIS 5e) West Caicos Island, Turks and Caicos, B.W.I.

Steve Bachtel, Charles Kerans, Neil Hurley*, and Nathaniel Miller

*Chevron Exploration Technology Co., 1500 Louisiana, Houston, TX 77002, USA

e-mail: co3hipster@comcast.net

Confocal petrography provides a new tool for the imaging of cements, pores, and internal structures of ooids and composite grains. Blocky cements, as recognized in TL images are highly zoned and display variable fluorescence, similar to zoning observed in CL petrography (controls on the zonation are currently being investigated). Imaging of isopachous cements are also greatly improved. Micritized ooid nuclei (in TL imagery) are observed to have a complex history including previous periods of coating and microborings. Many ooids that appear to have single nuclei in transmitted light actually are composite grains when viewed with confocal microscopy. Boat Cove, West Caicos Island contains a classic vertical section through an upper shore face to foreshore system (MIS 5e). The section provides excellent control on a single sea level cycle that has experienced constant exposure for 129,000 years. This is important because the effects cementation and dissolution of a single exposure event can be isolated and documented without the complexity of overprinted events as seen in the ancient rock record. Cements observed include a coarse, clear blocky cement (low Mg calcite), a finer crystalline blocky cement, an isopachous blocky cement (multi-generational, high-Mg calcite), and rare needle cements (aragonite). The blocky cements are observed in confocal imagery to be scalenohedral in form and highly-zoned. The blocky cements are most common in areas where voids are being dissolved, like in burrows or in finer grained laminae (due to capillary forces). Alveolar structure is observed in foreshore sediments and meniscus fabrics are present throughout the section. The cements are interpreted to be primarily meteoric cements with minor isopachous and mold-filling cements precipitated from marine fluids (probably beachrock). Moldic porosity is common and is represented by partial to total dissolution of ooid cortices.

Effects of micropores in limestones and dolostones on seismic rock properties—a review

Gregor Baechle*, Gregor Eberli, and Ralf Weger

*Consultant, 22510 Oak Mist Lane, Houston, TX 77494, USA

e-mail: gregor.baechle@gmail.com

The elastic properties in carbonate rocks are affected by three main factors: pore fluids, composition of the rock framework and pore space texture. It is important to revisit those fundamental controls of elastic rock property relationships for an accurate quantitative interpretation of conventional and unconventional carbonate plays. In this review, we concentrate specifically on the effects of microporosity on elastic properties of seven different carbonate rock datasets in age ranging from Neogene to Devonian age. We also review if the acoustic characterization of microporosity shows a unique correlation to reservoir quality (permeability). The Extended Biot Theory (EBT) is successfully utilized to approximate the Differential Effective Medium (DEM) trend lines of conceptual pore aspect ratios of 0.1, representing the elastic behavior of micropore-dominated limestones and dolostones. Both models are of equal applicability to quantify the effect of micropores on the velocity-porosity relationship. Out of seven carbonate datasets, five formations show a unique relationship with microporosity correlating with high frame flexibility factors (low acoustic velocities at a given porosity) and a low permeability. Two dolomite formations with micropores within a sucrosic fine crystalline texture show as well a correlation with high frame flexibility factors but display relatively high permeability. There is no unique relationship over all our carbonate datasets between frame flexibility factor and mineralogy and/or permeability. Hence, successful quantitative seismic interpretation requires integration of core and log data to put the elastic properties in the context of what drives reservoir performance. Calibrated rock physics models can uniquely identify and predict the low p-wave and s-wave velocity of microporosity dominated facies at a given porosity, hereby emphasizing the potential of improved reservoir characterization using formation specific calibrated rock physics models.

**Facies and diagenesis on a steep-sided Late Paleozoic isolated platform:
Karachaganak Field, Republic of Kazakhstan**

James W. Bishop*, Steve Bachtel, Alex J. Parker, and Marina Borovykh

*Chevron, 1500 Louisiana St—HOU150/31138, Houston, TX 77005, USA

e-mail: James.Bishop@Chevron.com

The Karachaganak gas condensate reservoir is an isolated platform that grew from Devonian through Permian time in the Pricaspian Basin. Two new cores provide insight into the lithologic makeup of the prograding Lower Carboniferous strata as seen in 3D seismic. The cores illustrate thick, vertical accumulations of microbial boundstones that host Neptunian fissures and caves. The wells recovered 564 m and 474 m of continuous core and are located on the southeast side of the western and main buildups of the field. Their prograding facies successions capture lower slope, middle slope, upper slope, and platform facies prior to subaerial exposure and a ~24 MY unconformity at the Serpukhovian Super-Sequence Boundary (SSB). Slope facies include in situ boundstone, as well as mud-, grain-, and debris-dominated gravity flow deposits. Grain and mud-dominated facies are common in lower slope environments, occurring as calci-turbidites and mass transport deposits. Debris-dominated facies occur in middle slope environments and consist of slope- and platform-derived breccias. Microbial and algal boundstones prevail in upper slope environments. In one of the wells, 440 m of near-continuous boundstone were penetrated, indicating that boundstones extended to middle slope environments, several hundred meters below sea level. Boundstones grade up-section into platform grainstones and packstones of the outer platform, as indicated by faunal assemblages and shallowing bed dips. The prograding succession is capped by the Serpukhovian SSB, recognized by distinct vadose diagenetic fabrics. Permian-aged slope sediments then buried the Carboniferous platform. In both wells, Neptunian dikes are recognized as sub-vertical fissures through boundstone wall-rock. Fissures are commonly encrusted by laminated microbialite and filled by muddy to grainy sediment. Final fissure porosity is commonly occluded by anhydrite. Neptunian fissures are common in Paleozoic steep-sided platforms in the Pricaspian Basin, where they are commonly unfilled and correspond to core breaks, lost circulation, and bit drops. Their preservation in Karachaganak core is owed largely to plugging by anhydrite, uncommon in other fields.

NMR characterization of microporosity in the Mississippian-aged carbonates of the southern mid-continent

Ibukun Bode*, Michael Grammer, and Chi Zhang

*Boone Pickens School of Geology—Oklahoma State University, 105 Noble Research Center, Stillwater, OK, 74078, USA

e-mail: ibukuno@okstate.edu

Carbonate reservoir rocks are particularly difficult to characterize due to a complex spatial distribution of pores and pore connectivity that have a significant impact on flow properties. Studies have shown that in carbonate pore systems, the largest pores may not form part of the connected cluster and that pores of varying sizes may contribute to the connected porosity. This heterogeneity highlights the need to integrate contributions of microporosity into carbonate pore characterization workflows. This study focuses on characterizing micro-nanometer sized pores in a wide range of carbonate fabrics by combining NMR response with multiscale digital image analysis (DIA), and facies descriptions. NMR transverse relaxation times (T₂) provide direct information on porosity and pore size distribution. Consequently, rock fabric has an implication on the overall geometry of the T₂ distribution signals. Also, empirically-derived T₂-cutoff values are used in partitioning bound fluids associated with microporosity from free movable fluids associated with larger pores. By comparing the T₂-cutoff to microporosity estimated from DIA, there is an additional insight into the contribution of microporosity in different facies.

Facies observed in core include skeletal peloidal packstones–grainstones, diagenetically altered spiculitic chert, dolomitized grainstones, and skeletal wackestones to mudstones. Based on dominant pore type and overall fabric, these facies are grouped into four distinct petrophysically-significant classes: intergranular, intragranular, enhanced, and tight. Porosity ranges from 3.6% to 46%, with associated permeability measuring between 0.02 mD and 56 mD. DIA measured pore sizes range from 84 nm to 3.08 mm, over four orders of magnitude. Microporosity contribution is as low as 5% in dolomitized grainstones and up to 90% in skeletal wackestones. Preliminary assessment of NMR response shows a grouping of fabrics correlative to the petrophysically-significant classes. In general, T₂ curves exhibit up to three modes: varying by facies, pore size distribution, and pore types present. Fabrics with minimal solution enhancement or diagenetically-reduced cementation show T₂ curves with the lowest amplitudes and shorter relaxation times, whereas high amplitudes characterize rocks that are associated with a higher abundance of pores. In addition, T₂-cutoff values vary by an order of magnitude, depending on the pore types and the amount of microporosity present in the samples.

Continued work will include larger sample numbers from different carbonate facies and geological ages. Relating NMR response and T₂-cutoff to qualitative properties—facies and dominant pore types—and quantifiable parameters such as pore-size distribution and microporosity validates the importance of utilizing a petrophysical-geological approach in carbonate pore-system characterization.

Thermochemical alteration of an immature calcareous mudstone by hydrous pyrolysis

Adam R. Boehlke* and Justin E. Birdwell

*Central Energy Resources Science Center, U.S. Geological Survey, Denver, CO 80225, USA

e-mail: aboehlke@usgs.gov

Evolving technology and increased economic interest has prompted the development and implementation of new exploration techniques for unconventional petroleum reservoirs. This has created a need to better understand the reservoir characteristics governing storage and extraction of oil and gas. To address this need, we have examined changes in rock characteristics before and after hydrous pyrolysis (HP) using field emission scanning electron microscopy (FE-SEM) and energy-dispersive X-ray spectroscopy (EDS). Rock matrix images were taken under various conditions to best document physical and chemical rock properties before and after HP in an attempt to document changes in organic-mineral interfaces and the rock matrix following thermal maturation. Studying systemic changes of thermal alteration on mudstones in nature is complicated due to uncertainties related to thermal history, burial stress and fluid composition amongst others. HP experiments provide a useful alternative approach for documenting these changes under controlled conditions.

Mudstone samples were collected from the Late Cretaceous Boquillas Formation at a roadcut near Del Rio, Texas. These mudstones were immature with a total organic carbon content approaching 5 wt.%, a hydrogen index around 600 mg/g, and significant amounts of calcite content (~65 wt.%). The mudstone was trimmed into a cube, and then bisected to obtain two nearly identical imaging surfaces. One of the imaging samples was left untreated, while the other was heated to 330° C for 72 hours with deionized water in a closed stainless steel reactor to assess changes in rock characteristics after laboratory-induced thermal maturation (samples are just into the oil window under these conditions). Following HP treatment, the samples were argon ion milled (AIM) and high-resolution backscatter and secondary electron images were collected under different accelerating voltages. In addition to imaging, EDS measurements were performed to examine the original mineralogy and any resulting thermochemical alteration products following HP.

Images taken before and after HP reveal several potentially important changes in the mudstone matrix. Framboidal pyrite appears to undergo a dissolution reaction during HP where void space created by pyrite dissolution appears to be somewhat filled with clay particles leaving a “sponge” texture (figure 1, panel a). Calcareous foraminifera, initially filled with organic matter or authigenic minerals such as kaolinite, dolomite, quartz and illitic clays, are replaced with a “sponge” of altered kaolinite, smectite/serpentine, and in some cases talc (figure 1, panel b). Secondary electron images of relatively low-magnification areas reveal thermochemical alteration has created void space at grain boundaries, dissolution cavities in pyrite, foraminifera tests and coccolithophores, as residual porosity as immature kerogen was converted to bitumen and expelled oil and gas, forming a network of void space resulting from the migration of petroleum out of the rock (figure 1, panel c). It is unclear if the extensive void space generated during these experiments would be present under natural conditions. However, this combination

of HP and high-resolution SEM imaging can provide insights into the properties of source rocks after thermal maturation that would be difficult to obtain from natural samples.

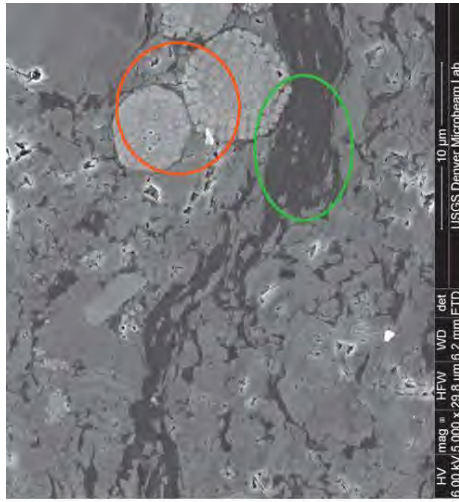


Figure 1, panel c.

Top: a secondary electron image of the untreated sample with a wider field of view showing good examples of pyrite (orange) framboids and organic matter (green) infilling fracture paths as well as interparticle space (the relative lack of void space is indicated by the bright white color representing electron charge at the edge of a void); Bottom: a secondary electron image of the post-pyrolysis sample (wide field of view) showing dissolved pyrite (orange), porosity development (bright white edges), and a textural difference in organic matter (green) from that of the unpyrolyzed sample.

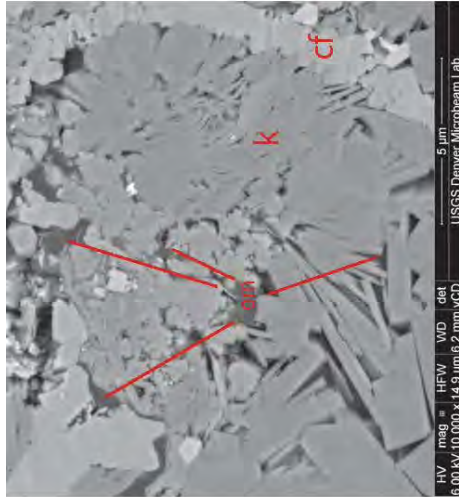


Figure 1, panel b.

Top: backscatterer image of authigenic kaolinite, quartz, dolomite, and other minerals in the untreated sample filling another foraminifera (cf) showing essentially no void space (black) between the sheets of the kaolinite (k) books (most of the void space appears to be filled with organic matter (om), shown in dark grey); Bottom: composite backscatterer/secondary electron image of the HP samples showing a kaolinite-filled foraminifera (cf) with clear void space between the sheets of the kaolinite (k) books accompanied by a fibrous aluminosilicate (al-f) of similar morphology to that shown infilling dissolved pyrite framboids in panel a.

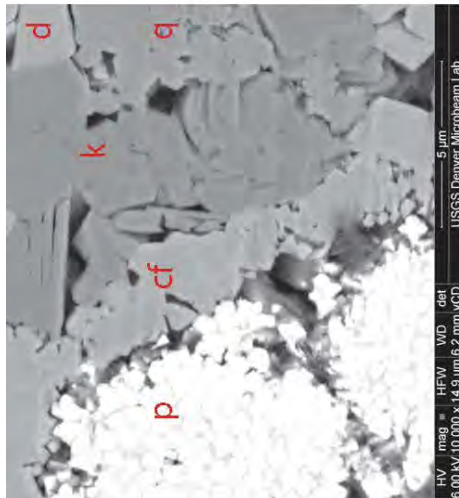
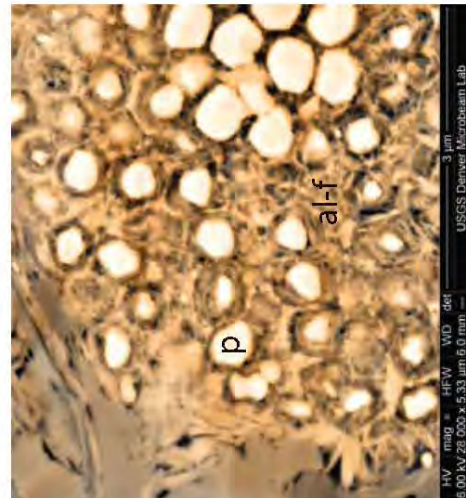
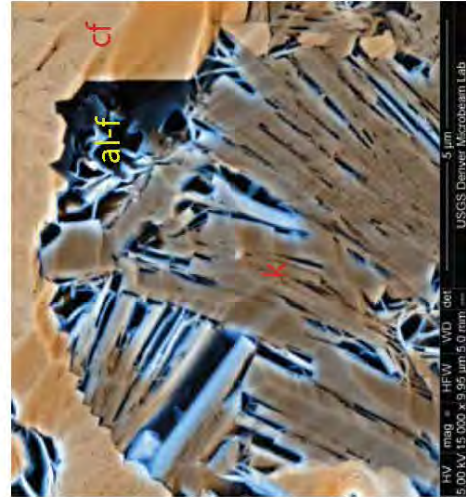
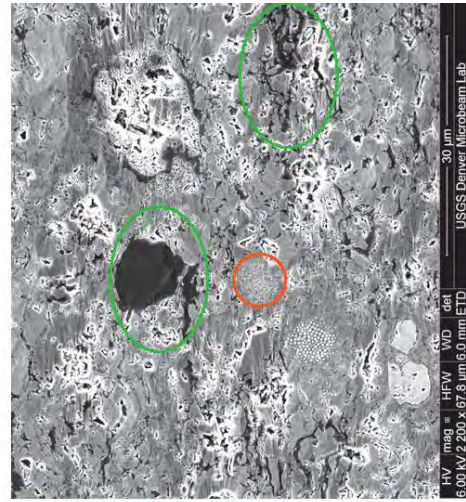


Figure 1, panel a.

Top: backscatterer electron image of the untreated sample showing framboidal pyrite infilling calcareous foraminifera adjacent to authigenic kaolinite (k), dolomite (d), and quartz (q); Bottom: composite backscatterer and secondary electron image of the sample following hydrous pyrolysis (composite image provides information on both texture and composition) showing framboidal pyrite (p) that has been replaced by a fibrous aluminosilicate (al-f) mineral containing Mg, Ca and Fe, possibly a product of pyrite dissolution during pyrolysis related to the oil generation process.



High-resolution large area low vacuum scanning electron microscopy (LV-SEM) imaging for microporosity and diagenesis of carbonate rock systems, and carbonate cemented sandstones

Jim Buckman*, Elma Charalampidou, Stephanie Zihms, Helen Lewis, Gary Couples, Patrick Corbett and Zeyun Jiang

*Institute of Petroleum Engineering, Heriot-Watt University, Riccarton, Edinburgh, EH14 4AS, Scotland.

e-mail: j.buckman@hw.ac.uk

Automated scanning electron microscopy (SEM) image collection from geological polished thin-sections, in conjunction with autonomous stitching, can be used to construct high-resolution (micron to sub-micron resolution) image montages, over areas of several square centimeters. Such montages can be formed from any available detector, including backscattered (BSE), secondary electron (SE) and cathodoluminescence (CL), and may comprise many thousands of images. The technique is applied to carbonates and a carbonate cemented sandstone to illustrate its application as a tool in the study of microporosity and diagenesis.

Imaging was carried out under low vacuum (0.8 Torr), without coating, utilizing both BSE and gaseous secondary electron (GSE) imaging. BSE imaging provides excellent data on porosity and micro-porosity (as well as variation in particulate and cement composition and general fabric), while using charge contrast imaging (CCI), GSE imaging provides details on cementation at a variety of scales, in a similar fashion to that of CL.

BSE montages can be collected and individual tiles batch thresholded and binarized, using image analysis software, for calculating porosity. Quantitative data on the porosity of each tile can then be plotted and contoured to quantify and visualize changes in porosity across the examined thin section (Fig. 1). Alternatively complete BSE montages, parts of montages, or individual tiles, can be selected, thresholded (binarized) for porosity, then used as the input parameters for stochastic construction of 3D models. Pore Architecture Modeling (PAM) and Pore Analysis Tools (PAT) can be applied to model porosity, permeability and fluid flow (Fig. 2).

Utilizing the GSE detector, charge contrast imaging (CCI), can be used at a variety of scales in examining the evolution of carbonate cements and their modification of pore systems. For example in oolitic limestone, illustrating the formation of grain lining and pore occluding cements (Fig. 3), as well as recrystallization.

CCI montages commonly have a variety of contrast/brightness artifacts due to variation in charge distribution across the individual scanned image tiles (Fig. 4). A variety of remedies are discussed, that can reduce these artifacts, making it easier to apply image analysis techniques across montages.

High-resolution montaged images can be used to later analyze samples in the fashion of a 'virtual SEM'. Images can be automatically collected at night or over weekends, which

effectively releases SEM time, and provides the opportunity for much more detailed coverage of thin sections. The technique is therefore ideal for archiving petrographic information from thin sections.

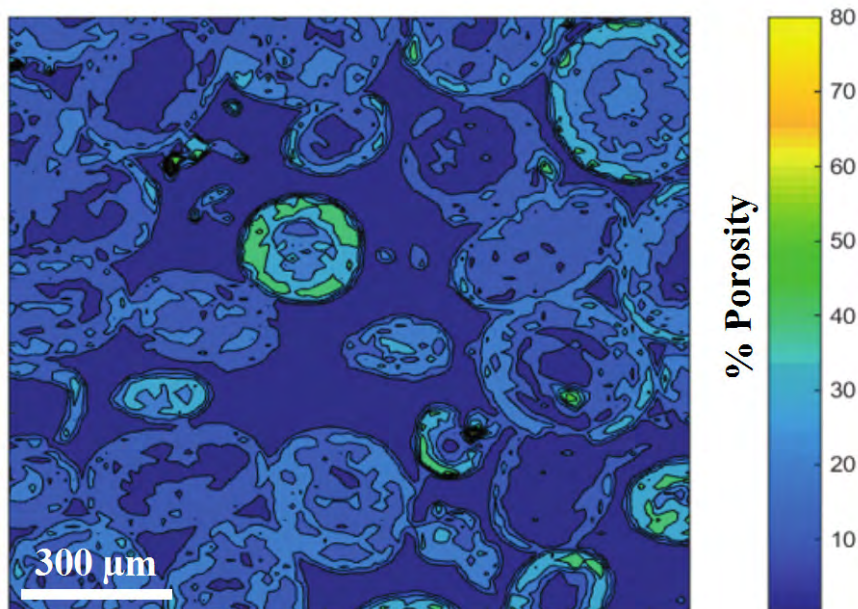


Figure 1: Porosity variation associated with oolitic limestone, based on individual tiled BSE images (each 23 µm horizontal field of view) thresholded and binarized for porosity.

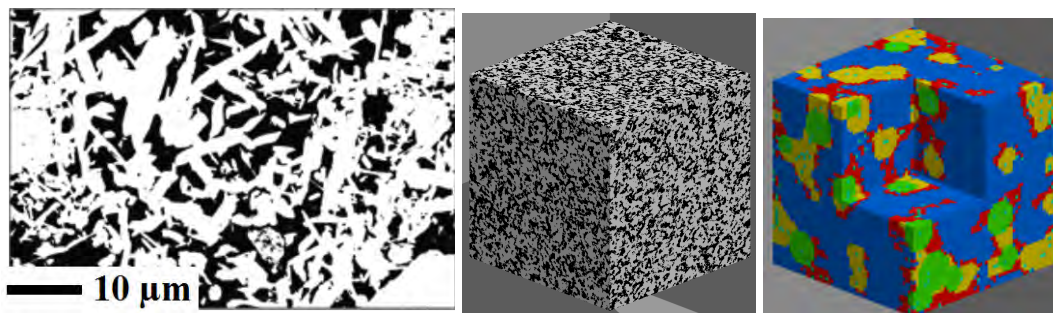


Figure 2: SEM image of pore containing acicular aragonite crystals, thresholded and binarized for porosity (left). Used as basis for stochastic construction of 3D PAM model (centre), with black representing pores (500 x 500 x 500 voxels). Model of nodes and connections, generated through PAT (right), blue represents solids (aragonite crystals), green spherically modeled pores, yellow cylindrical modeled pore connections and red as other pores (50 x 50 x 50 voxels). Both models visualized using Slicer software program.

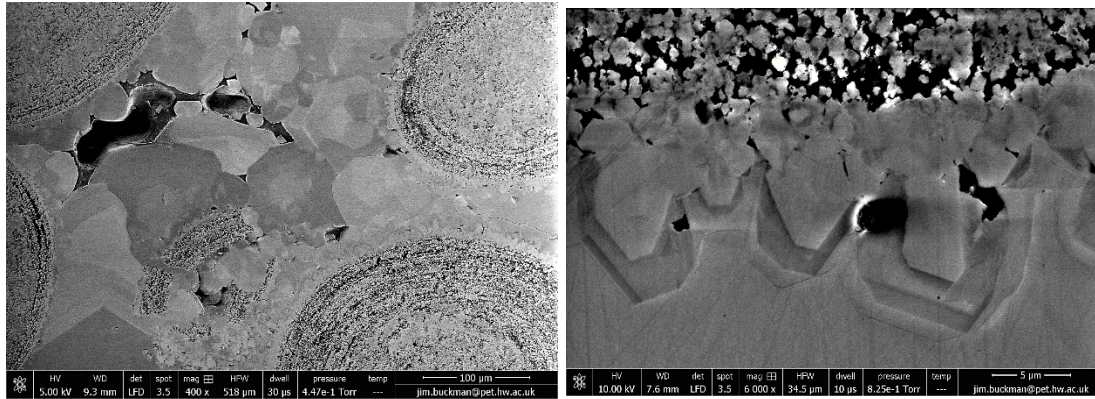


Figure 3: Examples of charge contrast imaging (CCI): showing coarse pore occluding calcite (left) and fine calcite that rims ooids (right).

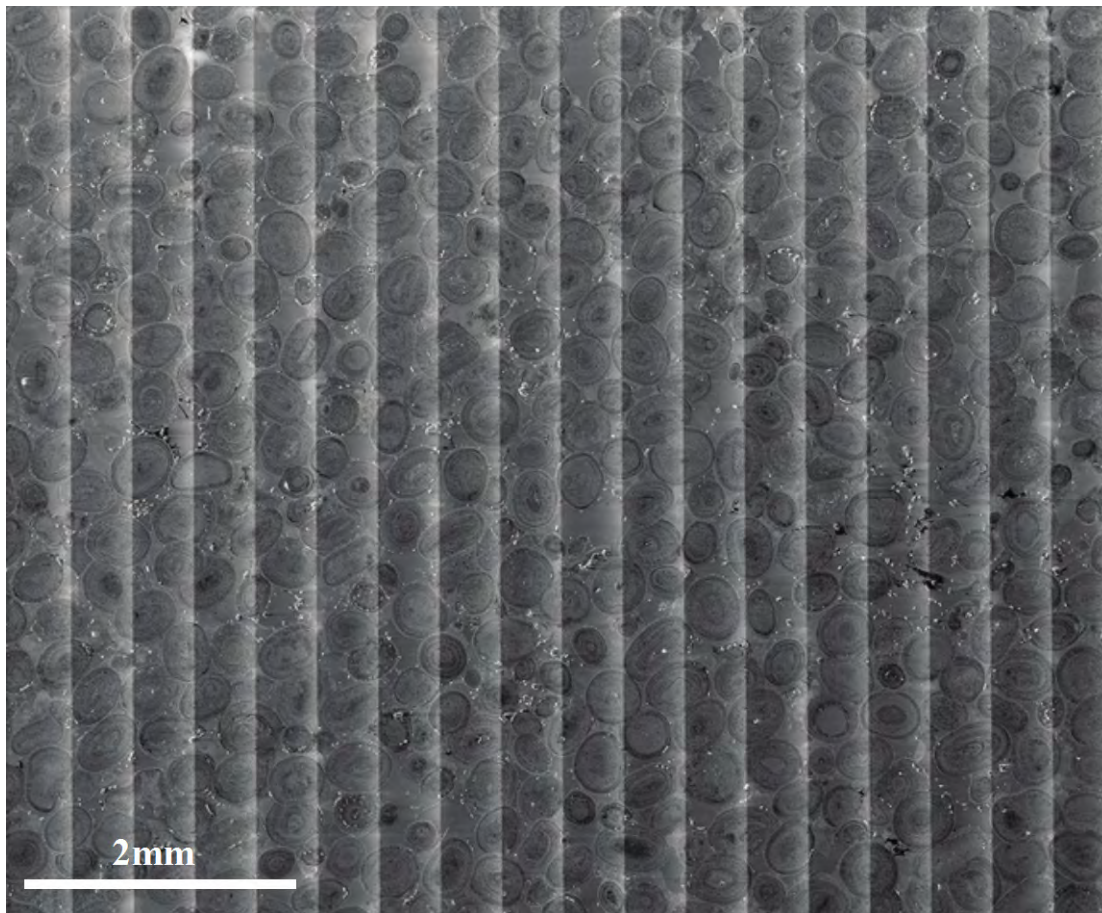


Figure 4: Oolitic limestone polished thin section, showing typical vertical bar artifacts, associated with high-resolution large area montages, observed during charge contrast imaging, using the GSE detector.

Quantitative digital petrography: Thin section to plug scale quantification of pore space, grains, and connectivity

Antonio Buono*, Shawn Fullmer, Hubert King, Mike Sansone, Bill Lamberti, and Keith Peterson

*ExxonMobil, 22777 Springwoods Village Parkway, Spring, TX, 77389, USA

e-mail: antonio.s.buono@exxonmobil.com

Carbonate reservoirs are often comprised of a heterogeneous pore system within a matrix of variably distributed minerals including anhydrite, dolomite, and calcite. When describing carbonate thin sections, it is routine to assign relative abundance levels to each of these components, which are qualitative to semi-quantitative (e.g., point counting) and vary greatly depending on the petrographer. Over the past few decades image analysis has gained wide use among petrographers, however, thin section characterization using this technique has been primarily limited to the pore space due to the difficulty associated with optical recognition beyond the blue-dyed epoxy associated with the pores. Here, we present a new method of computerized object-based image segmentation (Quantitative Digital Petrography: QDP) that relies on a predefined rule set to enable rapid, automated thin section quantification with only minor human interaction.

We have developed a novel work flow that automatically isolates the sample on a high resolution (i.e., $<1 \mu\text{m}/\text{pixel}$) scanned thin-section, segments the image, and assigns those segments to predefined categories—e.g., pores, cement, grains, etc. Using this technique, statistically relevant numbers of thin-sections can be rapidly processed and quality controlled, thereby allowing quantitative data such as MICP, NMR, SCAL properties, and surveillance data to be integrated with the petrographic observations for a more complete description of the carbonate rock. Our technique can also incorporate multiple layers, such as cross-polarization, Back Scatter Electron imaging (BSE), and elemental maps, which allow additional information to be easily integrated with results from QDP. The QDP approach is a significant improvement over previous digital image analysis methods because it 1) does not require binarization, 2) eliminates the subjectivity in assessing abundance levels, 3) is much less time-consuming for the petrographer, and 4) provides a much fuller dataset that can be incorporated across an entire well or field to better address common challenges associated with carbonate reservoir characterization, such as understanding pore type and cement abundance, pore connectivity, and grain distribution. These data can then be combined with Dynamic CT to expand the 2D understanding of pore space to a 3D understanding of connectivity and bypass zones.

Petrophysical characterization of Albian carbonate reservoir in Campos Basin using a multivariate approach with well logs and laboratory measurements

Abel Carrasquilla* and Raphael Silva

*UENF/CCT/LENEP, Macae—RJ, Brazil

e-mail: abel@lenep.uenf.br

Summary

An Albian carbonate reservoir from Oilfield B in the Campos Basin was characterized using a database of geophysical and petrophysical laboratory data. Porosity, permeability and water saturation logs were derived from the reference well and adjusted to laboratory measurements. Hereafter, statistics, regression, clustering and cross graphic techniques supported the initial interpretation, helping to determine electrofacies and flow zones, as well as, improved the experimental data fits. Finally, all of this methodology was successfully used to predict the same petrophysical parameters in a neighboring well without laboratory data.

Introduction

Campos is the most producing oil basins in the Brazilian continental margin, accounting for over 80% of national production (Fig. 1). In it there are fields with the presence of carbonate Albian reservoirs with medium porosity and permeability of 250 mD and 25%, respectively. These reservoirs are characterized as being heterogeneous, having a textural variety and are typically broken, which leads to a generally low recovery factor and complex relationship between the properties of the rock and geophysical data. For both, characterizing carbonate reservoirs through a combination study of their petrophysical properties and their well geophysical logs provides a fundamental understanding of reservoir geometry and dynamic properties (Bruhn et al. 2003).

While some porosity and other physical properties are routinely evaluated from well log, the measurement in situ of permeability is usually not feasible at low cost, being made by formation tests. Furthermore, it is recognized that permeability is a property depending on the measuring scale, so that its measurement on cores cannot be directly used for the evaluation of the permeability in the reservoir scale. Thus, the ability to estimate petrophysical properties of a reservoir rock from other more easily measured parameters or by means of laboratory tests is of great value to the oil industry. The petrophysical characterization using geophysical logs, for example, is of great importance to the discovery of new hydrocarbon reservoirs and aims to reduce the uncertainty and risks associated with oil exploration. Just as important are the early stage of development of an oil field, helping to define the best development strategy through the petrophysical and geological characterization (Lucia 1999).

So, well logs and analysis of rock samples in the laboratory are methods widely used to evaluate the physical properties of geological formations in the petrophysical characterization of carbonate reservoirs (Aguilera and Aguilera 2001). The data resolution and the spatial coverage in these two methods, combined with the number of measured parameters, occur in different

ranges to obtain knowledge of the lithology and subsurface structural information (Shenawi et al. 2007). Thus, the proposed study aims to explore the advantages of these two techniques, even adding the geological interpretation, to evaluate, from the petrophysical point of view, a set of data from a carbonate reservoir in Oilfield B in Campos Basin.

Materials and Methods

The methodology used in this study was as follows (Silva 2016):

- a) Initially, two wells were selected in this field, called X and Y, having the first well logs and laboratory petrophysical data and the second only well logs. The well X was used as a reference and Y as a blind test, whereas the distance between them is small (180 m), which have similar geological characteristics.
- b) Gamma rays, resistivity, sonic, density and neutron logs in reference well X were interpreted by deriving petrophysical parameters such as porosity, permeability and saturation, which were compared with the same parameters measured in the laboratory, allowing a more reliable reservoir characterization.
- c) These initial estimates were subject to statistical analysis using parameters such as maximum, minimum, average, median, mode, standard deviation, and histograms, which served to have a broader understanding of these petrophysical parameters.
- d) Linear regression and multiple linear regression techniques were used to estimate both the porosity from neutron porosity, density, sonic, such as permeability, exploiting its linear dependence of porosity.
- e) Cluster Analysis for Rock Typing module of Interactive Petrophysics software (LR Senergy 2017) was used to estimate porosity and permeability values aiming at a better correlation with laboratory data.
- f) Cross-correlation, Pickett and Winland graphs were built to assist the initial interpretation, helping in determining electrofacies, location of flow areas and better adjusting with laboratory parameters.
- g) Finally, all the methodology applied to the well reference X was used to infer the same petrophysical parameters in a blind test, nearby well Y, which lacked laboratory data.

Results

The histograms of both well logs indicate that there are logs with mono (density, neutron porosity and sonic) and bimodal (gamma and resistivity rays) characteristics (Fig. 2), and that the correlation between the two wells showed that reservoirs with hydrocarbons are deeper in the well X (Fig. 3). Laboratory data show a strong linear dependence between permeability and porosity (Fig. 4), with the porosity data ranging from 0.7–35% by focusing between 20–24%, as the permeability range between 0.1–40 mD and focus between 1.6–1.8 mD (Fig. 5).

The results of the clustering to density, neutron and sonic logs in wells X and Y have up to 10 electrofacies (Fig. 6), wherein the depths with those values above 9, have the best reservoir characteristics (Fig. 7). The determination of these electrofacies served as guidance to make a better estimate of the porosities and permeabilities derived from these logs. To the well X, when comparing with laboratory data, we observe fine adjustments to all estimates of porosity and permeability, but multiple linear regression resulted to be the best be compared with laboratory data (Fig. 8).

The Pickett (1966) plot proved to be similar in both wells, which served to estimate the value of the parameter m from the Archie Equation ($m = 2$) and hence the water saturation using Archie's equation as well as the volume of clay V_{SHALE} , which resulted with low values (<20%). The water resistivity formation R_w of this equation was estimated using the Schlumberger (2013) charts (Fig. 9). The best correlation between calculated porosity and permeability data and laboratory data using multiple linear regression it was used to generate the Winland (1972) graphic. Three flow units in Albian reservoir of well X were identified in this graphic and pore throats with values lower than 2 mm (Fig. 10).

The first flow unit is characterized by having micro pores, with a good total porosity, but very low permeability. The second has micro pores and meso pores, with good porosity but low permeability. The third presents meso pores, with great porosity, reasonable permeability and high oil saturation, thus constituting itself in the unit with better characteristics for hydrocarbon production (Fig. 11). The same 3 units of flow are identified in well Y, allowing the identification points which the porosity and permeability have incorrectly calculated by multiple linear regression (Fig. 12).

Conclusions

We characterize the Albian carbonate reservoirs of Oilfield B in the Campos Basin by integrating the results derived from the interpretation of well logs with petrophysical properties measured in the laboratory. We have shown that the proper use of this database, using the abundant well logs in front of the sparseness and targeting of laboratory tests, taking at the same time the advantage of the mathematics and geological interpretations, leads us to derive a wide range of petrophysical parameters that give us a broad view of the reservoir. This results in greater confidence in the estimates, which allowed us to extend the obtained results from the reference Well X to Well Y, which is considered as a blind test. In the study, this extension was made successfully only for one well, however, the methodology can be spread over the next wells with similar geology within the same reservoir.

Acknowledgments

The authors would like to thank the Carbonates Science, Training and Technology System (SCTC) of Petrobras for their cooperation in providing the data to publish this work.

References

- Aguilera R, Aguilera M. 2001. The integration of capillary pressures and Pickett plots for determination. SPE Conference, paper no. 71725.
- Bruhn C, Gomes J, Lucchese C, Johann P. 2003. Campos basin: reservoir characterization and management - Historical overview and future challenges. Offshore Technology Conference, Houston, Texas, paper OTC 15220, 14 p.
- Lucia F. 2007. Carbonate reservoir characterization. Springer-Verlag, Berlin, Heidelberg, 336 p.

LR Senergy. 2017. Interactive Petrophysics v4.3, Online user's manual (<http://www.lrsenergy.com/software/ip>).

Pickett G. 1966. A Review of current techniques for determination of water saturation from logs. JPT, vol. 18. p. 1425–1433.

Schlumberger 2013. Log interpretation charts. Educational Services. USA, 306 p.

Shenawi, S, White J, Elrafie E, El-Kilany K. 2007. Permeability and water saturation distribution by lithologic facies and hydraulic units: a reservoir simulation case study. Presented at the SPE Middle East Oil and Gas Show and Conference, Manama, Bahrain, SPE-105273.

Silva R. 2016. Petrophysical characterization of an Albian carbonate reservoir using well logs and laboratory measurements. Master Thesis, UENF/CCT/LENEP, Macaé – RJ, 157 p. (In Portuguese).

Winland H. 1972. Oil accumulation in response to pore size changes, Weyburn field, Saskatchewan: Amoco Production Company Report F72-G-25, 20 p. (Unpublished).

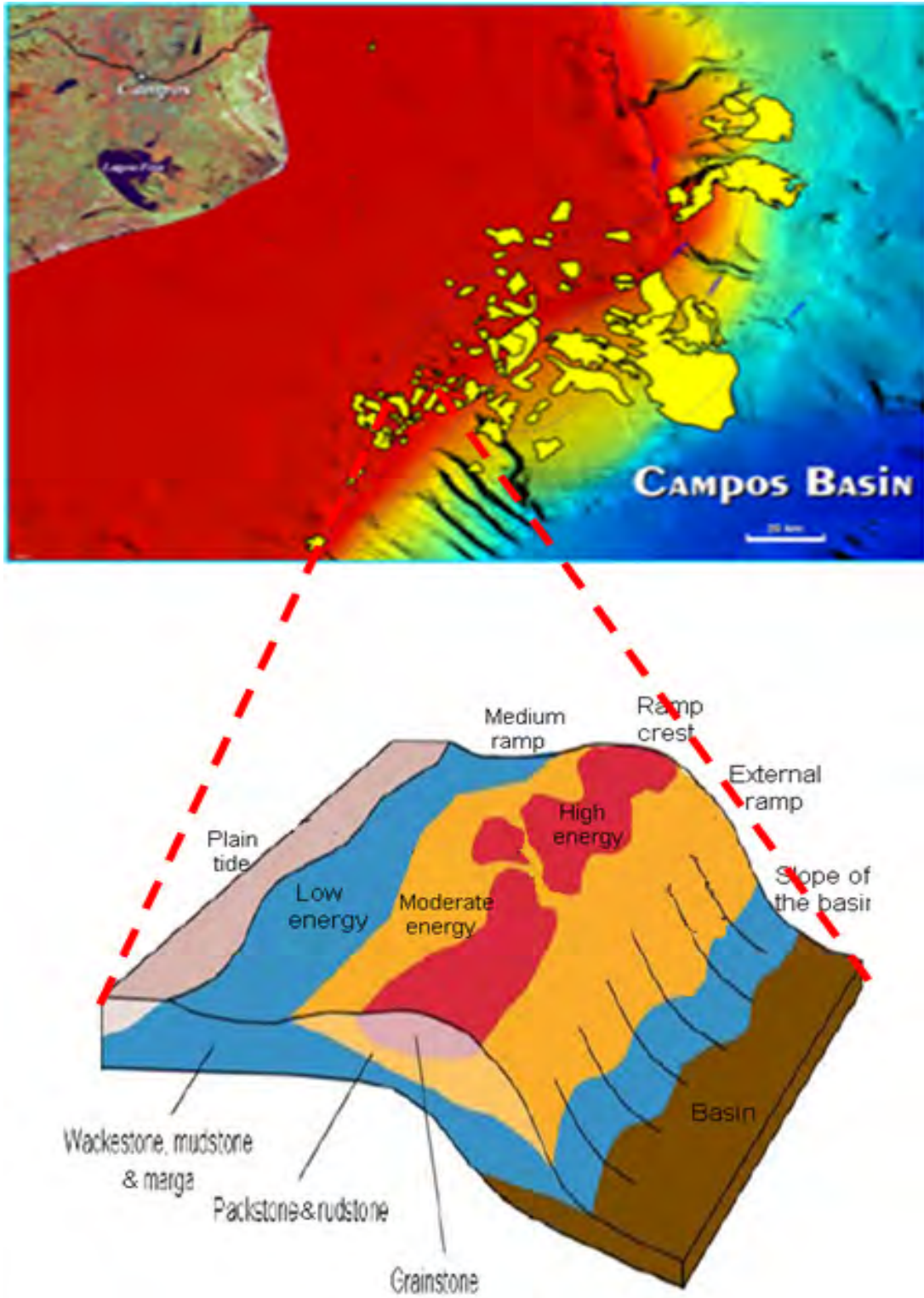


Figure 1. Albian carbonate reservoirs in Campos Basin (modify from Bruhn et al. 2003).

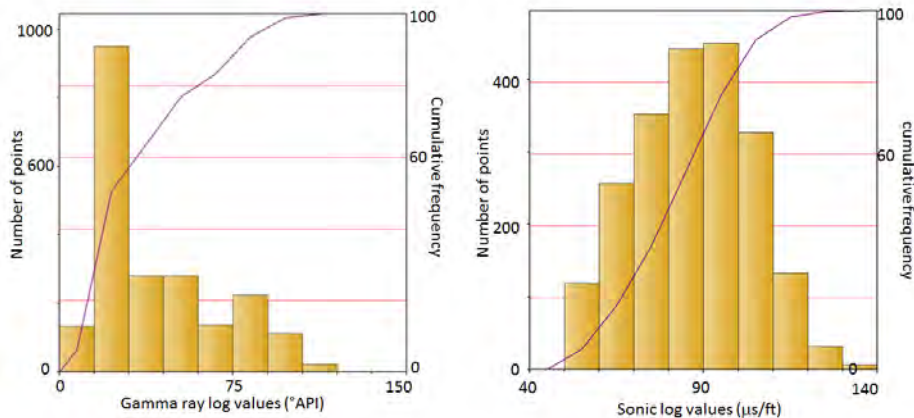


Figure 2. Histograms of gamma rays (left) and sonic (right) logs of Well X–Oilfield B.

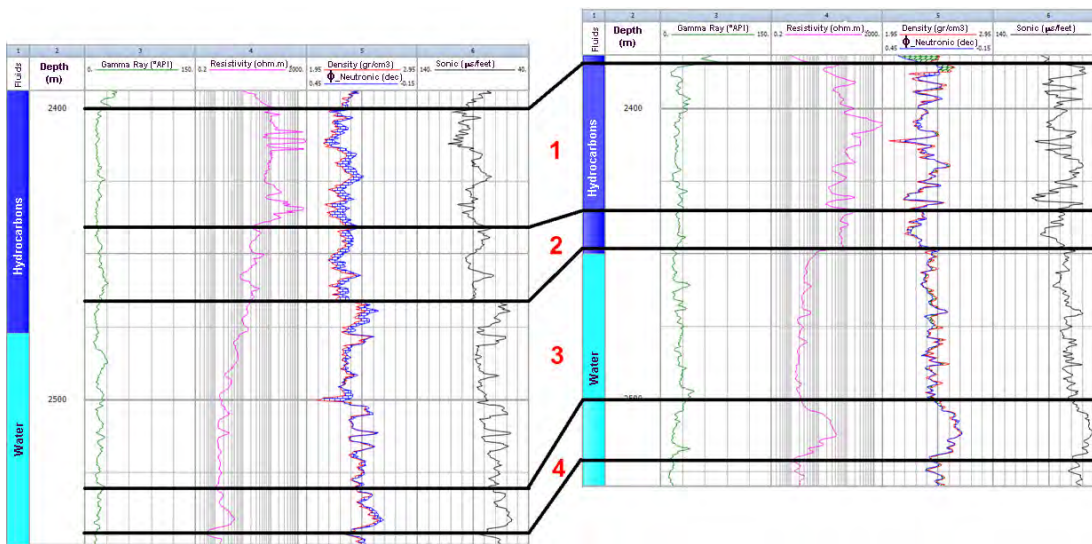


Figure 3. Correlation between gamma, resistivity, density, neutron porosity and sonic logs to the wells X and Y of Oilfield B in Campos Basin. The red numbers 1 to 4 indicate areas with similar characteristics.

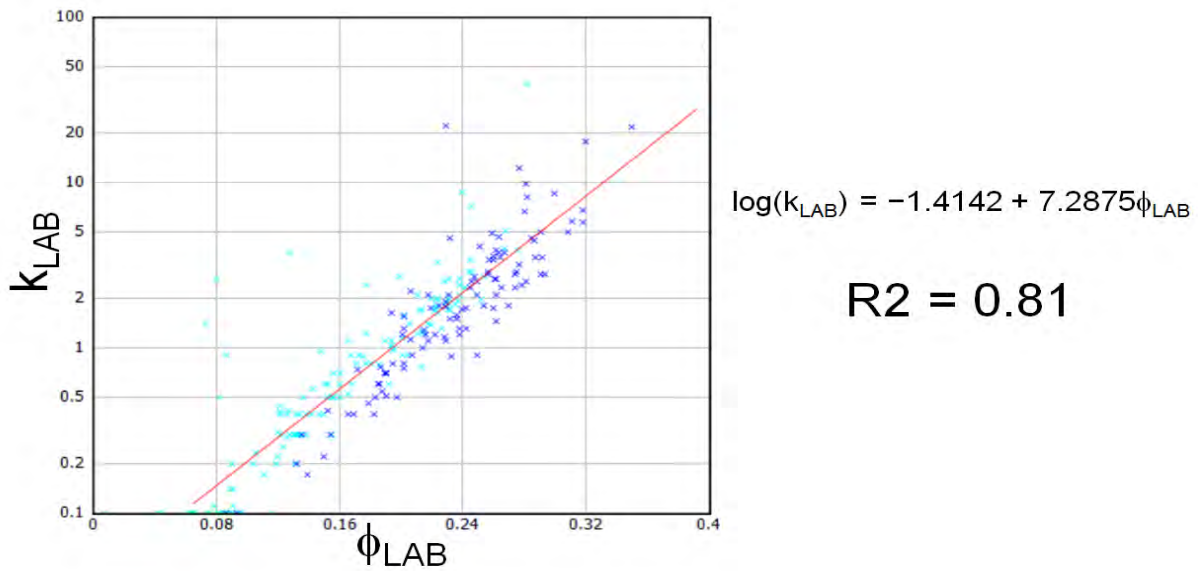


Figure 4. Porosity (ϕ_{LAB}) and permeability (k_{LAB}) laboratory data crossplot for Well X showing a strong direct relationship, with dark blue signifying the hydrocarbon zone and light blue the aquifer.

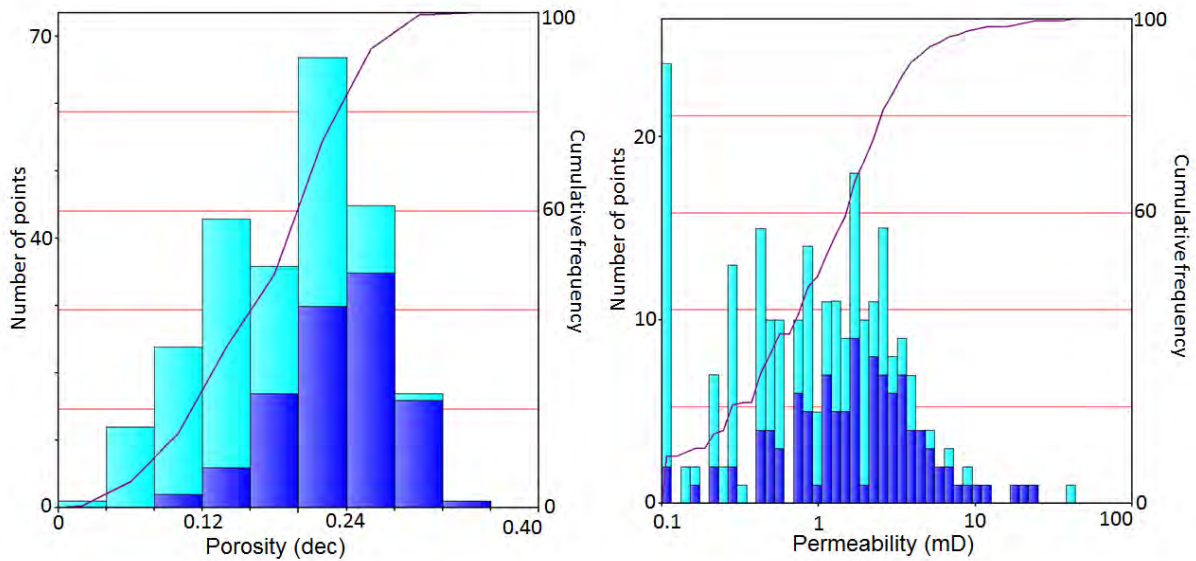


Figure 5. Porosity (ϕ_{LAB}) and permeability (k_{LAB}) laboratory histograms for Well X with dark blue meaning the hydrocarbon zone and light blue the aquifer.

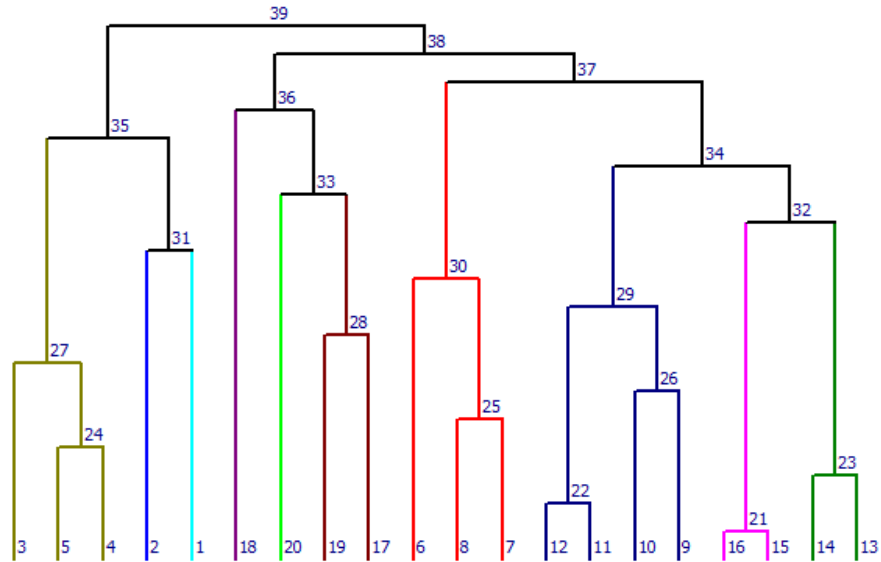


Figure 6. Clusters in 10 different colors, considering density, neutron and sonic logs of Well X, using the method of the sum of the square of the distance.

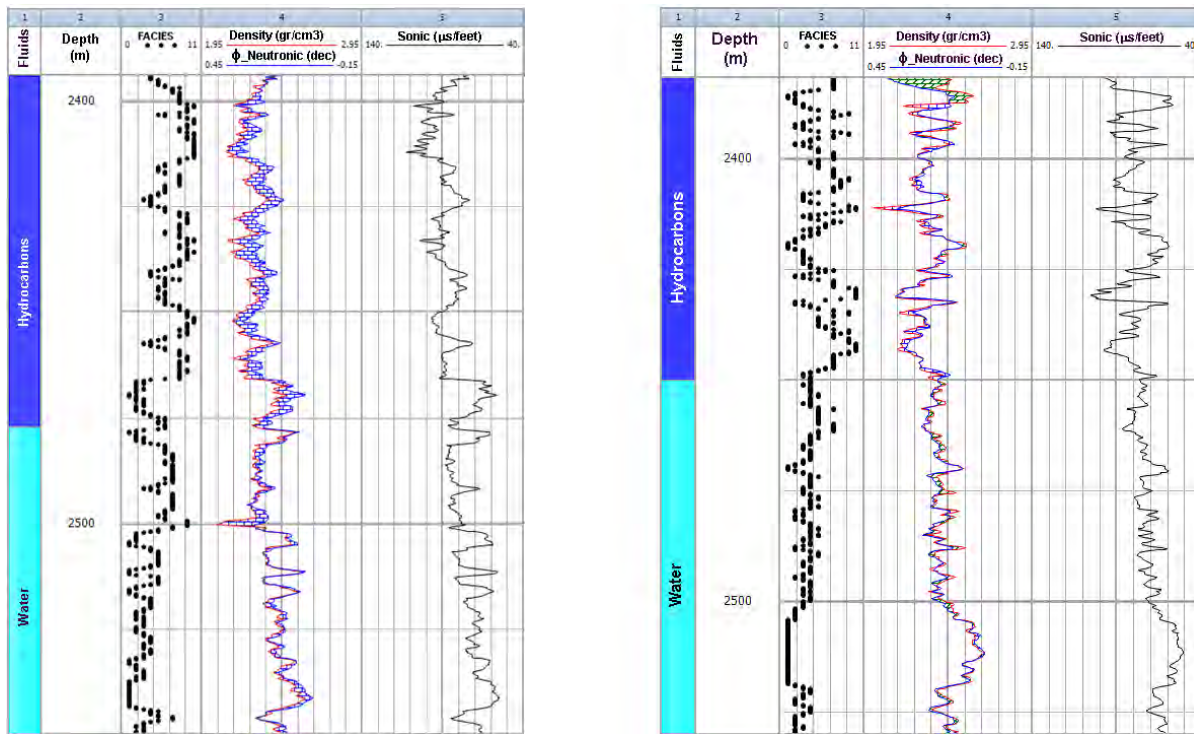


Figure 7. In the third track electrofacies for Well X (left) and Well Y (right) for each depth.

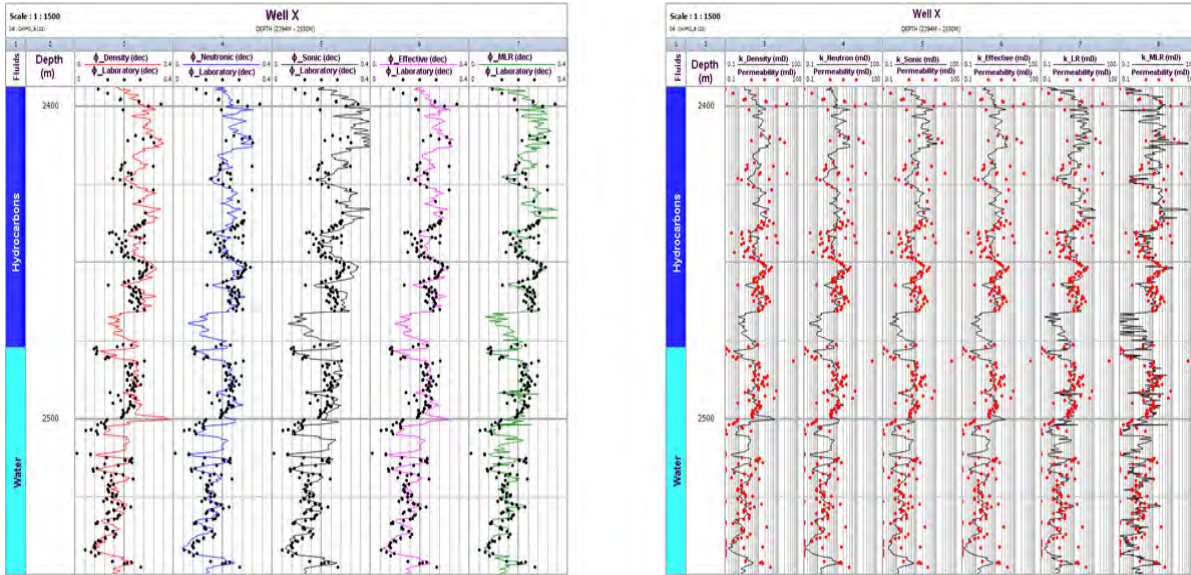


Figure 8. Estimated values of porosity (left) and permeability (right) for Well X compared with the respective data measured in the laboratory, using the estimates of density, neutron, sonic, effective, linear regression and multiple linear regression porosities.

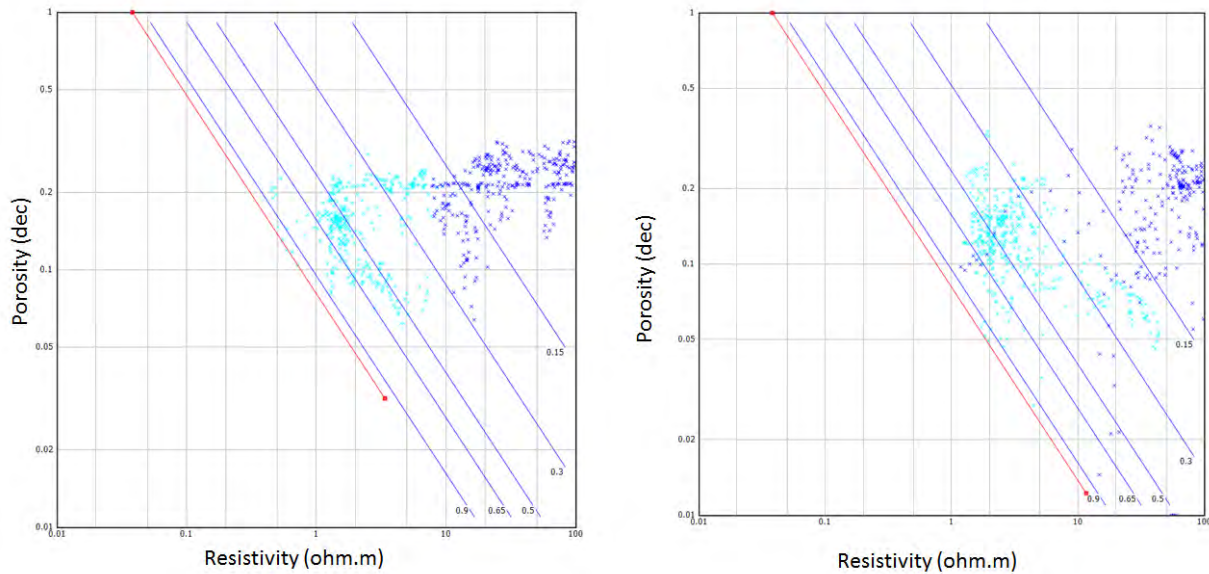


Figure 9. Pickett graph for Well X (left) and Well Y (right) of the Oilfield B, with light blue signifying the aquifer and dark blue zone hydrocarbon. Slopes of the straight lines are the parameter m of Archie equation ($m = 2$).

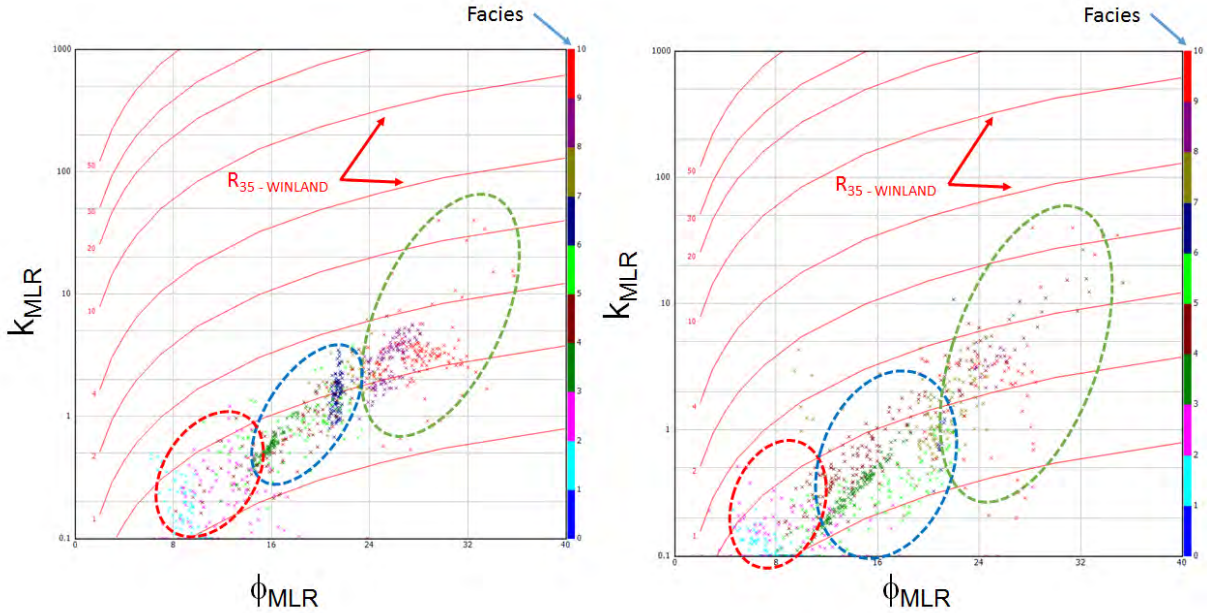


Figure 10. Winland graph for Well X (left) and Well Y (right) of the Oilfield B, where the different colors mean different electrofacies, red curves are the pore throat radius and ellipses mean flow zones, with red being the zone 1, blue is the zone 2 and green the zone 3.

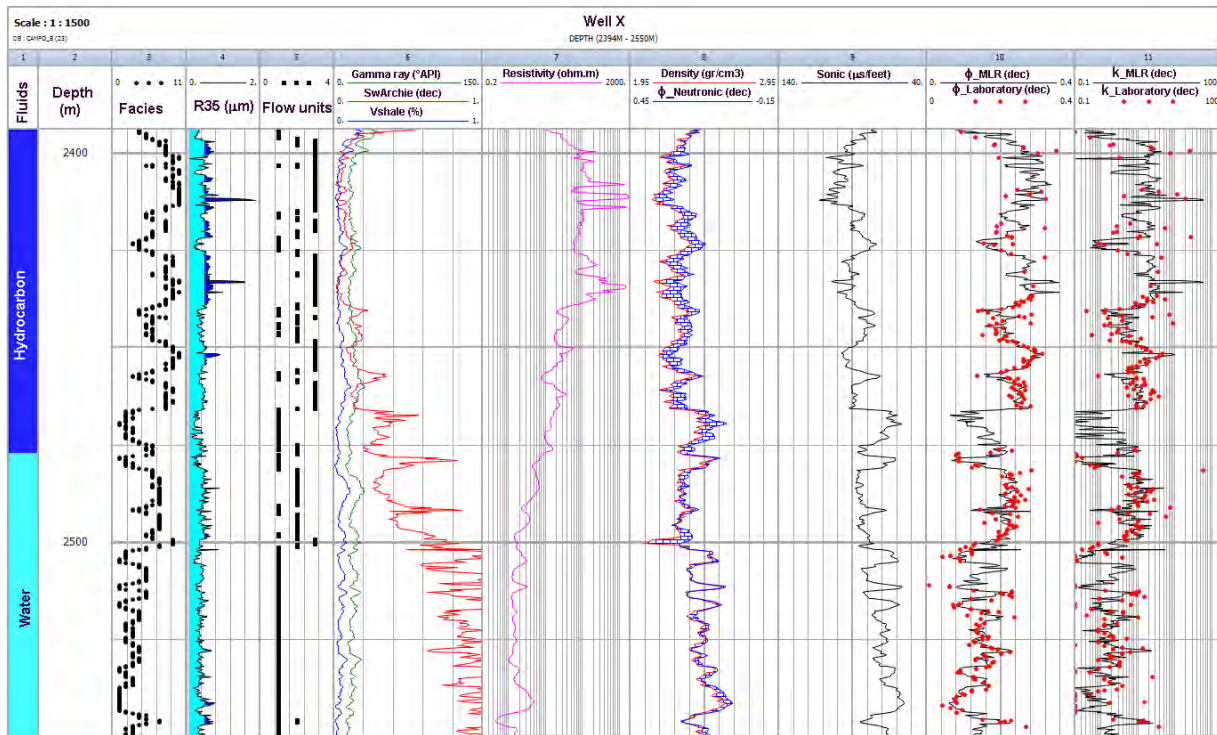


Figure 11. Complete interpretation for Well X, highlighting the electrofacies in the third track, the pore throat radius in the fourth, the flow units in the fifth and water saturation and volume of clay in the sixth.

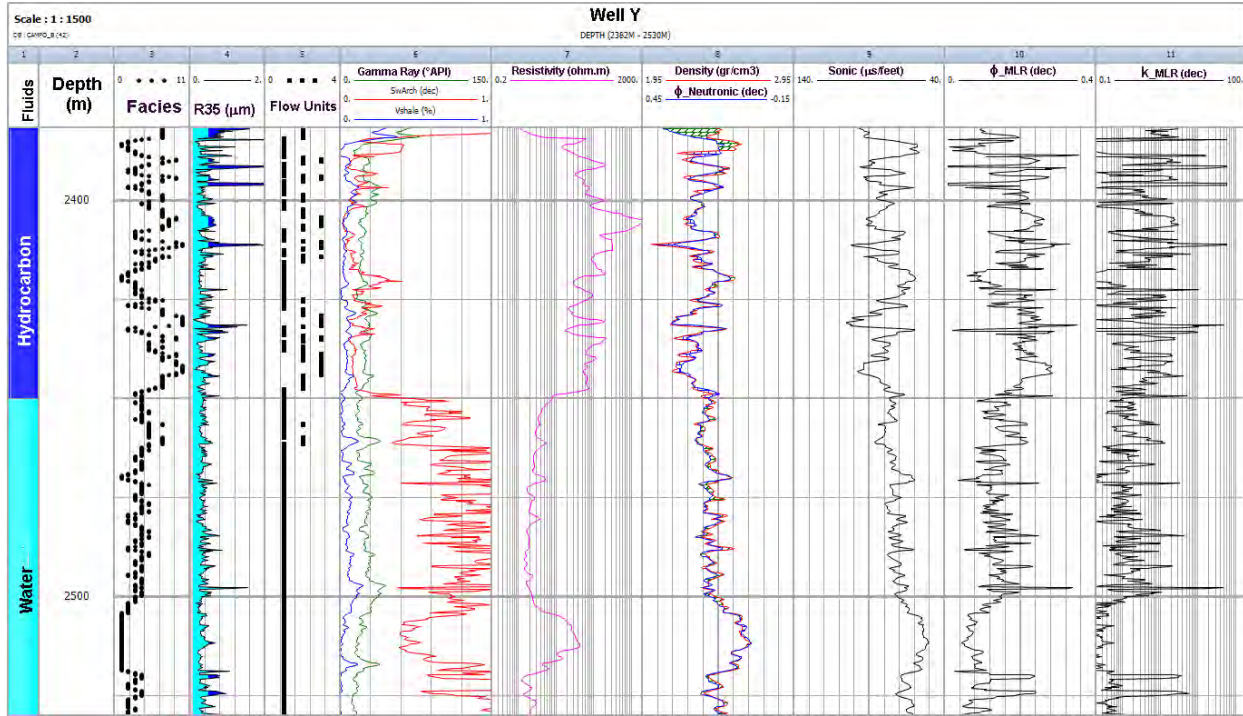


Figure 12. Full interpretation of the Well Y, highlighting electrofacies in the third track, the pore throat radius in the fourth, flow units in fifth and water saturation and volume of clay in sixth.

Unconformity-related porosity evolution in the Devonian Kwatabohegan Formation of the Moose River Basin, northern Ontario, Canada

Nancy Chow*, Matthew G. Braun, and Derek K. Armstrong

*University of Manitoba, 240 Wallace Building, 125 Dysart Road, Winnipeg, Manitoba, R3T 2N2, Canada

e-mail: nancy.chow@umanitoba.ca

The Lower to Middle Devonian Kwatabohegan Formation is considered to be one of the best potential petroleum reservoirs in the offshore Hudson Bay Basin but characterization of this formation and other potential Devonian reservoir rocks in the basin is primarily based on seismic and sparse petrophysical data. The adjoining Moose River Basin in northern Ontario offers Devonian outcrop exposures and core data that can be used to develop analogues for Devonian reservoirs in the Hudson Bay Basin. This study, undertaken as part of Natural Resources Canada's Geo-Mapping for Energy and Minerals program, investigates the stratigraphy and sedimentology of the Kwatabohegan Formation in selected cores from the Moose River Basin and characterizes the nature and distribution of porosity based on detailed core examination and petrography.

The Kwatabohegan Formation in the Moose River Basin consists of dolomitic skeletal limestones and dolostones. The formation is underlain by skeletal limestones and dolostones of the Stopping River Formation (Lower Devonian) and is conformably overlain by dolostones and nodular to massive gypsum of the Moose River Formation (Middle Devonian) which is capped by a regional unconformity. In the Kerr Addison Coral Rapids CR-78-08 core, located on the eastern side of the Moose River Basin, the Kwatabohegan Formation is about 66 m thick. It consists of a lower package of dolomitic coral-stromatoporoid floatstones, bituminous skeletal wackestones, and skeletal packstones-grainstones; and an upper package of predominantly microcrystalline to medium crystalline dolostones. The limestones typically have less than 5% porosity, whereas the dolostones have very good (up to 20%) intercrystalline, vuggy and moldic porosity. In the Schlievert Lake OGS 83-8D core, located about 140 km west-southwest of the Coral Rapids core, the Kwatabohegan Formation is about 51 m thick and dominated by dolomitic stromatoporoid bindstones, coral floatstones-rudstones, and skeletal packstones-wackestones. Moldic and vuggy porosity, up to 30%, occurs in most facies and increases up-section. Reservoir-quality porosity in the Kwatabohegan Formation is facies independent and mainly related to burial dolomitization coupled with later extensive dissolution of dolomite and neospar matrix. Dissolution is interpreted to be due to late-stage meteoric diagenesis, possibly related to uplift, erosion and formation of a regional unconformity, during one or more epeirogenic events on the Hudson Platform in the Middle to Late Devonian, and the pre-Mesozoic unconformity.

The use of micro-Fourier-transform infrared (micro-FTIR) reflectance spectroscopy for evaluation of composition, texture, and porosity in carbonate-rich shales and fine-grained carbonates

Hilary Corlett*, Tiffany Playter, Michelle Tappert, Ralf Tappert, and Tenea Dilman

*Alberta Geological Survey, 4999-98 Avenue, Edmonton, Alberta, T6B 2X3, Canada

e-mail: hilary.corlett@agr.ca

Hyperspectral imaging techniques based on micro-Fourier-transform infrared (micro-FTIR) reflectance spectroscopy allows for the creation of in situ, non-destructive mineral maps at the micrometer scale, where each pixel represents 2.7 μm . This technique is particularly useful in fine-grained basinal carbonates and carbonate-rich shales where the rock composition changes on a sub-millimeter scale. These fine-scale changes in mineralogy cannot be mapped using whole rock geochemistry or handheld x-ray fluorescence where the instrument window is 1 cm or more. Hyperspectral imagery was collected from the Duvernay Formation (Alberta, Canada) to produce mineral maps that show the distribution of quartz, biogenic silica, and clay in a <1 mm by 1 mm area. Mapping these microscopic changes in composition and texture, particularly the relationship of clay versus carbonate content or the presence and distribution of cement, can aid in predicting porosity and potential connectivity of pore networks. This technique also allows for differentiation of mineral phases such as crystalline or detrital quartz versus biogenic quartz. Making this distinction is of particular importance in carbonate-dominated shale reservoirs where intervals rich in detrital quartz have sometimes been found to have higher porosities than those rich in biogenic quartz (Ross et al. 2009), although the latter may contain a higher abundance of TOC. Micro-FTIR reflectance spectroscopy is also showing promise as a useful technique for the investigation of monomineralic rocks with fine crystal sizes, such as matrix dolomites, or pore-filling cements. Hyperspectral images of calcite and dolomite samples from Devonian rocks in the Western Canadian Sedimentary Basin were processed and analyzed to produce compositional maps that emphasize the crystal boundaries through identification of the individual mineral phase and the crystallographic orientation of each crystal. This image is then used to determine the arrangement of the crystals and the percentage of anhedral, subhedral, and euhedral crystals. The nature of crystal morphologies and boundaries in a recrystallized or neomorphosed matrix or cement ultimately affects its porosity and permeability.

References

Ross DJK, Bustin RM. 2009. The importance of shale composition and pore structure upon gas storage potential of shale gas reservoirs. *Marine and Petroleum Geology* 26:916–927.

The growth of calcite cement—porosity's nemesis!

J.A.D. Dickson

University of Cambridge, Department of Earth Sciences, Downing Street, Cambridge,
CB2 3EQ, United Kingdom

e-mail: jadd1@esc.cam.ac.uk

The morphological development of archetypal calcite cement, that is, polyhedral calcite monocrystals passively crystallizing from the walls of liquid-filled, static fissures or pores, is analyzed. The growth of spherulites, dendrites, split crystals and other bazar-shaped crystals, crystals growing in spaces only partly filled with liquid, and crystals growing in deforming spaces, are not included. Two examples of multiply zoned cements are used to reconstructed cementation in macropores.

The first sample is of a Permian bryozoan patch reef with cement that shows little textural maturation. The open framework of this reef was constructed by bryozoa (*Acanthocladia* and *Thamniscus*; Smith 1981) encrusted with a layer of dolomite crystals; calcite cement almost fills its irregularly-shaped pore network (Fig. 1). In cathodoluminescence (CL) the crystals are dominantly non-luminescent with bright yellow to orange colored narrow luminescent zones in the distal two thirds of each crystal (numbered 1 to 10, Fig. 2). The charge contrast image (CCI) shows a much finer zonation throughout and blocky structures in the proximal third of crystals; the bright luminescent zones appear black on the CCI.

The zonal succession in the Aberford cement crystals provides a time framework with which to reconstruct their growth. The oldest part of each crystal appears above the pore wall on Figure 2, which indicates these crystals nucleated out of the plane of the thin section. At the end of CL zone 1 precipitation, the pore wall was decorated by a few euhedral cement crystals adhering to its largely uncemented surface.

The crystallographic forms adopted by the Aberford crystals are identified from interfacial angles measured around individual CL zones and matched with published data (Palache et al., 1951). The transverse section through a crystal at the base of Figure 2 has a hexagonal outline to CL zone 1; its six interfacial angles of 60° are compatible with the principal prism $\{10\bar{1}0\}$ and its parallel-sides are capped by the $\{10\bar{1}1\}$ and $\{10\bar{1}4\}$ rhombohedra in longitudinal section. The large crystal, center right on Figure 2, shows thin orange luminescent facets $\{10\bar{1}0\}$ alternating with wider yellow luminescent facets $\{21\bar{3}4\}$. The yellow facets are arranged symmetrically in three sectors that shrink distally (Fig. 3).

Cementation of the Aberford pore proceeded centripetally until CL zone 7 when the original pore became subdivided into smaller pores that followed different paths (Fig. 2). Cementation of the upper central pore continued to completion whereas cementation in the left and right pores stopped becoming vugs lined by crystal faces.

The intercrystalline boundaries in the Aberford cement appear to be impingement or compromise boundaries but close examination of some boundaries show zones in adjacent crystals are offset (Fig. 4). This offsetting is likely caused by dissolution along this boundary after the crystal had impinged. No systematic distribution of these offset boundaries occurs in this cement between the margin and the center of the Aberford pore.

A pause in crystal growth of can cause ageing or alteration of the crystal's surfaces so seeding of subsequent cement on such surfaces becomes restricted to active sites. A pause in growth can also allow the precipitation fluid to alter causing a change in crystal habit. The second sample is a grainstone from the Blaen Onneu Oolite Formation that at one time had millimeter-sized shelter cavities beneath disarticulated bivalves separated by well-sorted sediment with intergranular pores hundreds of microns in diameter (Fig. 5); the shelter cavities were filled with cement that show an acute to equant habit change.

The CL image of the Abercriban cement (Fig. 6) shows multiple zoning that can be divided into 7 stages (labelled A to G, Fig. 7). Large cement A crystals are seeded on crinoids and prismatic calcite layers of bivalves; their distribution is shown in brown on Figure 7. The terminal surface of cement A has a simple zig-zag shape indicating it grew epitaxially but its internal structure and the stereom structure of most crinoids have been destroyed by recrystallization. Smaller cement A crystals occur in the intergranular pores between grains where its separation from cement B is obscured by recrystallization.

The largest syntaxial cement crystal shows cements B and C have orange colored luminescence, repeated oscillatory zoning, and a dominantly acute habit (Fig. 6); finally cement C formed an obtuse shrinking terminal cap. Cement D is dominantly non-luminescent with bright yellow or orange luminescent hairline zones a few microns wide. Cements B, C, and D grew centripetally into the larger shelter cavity forming progressively smaller concentric rings (Fig. 7). Cement C is prominently developed in the larger, compared to its thin development in smaller shelter cavity; cement D has the opposite thickness arrangement. Cement E seeds on the apex of the halted cement D surface marking a change from acute to equant habit; the diachronous contact between cement D and cements E, F, and G, is shown on Figure 7; cements F and G follow the equant rhombohedral form of cement E.

The filling of the upper smaller shelter cavity created two small pores that were eventually completely filled by stage D cement (Fig. 7). The hairline zones in cement D at the center of the right pore displays severe mismatches across intercrystalline boundaries (Fig. 8). The growth direction of four impinging crystals is normal to the hairline zones indicating these crystals grew together continuously to forming two enfacial junctions (Fig. 8).

The Abercriban cement is deformed by twin planes a few microns wide that cause jogs in the alignment of zones (Fig. 26E); they cross all generations of cement and hence post-dated cementation (Raven 1986).

Cement textures in the two Abercriban shelter cavities are partly controlled by variation in seed crystals forming their walls as these seeds are of variable size and orientation. The upper surface of the larger shelter cavity is composed of micrite that seeded cement crystals of uniform size

that competed against each other as they grew away from the micrite. The centripetal filling of the larger cavity was interrupted by the acute to equant habit change that disrupted textural maturation causing the pore center to be filled with randomly orientated crystals (Fig. 7).

Conclusions

1. Centripetal cementation of pores passes a threshold after which carbonate supply is confined to intercrystalline boundaries. Sheet pores along these boundaries are labile; they can change with time switching from above to below the percolation threshold so late cement distribution is erratic. Cement stages can be absent from some pores and the youngest cement does not necessarily occur at pore centers or line unfilled pores.
2. Determination of crystallographic form and habit is often sloppy or inaccurate, yet it controls the position and size of growth vectors, which in turn control cement morphology. An acute to equant habit change re-orientates a crystal's fastest growth direction sometimes by almost 90° resulting in "mushroom-shaped" crystals. The acute to equant or obtuse habit change has been identified in cements from carbonates of different ages and locations and may indicate a change in pore water chemistry that was widespread.
3. Crystallographic form and habit are determined by the precipitation environment; understanding how this works is far from complete but is improving; form/habit can indicate properties of the precipitation fluid that are otherwise difficult to determine. For instance, the change from synthetic rhombohedral to scalenohedral morphology is associated with increasing supersaturation and the anion/cation ratio of the fluid (Carmona et al. 2003).
4. Zonal offsets at intercrystalline boundaries formed by dissolution in nanometer-sized sheet pores can supply carbonate for simultaneous precipitation in adjacent macropores, due to a pore size effect. Zonal offsetting is minor in cements that incompletely fill pores but significant at the center of completely filled pores. This modification of cement boundaries shown by zonal offsetting could be commonplace in other materials where it is more difficult to demonstrate. The recycling of carbonate associated with boundary modification involves localized mass redistribution; its geochemical consequences need considering.
5. A high frequency of enfacial junctions is claimed to be one of the least equivocal criteria for identifying cement, however, none occur in the Aberford cement! The mechanism for forming enfacial junctions proposed by Bathurst (1964) is confirmed by the zonal reconstruction of cement at hiatus intercrystalline boundaries but their frequency is low. A new type of enfacial junction is identified that forms by boundary modification of pore center cements.
6. Many calcite cements preserved their original features for millions of years from deposition to maximum burial and back again. The use of their internal growth features to reconstruct the morphological development of calcite aggregates is only one use of this material that is a "treasure house" of information.

References

Bathurst RGC. 1964. The replacement of aragonite by calcite in the molluscan shell wall. *In* Imbie J, Newell N (Editors). *Approaches to Paleocology*: John Wiley and Sons, Inc., New York.p. 357–376.

Carmona JG, Morales JG, Clemente RR. 2003. Rhombohedral–scalenohedral calcite transition produced by adjusting the solution electrical conductivity in the system $\text{Ca}(\text{OH})_2\text{--CO}_2\text{--H}_2\text{O}$. *Journal of Colloid and Interface Science* 261:434–440.

Palache C, Berman M, Frondel C. 1951. *Dana's System of Mineralogy*, 7th edition, Vol. II: Wiley, New York. 1124 p.

Raven MJ. 1983. The diagenesis of the Oolite Group between Blaen Onneu and Pwll Du, Lower Carboniferous, South Wales, [Ph.D. thesis], University of Nottingham.

Smith DB. 1981. Bryozoan-algal patch-reefs in the Upper Permian Lower Magnesian Limestone of Yorkshire, northeast England. *In* Toomey DF (Editor). *European Fossil Reef Models*, Special Publication 30: SEPM (Society for Sedimentary Geology), Tulsa, Oklahoma. p. 187–202.

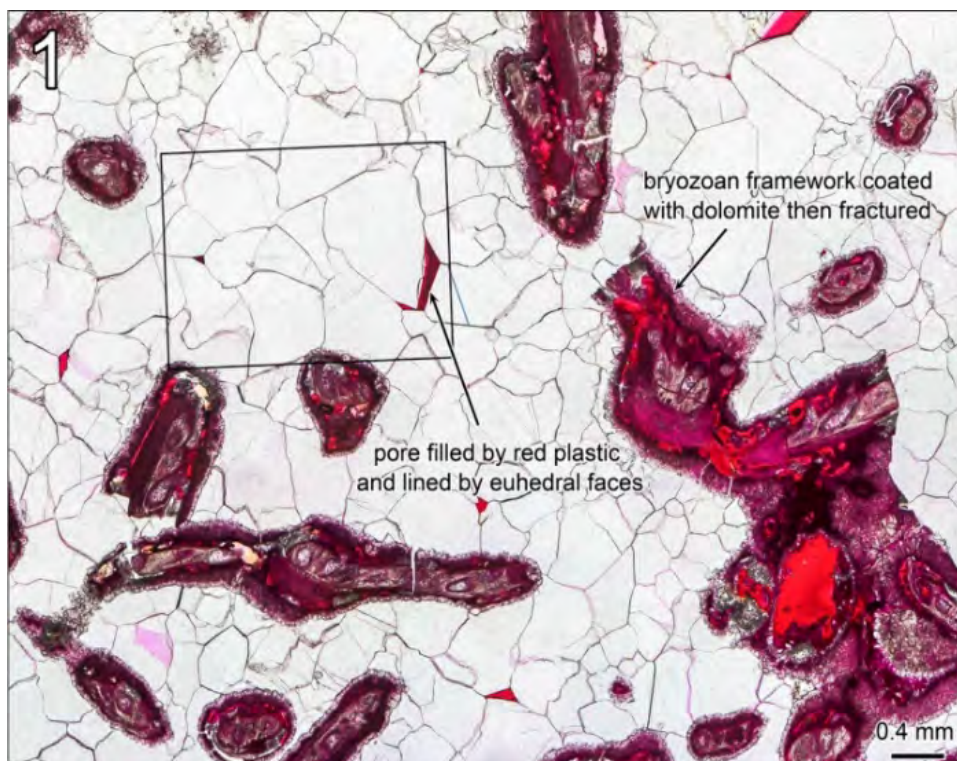


Fig. 1 --- Plane light image of thin section through patch reef formed of fragmented bryozoan colonies, Upper Permian, Aberford, near Leeds, Yorkshire, U.K. The interskeletal pores were largely filled by granular transparent calcite cement. Present pores are filled with red plastic.

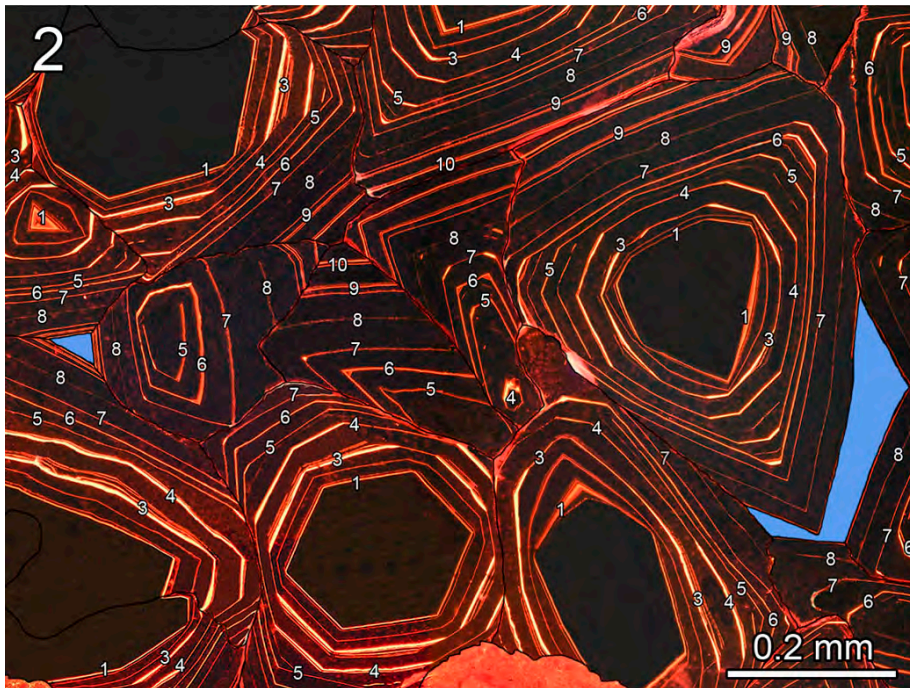


Fig. 2 --- CL image of box on Fig. 1, calcite cement crystals show thin luminescent zones (numbered 1 to 10) in dominantly non-luminescent calcite. Pore space is coloured blue and bryozoa with dolomite crusts are coloured orange.

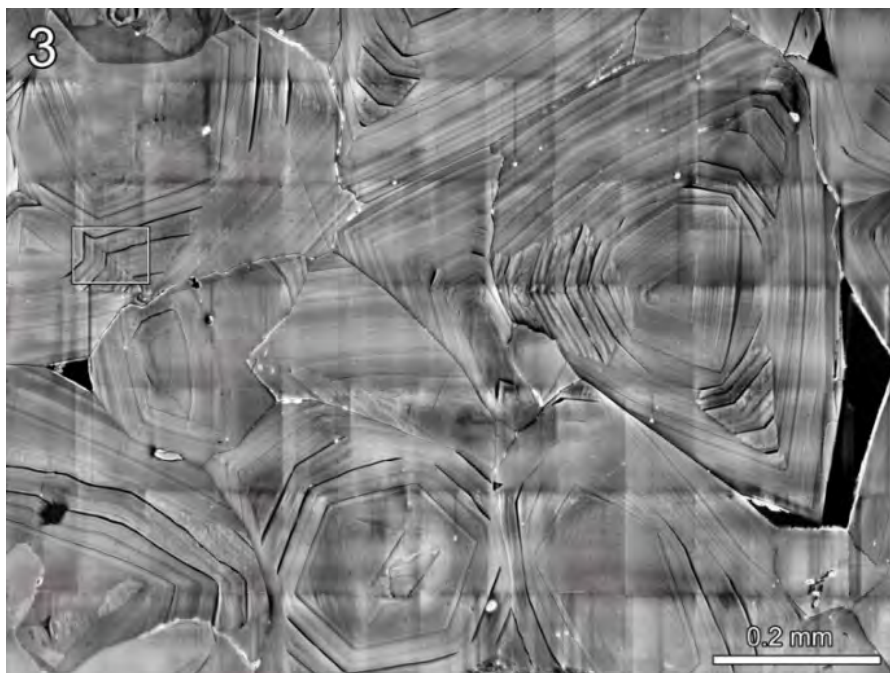


Fig. 3 --- Charge contrast image, same area as Fig. 2. The oldest portion of some crystals show eccentric blocky structures, whole crystal show fine growth layers and growth sector boundaries are prominent. Ten imperisistent black zones are equivalent to CL bright zones.

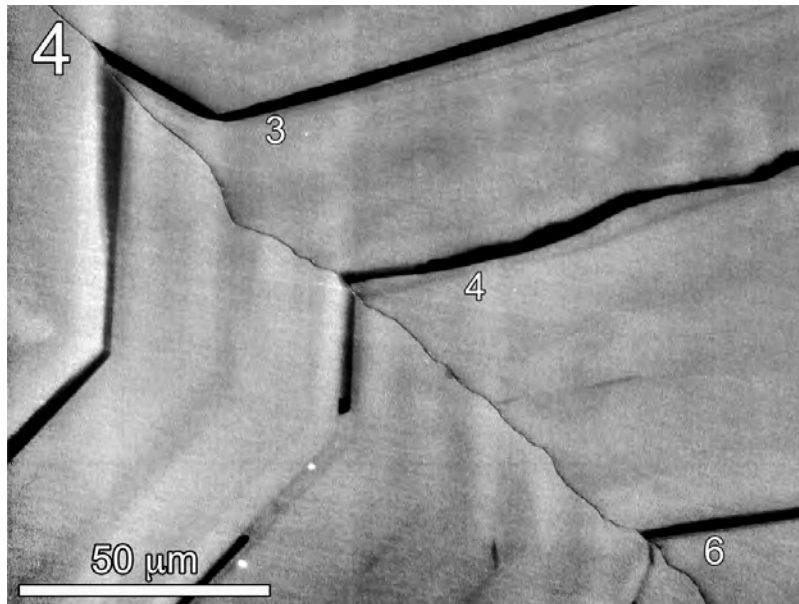


Fig. 4 --- CC image of boxed area on Fig. 3; one irregular diagonal intercrystalline boundary, runs top left to lower right with offset black zones 3, 4, and 6 in two impinging calcite crystals.

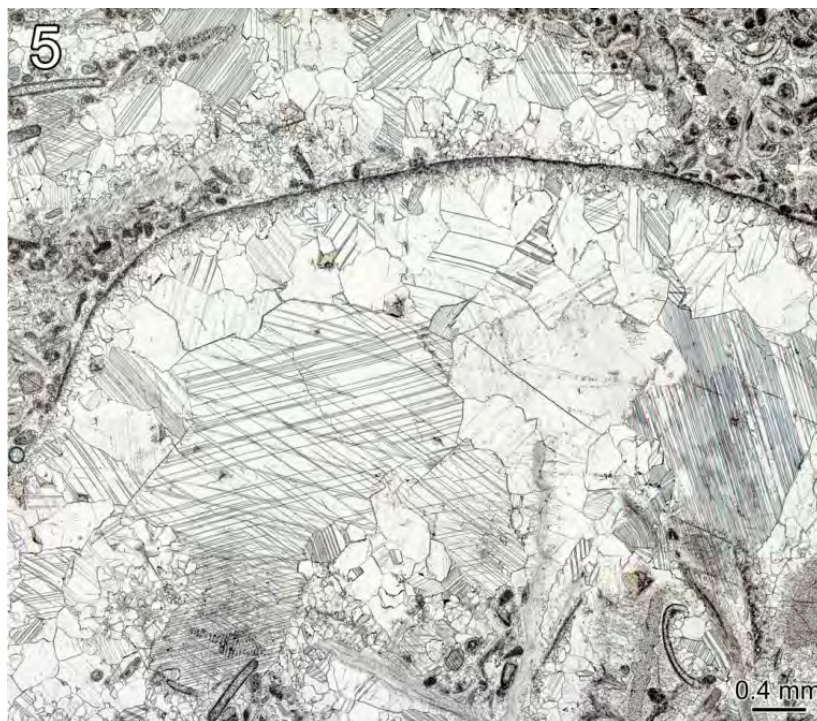


Fig. 5 --- Plane light image of a thin section from the Blaen Onneu Oolite, Abercriban Quarry, Pontsticill, Merthyr Tydfil, Wales, UK. Peloidal skeletal grainstone with convex-up disarticulated bivalve shells (dissolved) that protected shelter cavities now filled with coarsely crystalline calcite cement. Some cement crystals show rhombohedral twinning.



Fig. 6 --- CL image from same area as Fig. 5; shelter cavity cements showing multiple orange to black luminescent zoning.

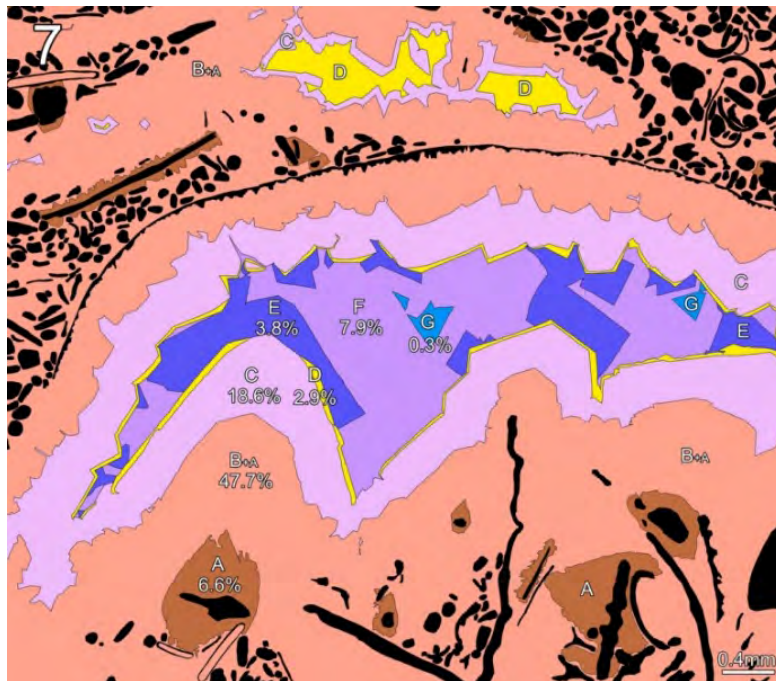


Fig. 7 --- Tracing from CL image Fig. 6 showing cement divisions in color A = brown, A+B = pink, C = pale mauve, D = yellow, E = dark blue, F = pale purple and G = blue; figures are counts for components as % of whole image area.

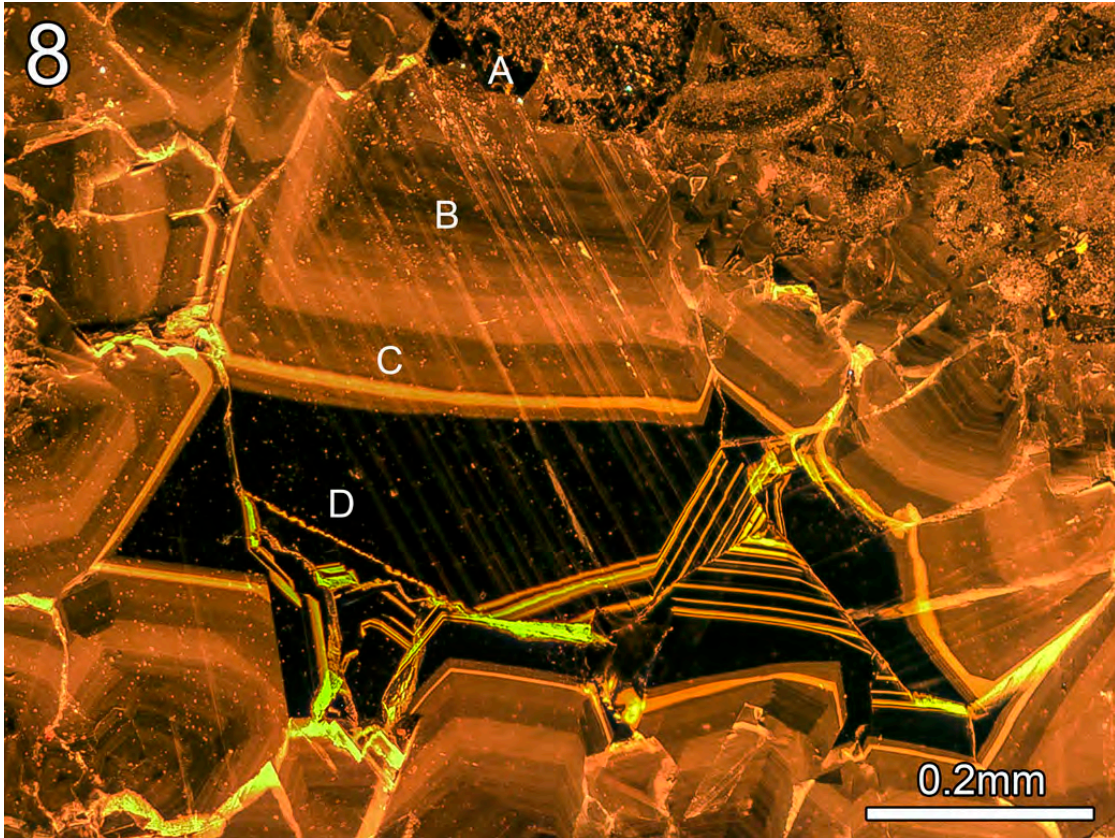


Fig 8 --- CL image of box at top of Fig. 6; cement D at the center of pore with offset and missing zones around two enfacial junctions.

Comparison of sedimentological, stratigraphic, and diagenetic controls on development of fracture porosity in dolostones of the Miocene Monterey Formation of California and Devonian Slave Point Formation of western Canada

John B. Dunham

Dunham Consulting, 1925 Terrace Drive, Ventura, CA 93001, USA

e-mail: johndunham76@gmail.com

Fractures are common in carbonate rocks and may account for some or all of the effective porosity in carbonate reservoirs (Nelson 2001). Fractures form in response to stress, but they will only form in brittle rocks. Stress is defined in units of force per unit-area, comparable to pressure for example; stress can be applied to rocks by means of tectonic compression, or through non-tectonic vertical loading by gravity.

It is common to observe fractured layers alternating with non-fractured layers; this results from variations in original sediment compositions that affect the mechanical properties of rocks. This report presents examples of fractured-carbonate reservoir rocks from the deep-water Miocene Monterey Formation of California, and the shallow-water Middle Devonian Slave Point Formation of Western Canada.

Fractures in the Monterey Formation developed from horizontal stress applied through tectonic compression. When subjected to horizontal stress, brittle layers became fractured while ductile layers underwent plastic flow. The result is interlayering of fractured and non-fractured rock. Burial diagenesis transformed original high-porosity biogenic carbonate and siliceous-ooze sediment into low-porosity brittle dolomite and chert layers. Biogenic sediments that were contaminated with only a few percent of terrigenous clay did not become brittle; these ductile rocks underwent plastic-flow during compression. The effect is that heavily fractured dolomite and chert layers alternate with non-fractured calcareous and siliceous mudstones within the Miocene Monterey reservoir. Fractures comprise all of the effective porosity in Monterey reservoirs in Point Pedernales field of the offshore Santa Maria basin, Central California.

In contrast, the fractures that are prevalent throughout Devonian dolostones of the Slave Point Formation formed by gravity-loading vertical-compression during burial, without horizontal tectonic compression. These fractures are related to stylolites. The fractures formed when brittle rocks were bent along uneven stylolite surfaces. The fractures are not as laterally extensive as tectonic fractures in the Monterey Formation, but they are pervasive throughout brittle-dolomite intervals within the Slave Point Formation. The fractures do not comprise the major proportion of porosity within the dolomite reservoir, but they were important to providing permeability pathways for corrosive fluids and hydrocarbons to flow through the rocks during burial. Large fossil molds account for the major proportion of reservoir porosity, while fractures contribute only a small quantity of additional porosity to the reservoir. Nevertheless, these stylolitic-fractures are important for providing interconnections among isolated moldic pores that are encased in low-permeability microcrystalline dolomite.

These examples of fracture development in dolostone come from formations of very different ages and depositional settings, but they demonstrate the same phenomenon: fractures will only form in brittle rocks.

Introduction

The idea for this submission came from the 2015 Mountjoy Meeting in Banff, where a speaker showed a core that had fractures in some layers, but not in others. This led to a discussion where I noted that it was a common to observe fractured and non-fractured rocks in the Monterey Formation of California, where brittle rocks are interlayered with ductile rocks. The following presentation for Mountjoy II is intended to document such examples, both from the Miocene Monterey Formation of California, and from the Devonian Slave Point Formation of Western Canada. I measured coastal-outcrop sections and described cores of the Monterey Formation for Union Oil Company of California, to aid exploration and development efforts in the Santa Maria, Santa Barbara, San Joaquin, and Los Angeles basins in California (Fig. 1). Work on Devonian carbonate cores supported exploration teams in the Calgary office of Union Oil Company of Canada.

Rock Strength and Fracturing

It is common to see fractured rock layers interbedded with non-fractured beds in Monterey outcrops and cores (Fig. 2). This derives from variations in original sediment compositions that influenced the mechanical properties of rocks, as described below. The first studies of mechanical properties of rocks came from the field of Engineering Geology, where unexpected encounters with weak rocks led to major problems with construction of buildings, bridges, tunnels, and dams (Fig. 3). Issues with weak rocks led to development of a formal engineering classification of rock strength, based on uniaxial compressive strength (UCS) tests (Fig. 4). Uniaxial compressive strength was recognized as an important factor that predicted whether a rock mass might cause trouble, or not. The UCS test applies compressive stress to a rock cylinder, while at the same time, measuring the change in length of the cylinder, to produce a stress-strain curve (ASTM 2010). Initially, strain is elastic, meaning that the rock will return to original length if stress is removed. Eventually the elastic limit is reached, where the rock begins to undergo non-reversible change in shape (plastic deformation). Finally, the yield point is reached, where strain becomes rapid with little additional applied stress. The slope of the straight line on the stress strain curve is Young's Modulus, which is a measure rock stiffness, or how much the rock squeezes per each unit of applied stress; imagine squeezing a cube of granite, or a marshmallow, between your finger and thumb.

Unconfined Compressive Strength tests provide a formal definition for brittle and ductile rocks. Rocks that are brittle undergo little plastic deformation before they fail-by-fracture soon after reaching the elastic limit. Rocks that are ductile will continue to deform by plastic-flow without fracturing, long after the elastic limit is reached (Fig. 5). Classic end-members of the brittle to ductile rock spectrum are seen in comparison of UCS tests of Granite and Rock Salt (Fig. 6). The granite core shows very little plastic deformation prior to fracturing, while the rock-salt core shows considerable plastic deformation and never does fail by fracture.

Extensive research (Deere and Miller 1966, Hoek and Brown 1997, Nelson 2001, Sone and Zoback 2013a, 2013b, among many others) has shown that rocks with high compressive strength tend to be brittle, while rocks with low compressive strength tend to be ductile. The properties of rocks with high compressive strength include having low porosity, low clay content, low kerogen content, high mineral toughness where mineral toughness is a function of mineral hardness and crystal cleavage, consider halite versus quartz as an example, and high degree of interlocking of crystals in the rock matrix (Fig. 7). Rocks with the opposite properties have low compressive strength. Examples high-strength rocks include granite, chert, and silica-cemented sands. Carbonates have moderate strength because of lower mineral toughness. Weak rocks include porous sands, evaporites, and mudstones. In any sequence of sedimentary rocks, it would not be unusual to encounter carbonates with moderate strength to be interlayered with shales with low strength. The concept of mechanical stratigraphy subdivides stratified rock into individual mechanical units defined by differences in rock strength, stiffness, and brittleness (Laubach et al. 2009).

Uniaxial Compressive Strength forms the basis for the National Engineering Handbook Engineering Classification of Rocks (NEH 2017). Rock classes that are defined by compressive strength also show differences in ability to withstand blows with a rock hammer. Table 4-3 (Fig. 8) divides rocks into 6 classes based on the way they behave in the field when struck with a rock hammer. Hard to very hard to extremely hard rocks are the ones that “ring” when struck with a rock hammer, and may require many hammer blows to break, if they break at all. My personal experience with the Ordovician Eureka Quartzite in Nevada is that the steel in my rock hammer splintered before the quartzite on the outcrop fractured. In contrast, the softer rocks will “thud” when hit with a rock hammer and will “dent” under a hammer blow. These hardness properties do correlate with Uniaxial Compressive Strength and rock stiffness. Hard rocks within the Monterey Formation include dolostone, quartz chert, and opal-CT porcelanite. Porcelanite is defined as a hard dense rock similar in appearance to unglazed porcelain, usually made up of nearly pure-silica opal-CT which is a mix of the cryptocrystalline SiO₂ minerals cristobalite and tridymite (Isaacs 1980). Dolostone, chert, and porcelanite are brittle and emit high-pitched rings when struck with a hammer, while ductile siliceous mudstones and organic-rich claystones emit a dull thud when struck with a hammer. Hard rocks are brittle and will fracture, while softer rocks will tend to be ductile.

Smart et al. (2014) showed that mechanical stratigraphy was an important input for modeling of fluid-injection hydraulic fracturing projects. In their study (Fig. 9), an outcrop was logged with a Schmidt Hammer, where quantitative hammer-rebound values are interpreted to correlate with relative rock-strength and stiffness properties. Their conclusion was that more induced-fractures will be found in strong layers, while few or no fractures may form in weak layers. Mechanical stratigraphy is an important consideration not only for naturally fractured reservoirs like the Monterey, but also for understanding the behavior of rocks subjected to fluid-injection-induced rock deformation (hydraulic fracturing).

Fractures in the Monterey Formation

The Monterey Formation is a naturally fractured reservoir, but fractures are not uniformly distributed within Monterey reservoirs. There are hard layers and soft layers that show great

variation in mechanical stratigraphy (Fig. 10). Quartz cherts, opal-CT porcelanites, and dolostones are brittle rocks that do contain fractures, but these hard layers are interlayered with soft, non-fractured siliceous shales and organic shales. The stratigraphy reflects differences in composition of the original sediments that were deposited during Miocene time.

The general Monterey story is that upwelling stimulated growth of calcareous and siliceous plankton in surface waters (Fig. 11). Decomposition of sinking plankton consumed oxygen and produced an oxygen-minimum zone about 200 meters water depth. In the open ocean, normal oxygen levels are restored in deeper waters, but in the California Borderland, there are ridges or “sills” that isolate individual basins and keep out deep oxygenated bottom water. The Recent silled-basins of the Borderland are anoxic, and accumulate and preserve sediments with TOC’s over 20%. Miocene Monterey organic-shales accumulated in similar anoxic environments and are the source for most of the oil within the Santa Maria, Santa Barbara, Los Angeles, and San Joaquin basins. Some of these basins were proximal to sources of terrigenous silt and clay, and others were more distal. The Santa Maria and Santa Barbara basins were remote from clastics, while the Los Angeles and San Joaquin basins received more terrigenous clay. During burial, siliceous plankton dissolved and re-precipitated as opal-CT and quartz silica phases, while calcareous nannoplankton dissolved and re-precipitated as microcrystalline dolomite. Both diagenetic tracks resulted in major decreases in porosity (Fig. 12). Original 70%+ porosity sediment is converted into very low porosity dolostone and chert. Monterey dolostones are “bacterial dolomites” (Fig. 13) as described by Baker and Kastner (1981), and Garrison et al. (1984) that replaced calcareous nannoplankton soon after burial, at shallow depths below the water bottom. Anoxic pore waters show the effects of microbial sulfate reduction within a few meters below the water bottom (Claypool and Threlkeld, 1983). Sulfate reduction within pore water can create conditions that are chemically conducive to dolomitization (Baker and Burns 1985; Machel and Mountjoy 1986, 1987). Garrison and Kastner tested their ideas about bacterial dolostone by participating in Ocean Drilling Program Leg 112 that drilled wells in an active coastal-upwelling area with an oxygen-minimum zone impinging on the western margin of Peru (reported in Suess et al. 1988). Pore waters showed the effects of sulfate-reduction and methanogenesis, and dolostones with isotopic signatures of bacterial metabolism were found at very shallow depths below the sea floor, documenting very-early diagenetic replacement of calcareous nannoplankton by microcrystalline dolomite (Fig. 14).

In the Southern California Borderland basins, silica-phase changes occurred at burial depths where increasing temperature drove the dissolution-reprecipitation reactions (Isaacs 1980, Behl 2012) at specific depths below the water bottom (Fig. 15). The end result of these burial-diagenetic carbonate and silica phase changes is the reduction of original 70%+ porosity sediment to a sequence of very low porosity chert and dolostones interlayered with mudstones with higher porosity (Fig. 16). The mechanical behavior of these different rocks can be understood in terms of listed in Figure 7. Chert is a rock composed of quartz, with high mineral toughness, in a matrix of fine, tightly interlocked crystals, with low porosity. Dolostone is a rock composed of dolomite with lower mineral toughness, in a matrix of tightly interlocked crystals with low porosity. Mudstone is a rock composed of some amount of silica and dolomite microcrystals in a matrix of clay; mudstone does not have an interlocked crystal mosaic and it has high porosity. Figure 17 summarizes the mechanical properties of these rocks.

Why don't all of the sediments become hard dolostone or chert layers? The answer is that the original depositional sediment contained a mix of siliceous plankton, calcareous plankton, and detrital clay. Rocks fitting the field description of dolomite or chert plot at the points of the ternary plot, only the purest siliceous or calcareous sediments became transformed into chert or dolomite (Fig. 18). Any sediment that contained more than about 10 weight percent detrital clay, evolved into calcareous or siliceous shale. These shale rocks have fissility and retain high porosity, and tend not to fracture. The presence of 10 weight percent clay is observed to be the dividing line that determines whether the rock is brittle or ductile (Fig. 19). Chert and dolostone are hard rocks that ring when hit with a hammer; siliceous mudstone, calcareous mudstone and claystone are soft rocks that dent when hit with a hammer; 10% clay appears to mark the dividing line.

TOC in Monterey shales often exceeds 5% and can exceed 25%. It is Type II marine kerogen. These shales record very slow sediment accumulation rates where organic carbon and phosphate became concentrated in the sediment. The high porosity, high clay content, and high TOC content in Monterey shales result in low rock strength and ductile behavior (Fig. 20).

The stress applied to Monterey rock layers comes from tectonic compression that is ultimately related to transpression along the San Andres transform-fault system. The strain ellipse shows what happens when a circle is stressed and undergoes strain into an ellipse. The system of fractures observed in Monterey outcrops shows the direction of the maximum compressive stress, which is horizontal compression. The fractures are arranged in very orderly patterns that can be predicted from the shapes of folds visible on seismic lines, and the directions of horizontal wells can be oriented to intersect an optimal number of fractures (Fig. 21).

To summarize the Monterey Formation, it contains layers of fractured and non-fractured rock because diagenesis has reduced porosity in original low-clay calcareous and siliceous sediments, leading to brittle behavior. In contrast, mudstones with high clay and kerogen content are ductile and do not fracture. Tectonic compression results in brittle fracture of hard rocks and ductile deformation of soft rocks.

Fractures in the Slave Point Formation

The story of brittle and ductile rocks isn't just limited to zones of tectonic compression. Middle Devonian dolostones of the Slave Point formation in Alberta contain a range of different facies types interlayered with one another, that include both brittle and ductile rocks (Fig. 22). The Slave Point Formation consists largely of dolostone, but there are differences in clay content from layer to layer within the sequence. Argillaceous dolostones (Fig. 23) show wispy stylolites that record significant compaction and plastic flow of more-clay-rich layers with the result that all vertical compaction results in ductile deformation. In contrast, pure dolostone layers do not show ductile deformation. In the examples on the right of Figure 23, large fractures have formed in pure dolostone cores. All the fractures in these pure dolostones can be traced into stylolites. As stylolites formed, the brittle dolostone became flexed due to uneven dissolution on the stylolite surface. The pure dolostone could not deform by plastic flow, it could only fracture. The greatest principal stress is gravity, oriented vertically. Vertical stress formed the horizontal stylolites, and the vertical fractures. Similar stylolite-fractures are present in rocks of all ages, wherever

stylolites are present in brittle rocks (Nelson 2001). Look for these fractures whenever you see stylolites in brittle rocks.

Summary and Conclusions

In summary: (1) Brittle versus ductile behavior is defined by the Unconfined Compressive Strength test. (2) Brittle rocks have well-defined physical properties. (3) Rocks in any layered sequence may have different rock strengths, high-strength hard layers in the sequence will fracture while soft layers will not. (4) Interlayered chert, dolostone, and organic shale comprise the mechanical stratigraphy of the Monterey Formation; hard layers are brittle and soft layers are ductile. Hard layers consist of nearly pure silica or nearly pure dolomite; only 10% clay leads to ductile behavior. (5) Horizontal compression related to transpression along the San Andreas Fault system applied stress to the Monterey Formation in Southern California. (6) Gravity loading applied vertical stress to Devonian dolostones of the Slave Point Formation in Alberta.

The ultimate conclusion for both the Miocene Monterey Formation of California and the Devonian Slave Point Formation of Alberta is that if brittle rocks are subjected to stress, they will fracture. Interlayers of fractured and non-fractured rocks record differences in mechanical properties within the rock successions.

References

- ASTM. 2010. Standard test method for compressive strength and elastic moduli of intact rock core specimens under varying states of stress and temperatures: American Society for Testing and Materials Designation: D 7012-10, p. 1-8.
- Baker PA, Burns SJ. 1985. Occurrence and formation of dolomite in organic-rich continental margin sediments: American Association of Petroleum Geologists v. 69, p. 1917–1930.
- Baker PA, Kastner M. 1981. Constraints on the formation of sedimentary dolomite: Science v. 213, p. 214–216.
- Behl RJ, Garrison RE. 1994. The origin of chert in the Monterey Formation of California (USA): Proceedings of the 29th International Geological Congress, Part C, A. Ijima, A., Abed, and R. Garrison (eds), Utrecht, p. 101-132.
- Behl RB. 1999. Since Bramlette (1946): The Miocene Monterey Formation of California revisited: Geological Society of America Special Paper 338, p. 301-313.
- Behl RB. 2012. The Monterey Formation of California: New Research Directions: AAPG Search and Discovery Article #10435.
- Blake GH. 1981. Biostratigraphic relationship of Neogene benthic foraminifera from the southern California outer continental borderland to the Monterey Formation: in Garrison, R.E., Douglas, R.G., Pisciotto, K.E., Isaacs, C.M. and Ingle, J.C. (eds.), The Monterey Formation and

Related Siliceous Rocks of California: Pacific Section, Soc. Econ. Paleontologists and Mineralogists, p. 1-13.

Burns SJ, Baker PA. 1987. A geochemical study of dolomite in the Monterey Formation, California: *Journal of Sedimentary Petrology* v. 57, p. 128–139.

Claypool G, Threlkeld C. 1983. Anoxic diagenesis and methane generation in sediments of the Blake Outer Ridge, Deep Sea Drilling Project Site 533, Leg 76, in R. Sheridan, F. Gradstein, et al. *Initial Reports of the Deep Sea Drilling Project*, v. 76, p. 391-402.

Compton JS. 1991. Porosity reduction and burial history of siliceous rocks from the Monterey and Sisquoc Formations, Point Pedernales area, California: *Geological Society of America Bulletin*, v. 103, p. 625-636.

Deere DU, Miller RP. 1966. Engineering Classification and Index Properties for Intact Rock: USAF Technical Report no. AFWL-TR-16-116 (this can be found by copying this reference into Google Search).

Dunham JB, Blake GH. 1987. Guide to coastal outcrops of the Monterey Formation of Western Santa Barbara County, California: Pacific Section, Society of Economic Paleontologists and Mineralogists, Book 53, p. 1-36.

Dunham JB, Cotton ML. 1990. Lithology of the Monterey Formation in the Western Santa Maria Valley Field, Santa Maria Basin, California: *Society of Economic Paleontologists and Mineralogists Core Workshop* v. 14, p. 203-243.

Dunham JB, Watts N. 2017. Moldic Pore Distribution, Basement Paleotopography, and Oil Production from a Devonian dolostone reservoir, Peace River Arch, Western Canada: *Society of Economic Paleontologists and Mineralogists Special Publication 109* (in press).

Garrison RE, Kastner M, Zenger DH (eds). 1984. Dolomites of the Monterey Formation and Other Organic-Rich Units: Pacific Section, Society of Economic Paleontologists and Mineralogists, 215 p.

Hoek E, Brown T. 1997. Practical estimates of rock mass strength: *International Journal of Rock Mechanics and Mining Sciences*, Vol 34, No 8, 1997, p. 1165-1186.

Isaacs CM. 1980. Diagenesis in the Monterey Formation examined laterally along the coast near Santa Barbara, California: Stanford University, Ph.D. dissertation, 329 p.

Isaacs CM. 1981a. Porosity reduction during diagenesis of the Monterey Formation, Santa Barbara coastal area, California. In Garrison, R. E., and R.G. Douglas, eds., *The Monterey Formation and Related Siliceous Rocks of California*. Pacific Section Society of Economic Paleontologists and Mineralogists, p. 257-271.

Isaacs CM. 1981b. Field characterization of rocks in the Monterey Formation along the coast near Santa Barbara, California: Guide to the Monterey Formation in the California Coastal Area, Ventura to San Luis Obispo, Pacific Section American Association of Petroleum Geologists Volume 52, p. 39-53.

Laubach SE, Olson JE, Gross MR. 2009. Mechanical and fracture stratigraphy: American Association of Petroleum Geologists Bulletin, v. 93, p. 1413-1426.

Liang W, Zhang C, Gao H, Yang X, Xu S, Zhao Y. 2012. Experiments on mechanical properties of salt rocks under cyclic loading: Journal of Rock Mechanics and Geotechnical Engineering, v. 4, p. 54-61.

Machel HG, Mountjoy EW. 1986. Chemistry and environments of dolomitization – a reappraisal: Earth Science Reviews, P. 23, p. 175-222.

Machel HG, Mountjoy EW. 1987. General constraints on extensive pervasive dolomitization and their application to the Devonian carbonates of Western Canada: Bulletin of Canadian Petroleum Geology, v. 35, p. 143-158.

NEH. 2017. National Engineering Handbook Part 631, Chapter 4, Engineering Classification of Rock Materials: <https://directives.sc.egov.usda.gov/viewerFS.aspx?id=3848>

Nelson RA. 2001. Geologic Analysis of Naturally Fractured Reservoirs, 2nd ed.: Gulf Professional Publishing, Houston Texas, 332 pages.

Smart KJ, Ofoegbu GI, Morris AP, McGinnis RN, Ferrill DA. 2014. Geomechanical modeling of hydraulic fracturing: Why mechanical stratigraphy, stress state, and pre-existing structure matter: American Association of Petroleum Geologists Bulletin, v. 98, p 2237-2261.

Sone H, Zoback MD. 2013a. Mechanical properties of shale-gas reservoir rocks – Part 1: Static and dynamic elastic properties and anisotropy: Geophysics, v. 78, p. D381-D392.

Sone H, Zoback MD. 2013b. Mechanical properties of shale-gas reservoir rocks – Part 2: Ductile creep, brittle strength, and their relation to the elastic modulus: Geophysics, v. 78, p. D393-D402.

Suess E, von Huene R. 1988. Site Reports, Ocean Drilling Program Leg 112, Sites 679 through 688 initial reports: http://www-odp.tamu.edu/publications/112_IR/112ir.htm

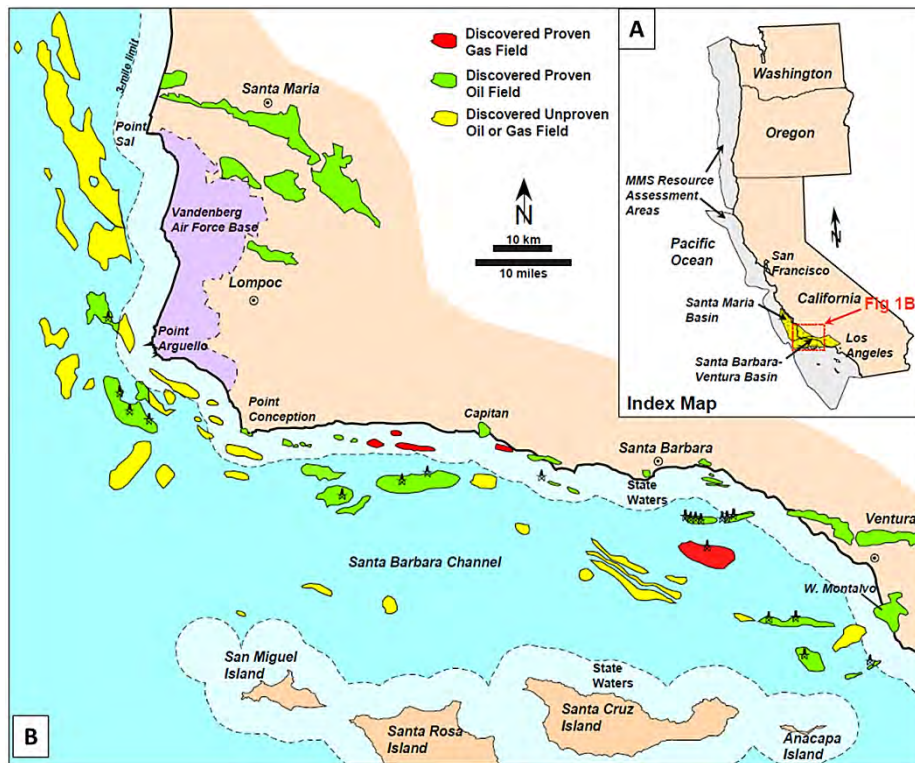


FIG. 1. – **A)** Index map showing location of Santa Maria and Santa Barbara – Ventura Basins in Southern California. **B)** Oil and gas fields sourced from the Miocene Monterey Formation. Reservoir rocks to the west of Santa Barbara are fractured Monterey Formation dolostone and chert; reservoirs to the east are mostly Pliocene sands of the Pico and Repetto Formations.

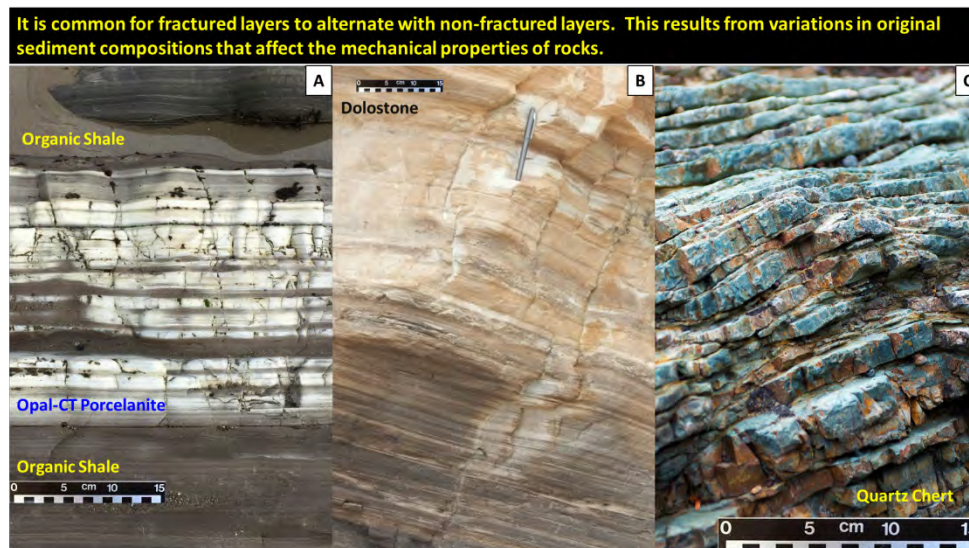


FIG. 2. – Monterey Formation outcrops from coastal Santa Barbara County, California. **A)** Non-fractured organic-rich claystone intercalated with fractured Opal-CT porcelanite. **B)** Fractured dolostone underlain by non-fractured organic claystone. **C)** Very hard, very brittle, glassy quartz chert.

- The first studies of the Mechanical Properties of rocks came from the field of Engineering Geology as applied to problems with construction of buildings, bridges, tunnels, and dams.
- Initial work was based on experience based on trial and error. When errors occurred, they had big effects.



FIG. 3. – “Weak” rock layers that put engineering projects at risk; failures like these led engineering-geologists to propose formal definitions and classifications of rock strength.

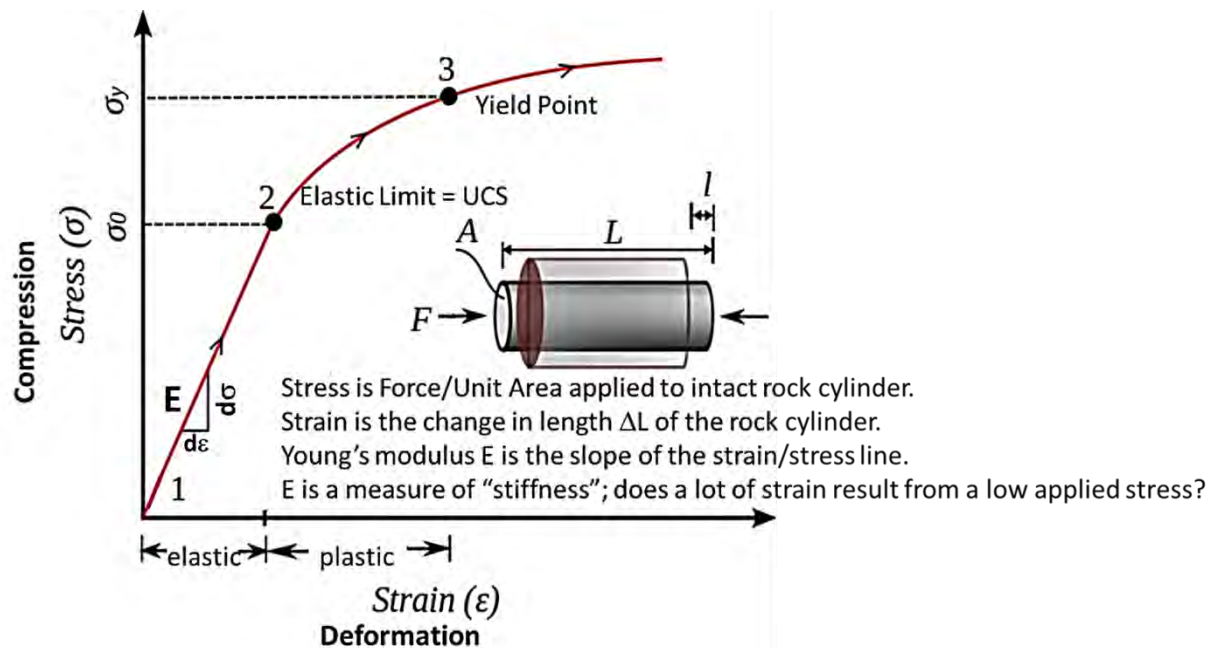


FIG. 4. – Strength classification of rocks is based on the Uniaxial Compressive Stress test, where an unconfined rock cylinder is squeezed, and a stress-strain plot shows how much deformation takes place per each unit of applied stress (ASTM 2010).

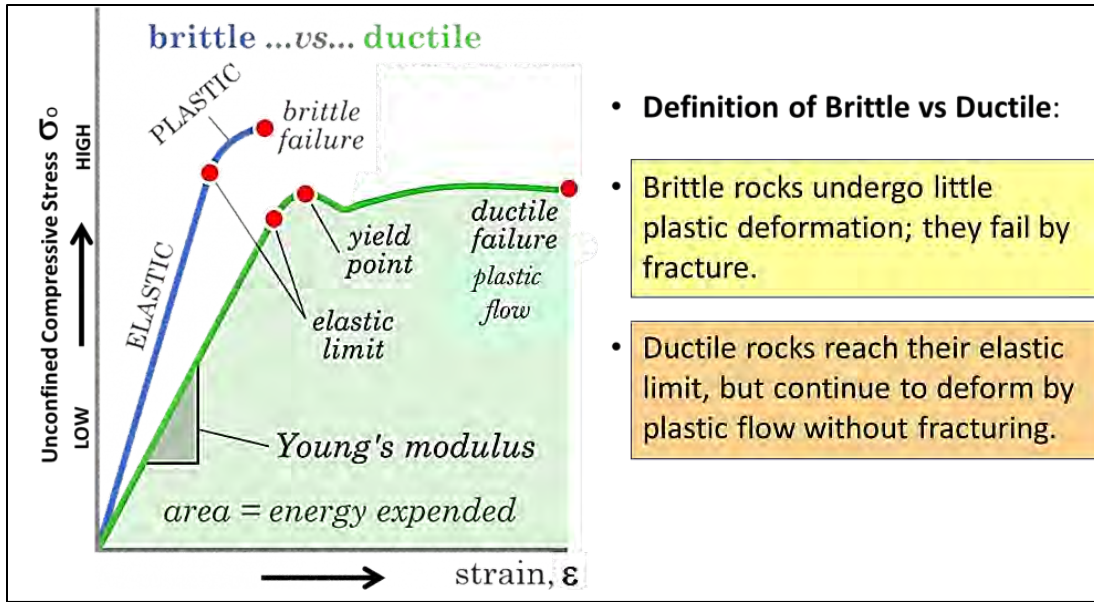


FIG. 5. – A brittle rock is shows little plastic deformation during a Uniaxial Compressive Stress (UCS) test. A ductile rock shows major plastic deformation during a UCS test.

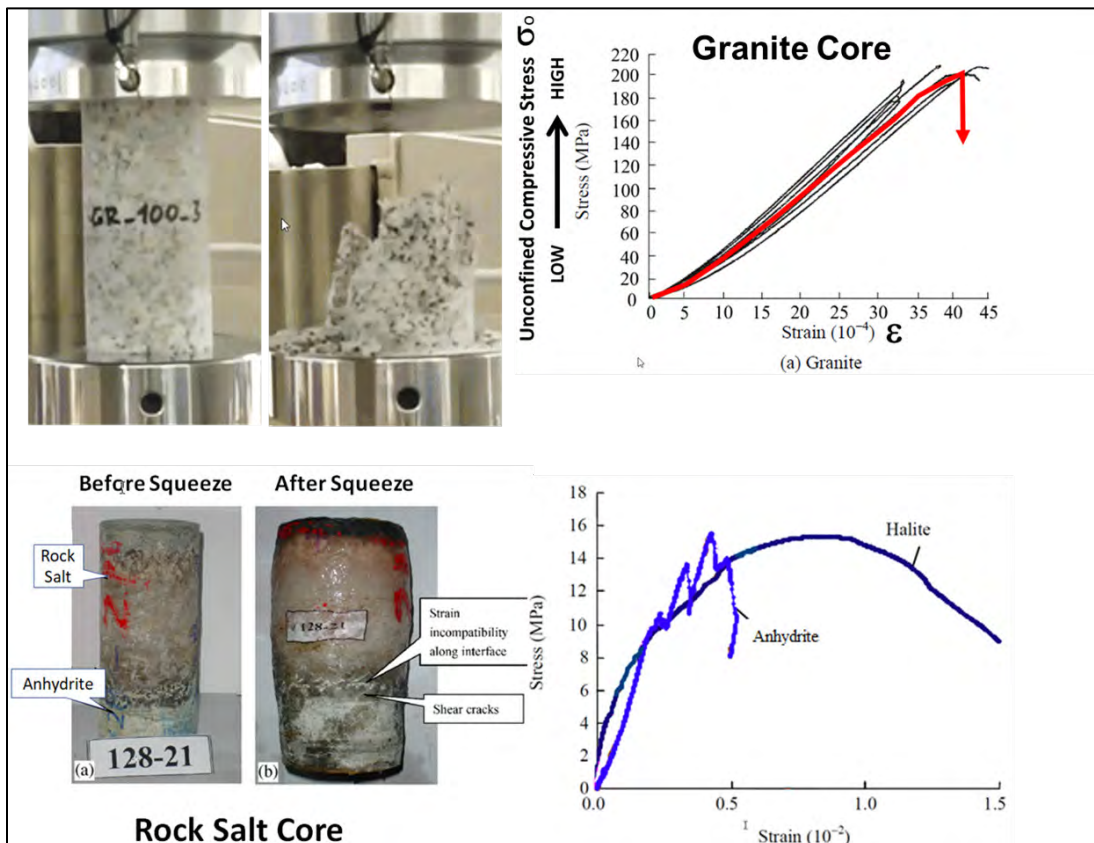
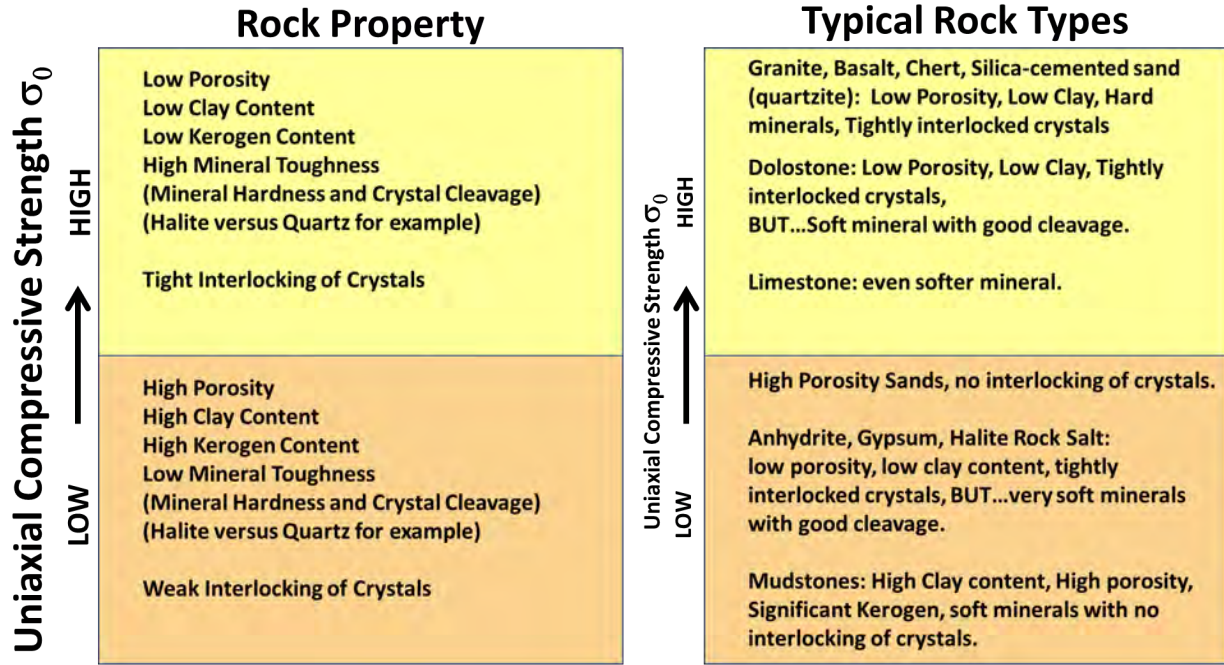


FIG. 6. – Classic comparison of brittle versus ductile rock. **A)** Granite core showing little plastic deformation prior to shattering at its yield point. **B)** Rock Salt core subjected to UCS test shows major plastic deformation without formation of fractures (modified from Liang et al. 2012).



(Deere and Miller, 1966; Hoek and Brown, 1997; Nelson, 2001; Sone and Zoback, 2013)

FIG. 7. – Specific properties determine whether a rock has low or high compressive strength. Rocks with high strength tend to be brittle, while low-strength rocks tend to be ductile.

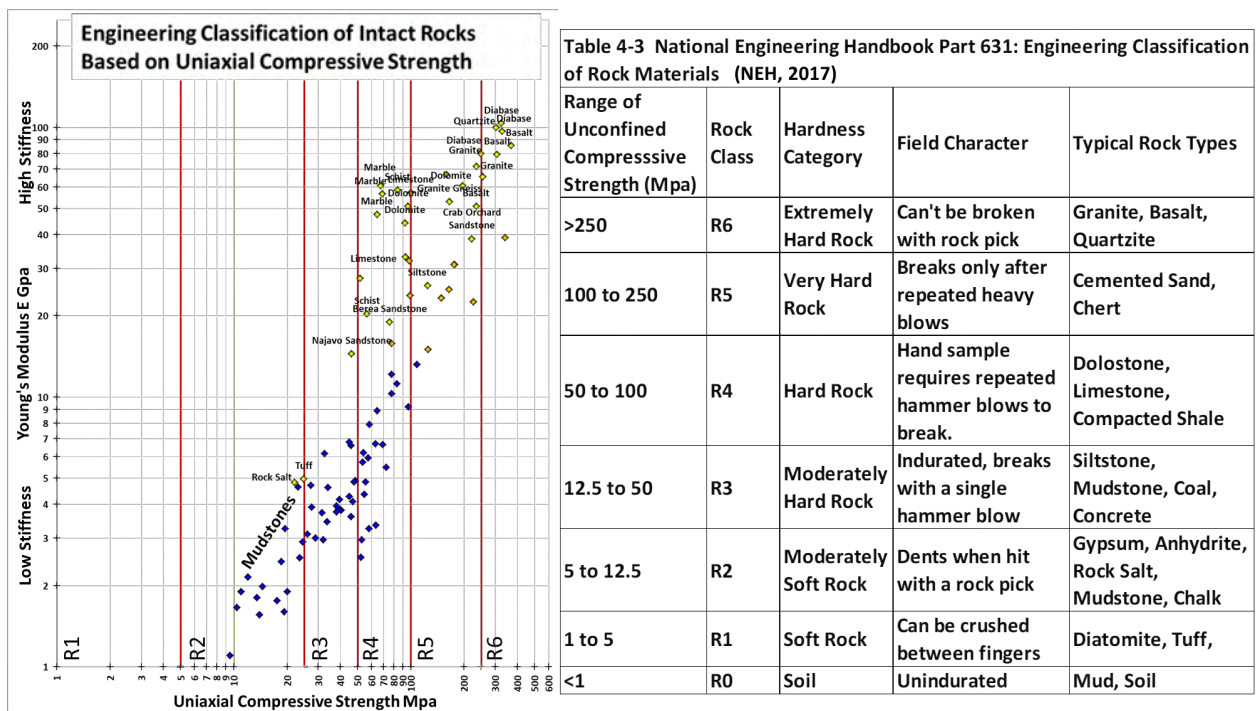


FIG. 8. – National Engineering Classification of Rocks based on Unconfined Compressive Strength (NEH 2017).

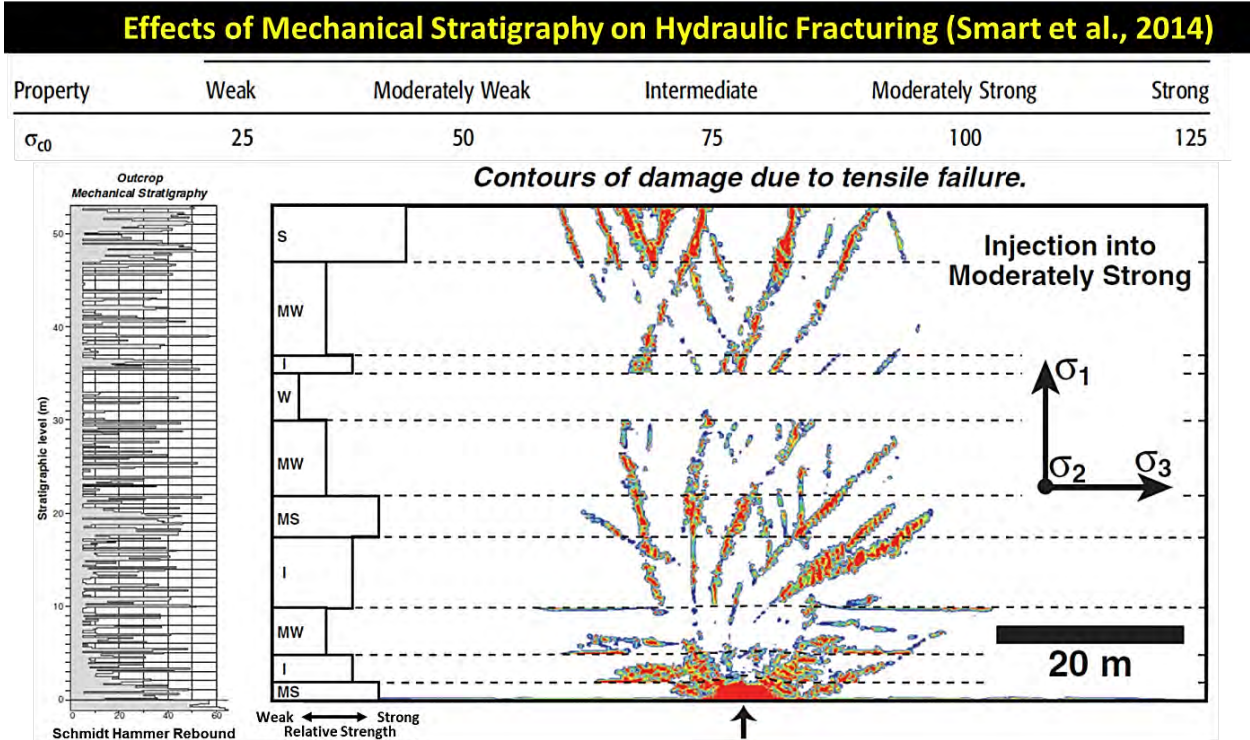


FIG. 9. – Predicted pattern of fracturing in layers of rock with different mechanical strengths; model interprets that few to no fractures will form in rock layers with low mechanical strength (modified from Smart et al. 2014).

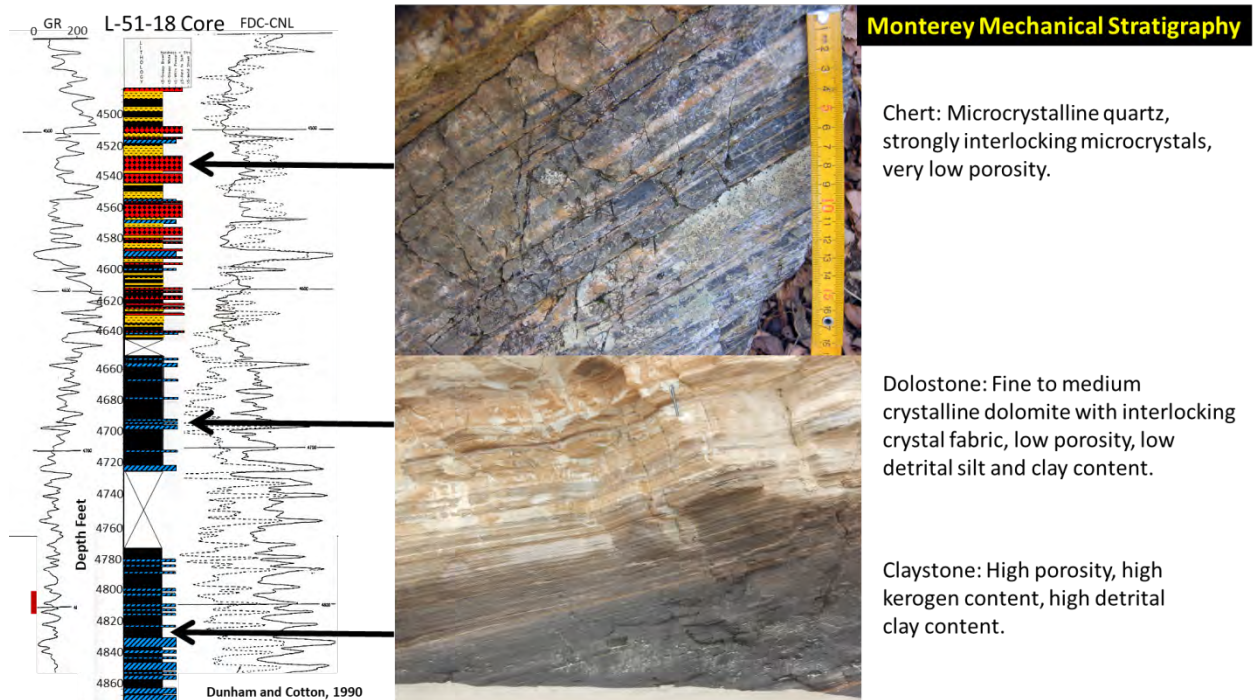


FIG. 10. – Mechanical stratigraphy of the Monterey Formation includes brittle cherts and dolostones interlayered with ductile organic-rich claystones. L-51-18 well (Western Santa Maria Valley Field) shows scale of interlayered beds.

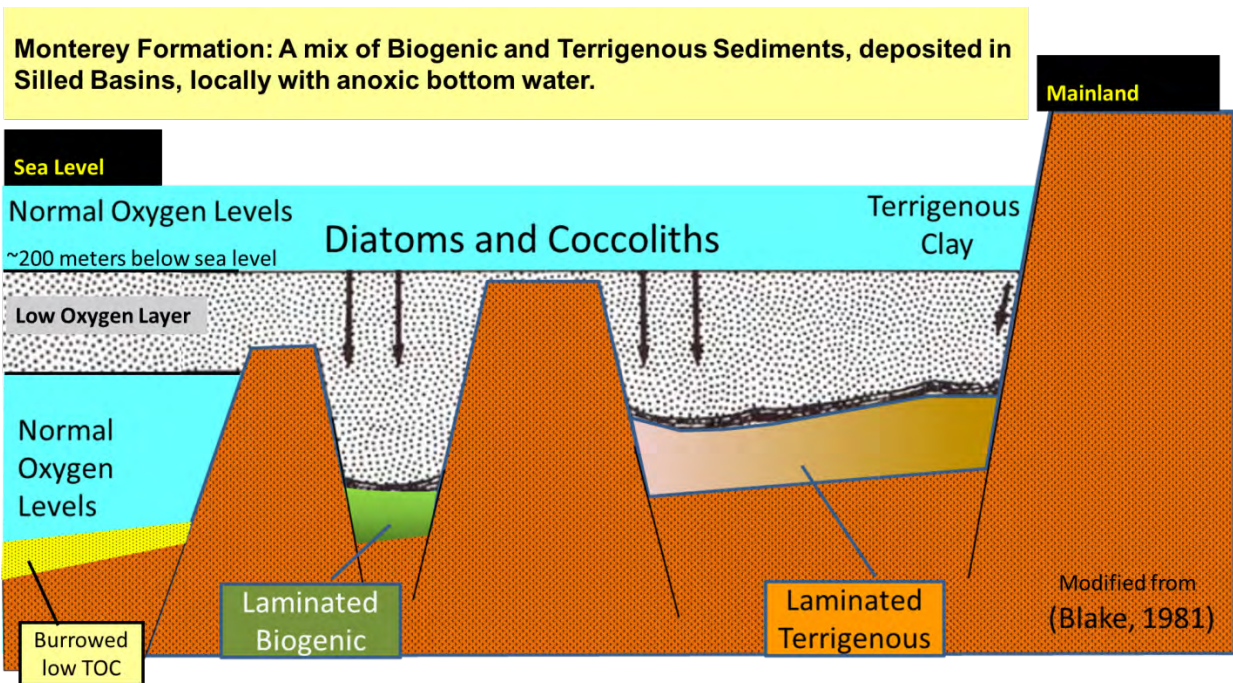


FIG. 11. – Monterey rocks formed through burial diagenesis of mixed terrigenous and biogenic sediments.

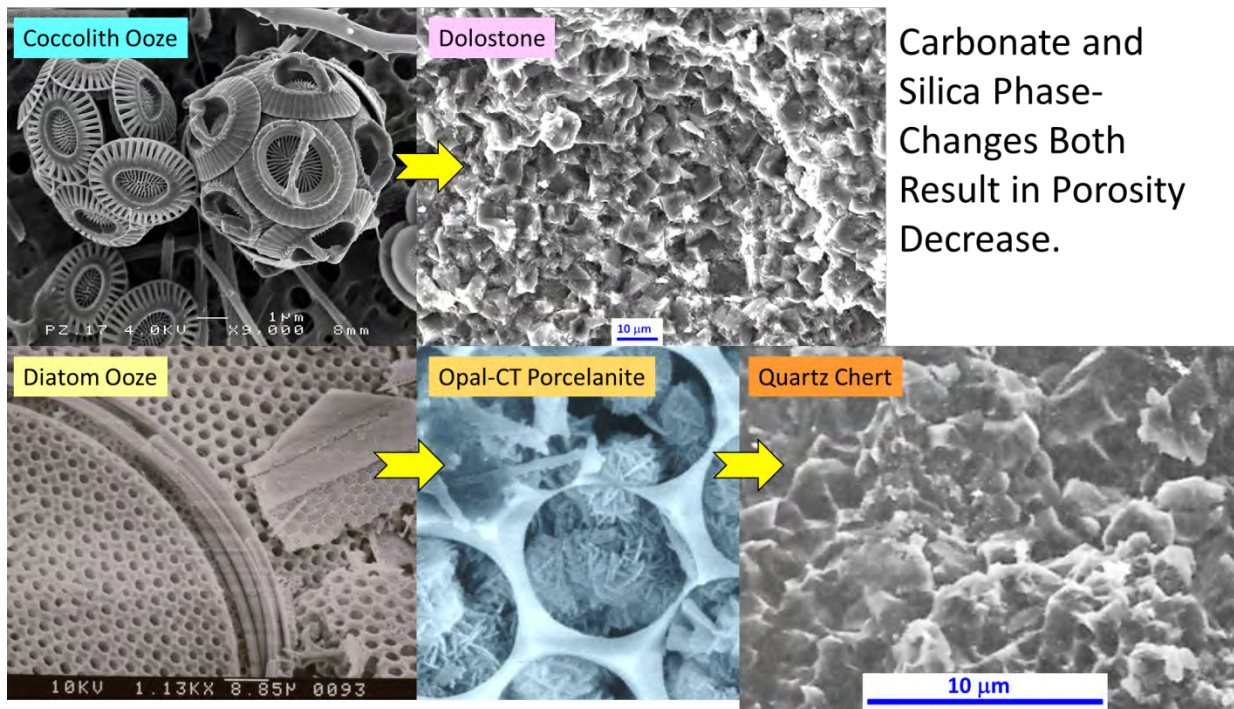


FIG. 12. – Calcareous nanoplankton dissolved and re-precipitated as microcrystalline dolomite; siliceous plankton dissolved and re-precipitated initially as opal-CT microcrystals and eventually as quartz microcrystals. In both cases, original high-porosity sediment evolves into low porosity rock.

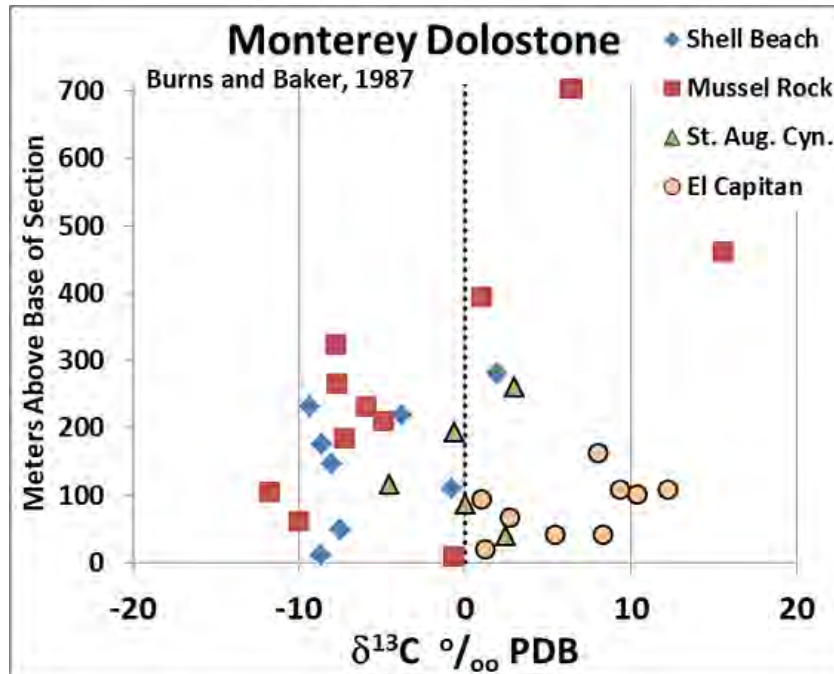


FIG. 13. – Monterey dolostones show the Carbon isotopic signatures of bacterial metabolism. Sulfate-reducing bacteria led to strong negative values while methanogenic bacteria produced strong positive values (Garrison et al. 1984, Burns and Baker 1987).

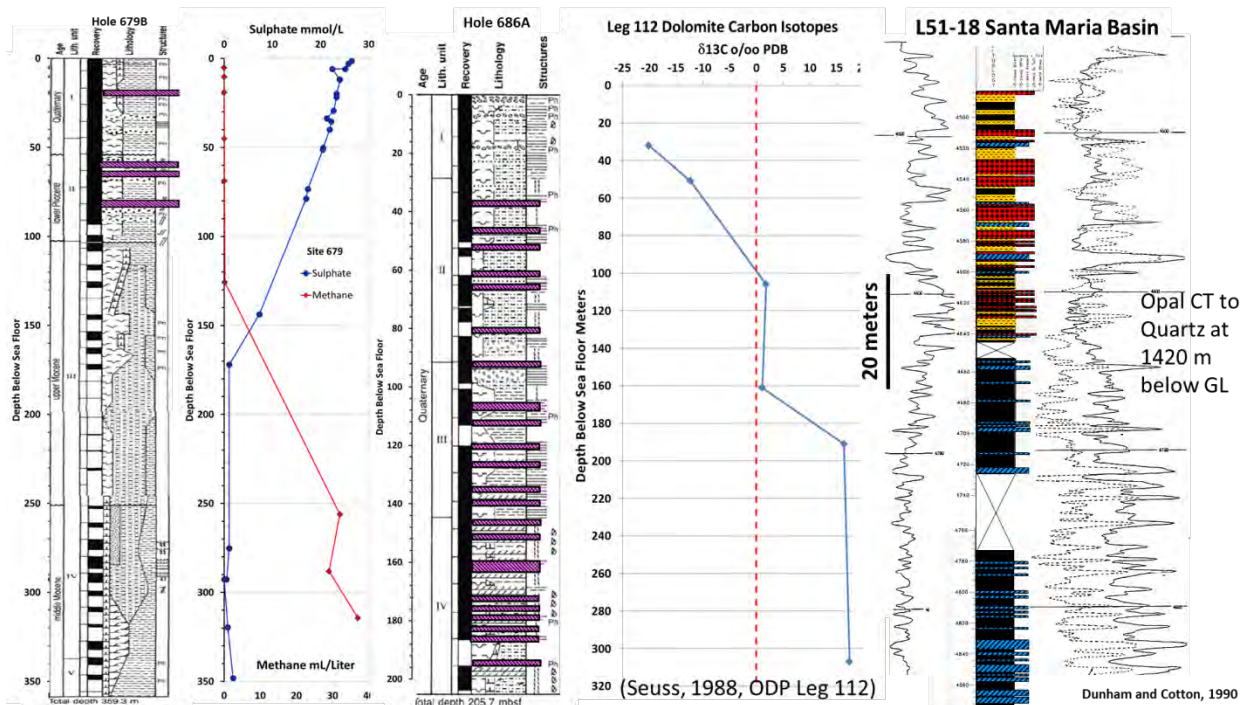


FIG. 14. – ODP Leg 112 cores from Peru had pore waters that showed the effects of both sulfate-reducing bacteria and methanogenesis (Suess et al. 1988). The thickness and vertical distribution of these early-diagenetic bacterial dolostones (purple layers) is similar to dolostones (blue layers) observed in Monterey cores (Dunham and Cotton 1990).

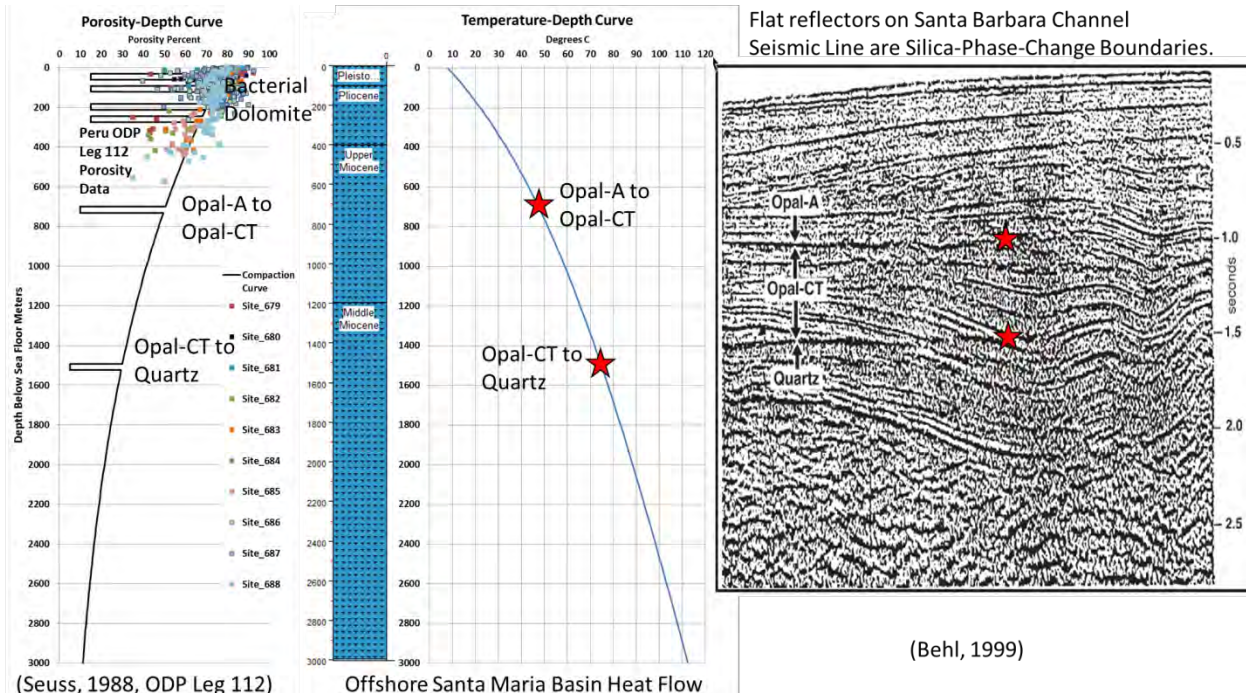


FIG. 15. – Original biogenic sediment has very high porosity, in the range of 70 to 80% or more (Seuss 1988). Normal compaction will reduce porosity on a typical exponential compaction curve, but in Monterey sediments, dolomite-replacement produces hard layers at shallow depth while temperature-controlled silica phase changes produce low-porosity layers at greater depths.

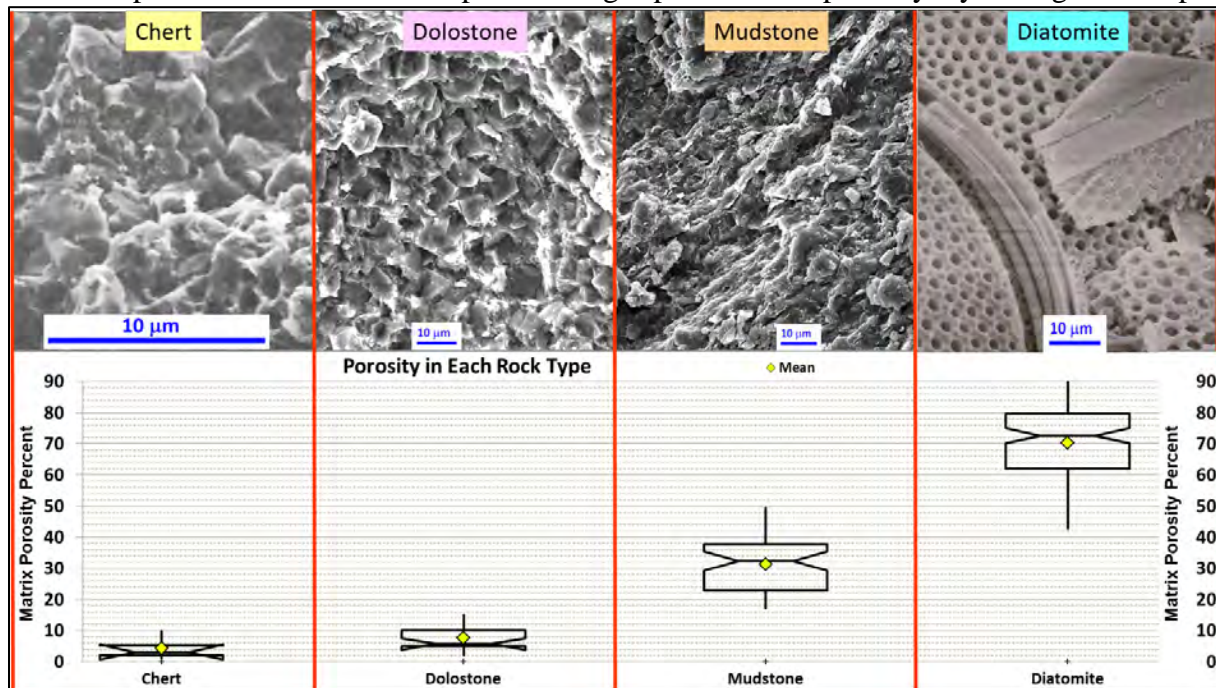


FIG. 16. – Notched-Box plots showing porosity distribution in Monterey rock types. Original 70%-plus porosity biogenic sediment evolves during burial into three different basic rock types: 1) Mudstone is a mix of terrigenous clay and biogenic plankton, it follows a normal-compaction trend during burial. 2) Dolostone is composed primarily of microcrystalline dolomite with very low porosity. 3) Chert is composed primarily of microcrystalline silica with very low porosity.

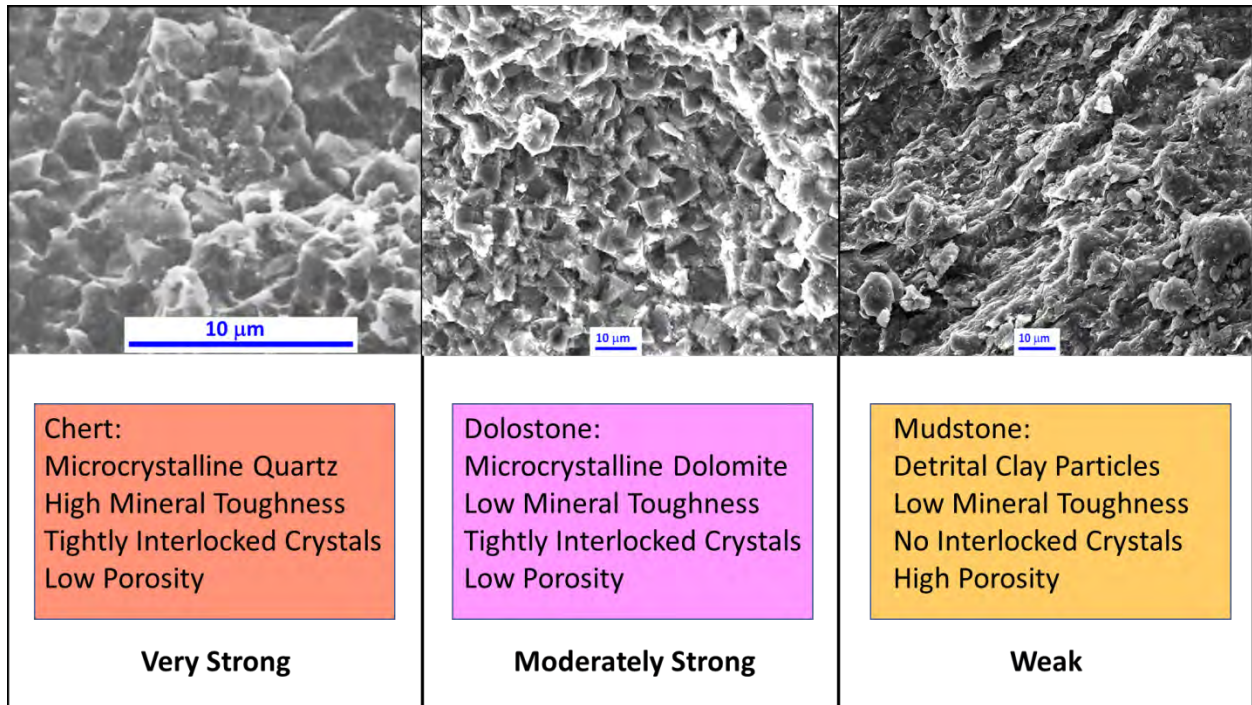


FIG. 17. – Mechanical properties of these rocks derive from specific physical properties.

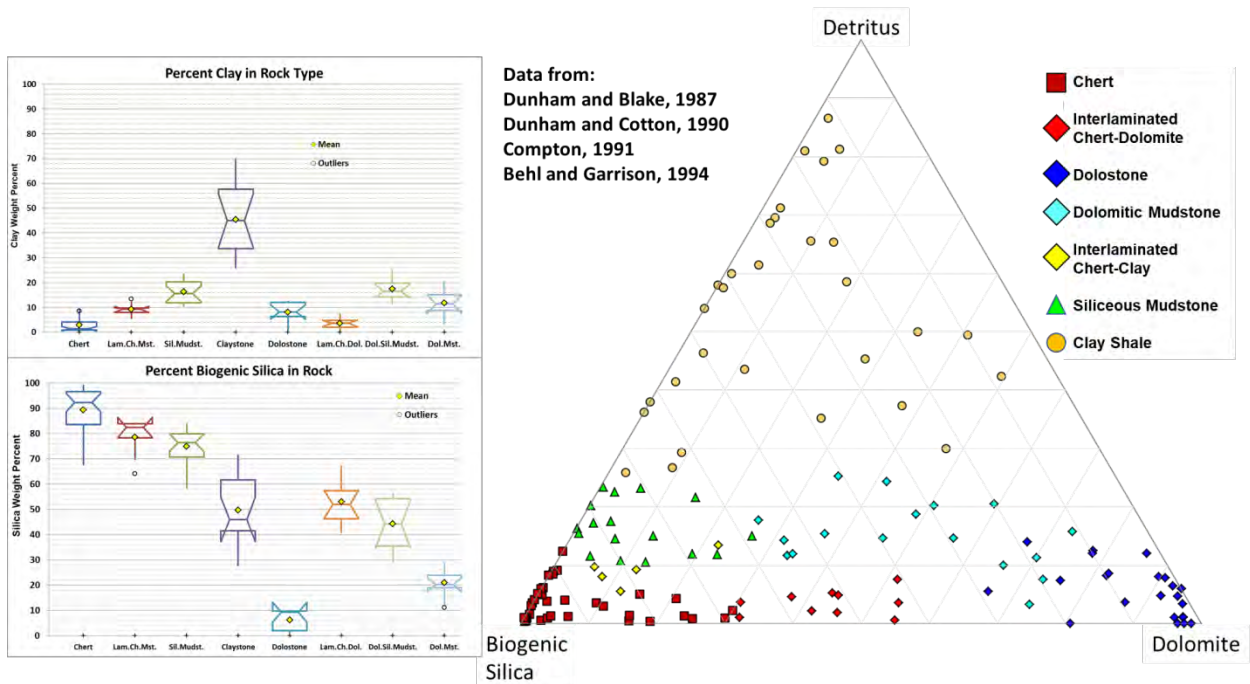


FIG. 18. – Chert and dolostone are brittle rocks while clay shale, dolomitic mudstone, and siliceous mudstone are ductile rocks. Chemical analysis shows that only very pure biogenic sediments evolve into brittle rocks. All rocks with more than 10 weight-percent clay are ductile rocks.

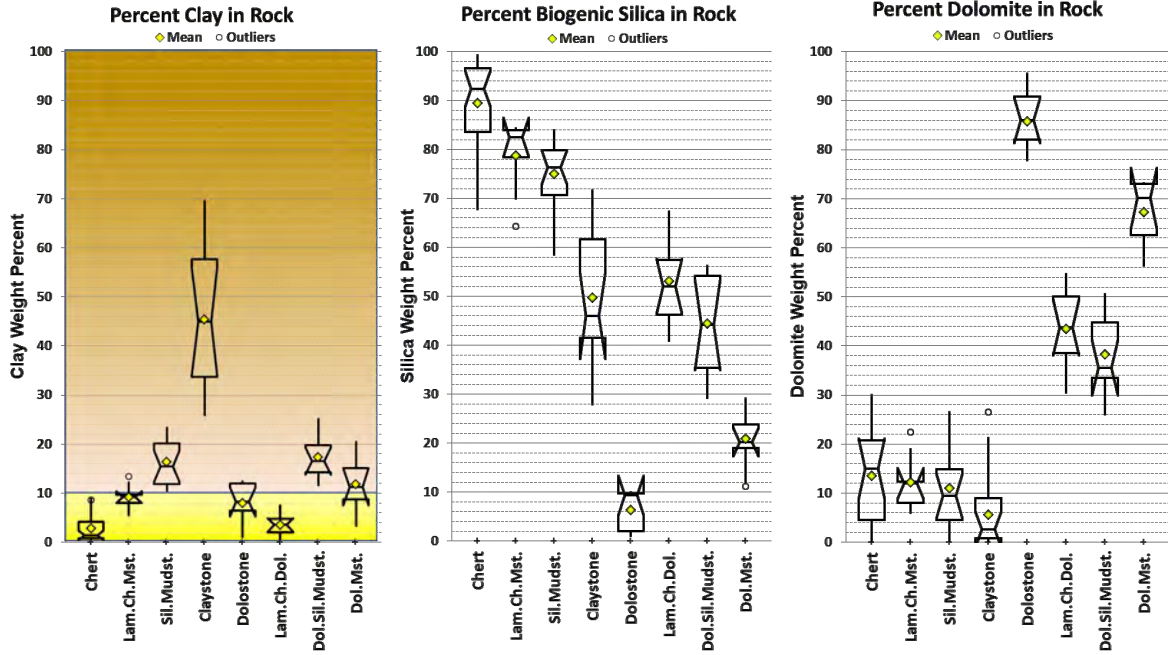


FIG. 19. – Ten weight-percent clay is the dividing line that separates brittle rock from ductile rock.



TOC in Monterey Shales ranges from 5% to over 25%. High Kerogen Content correlates with low strength.

High Porosity and High Clay Content in Monterey Shales correlate with low strength.

FIG. 20. – Layers with high porosity, high clay content, and high kerogen content make up the non-fractured layers within Monterey mechanical stratigraphy. Faults may cut and offset shale layers, but all fractures in mudstones will close shut due to ductile plastic-flow. Only hard, non-ductile rocks maintain open fractures.

- Fractures in the Monterey Formation formed through tectonic compression.
- When subjected to horizontal compression, brittle layers became fractured while ductile layers underwent plastic flow.
- The result is that heavily fractured dolomite and chert layers alternate with non-fractured calcareous and siliceous mudstones within the Miocene reservoir.
- Fractures comprise all of the effective porosity in Monterey Reservoirs in Point Pedernales field of the offshore Santa Maria basin, Central California.

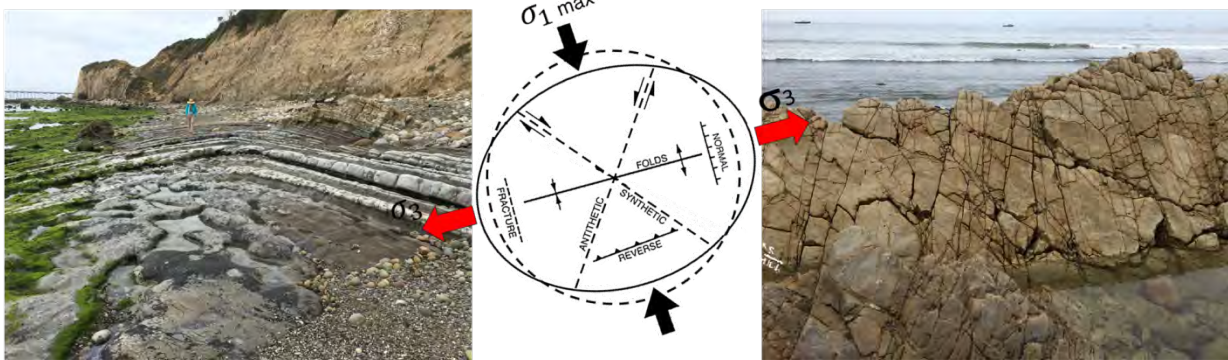


FIG. 21. – Tectonic compression applies horizontal stress to Monterey Formation rocks. Brittle rocks fracture, while ductile rocks undergo plastic flow without fracturing.

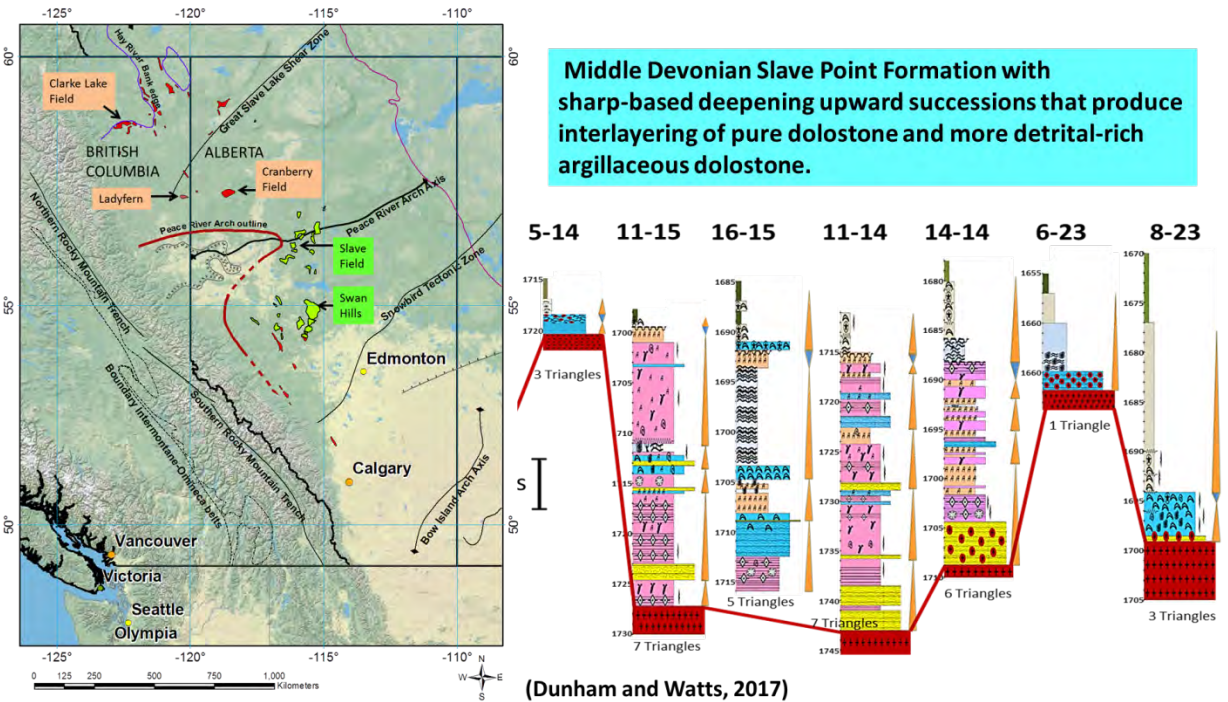


FIG. 22. – Brittle and ductile rocks are interlayered within the Devonian Slave Point formation of Alberta, Canada.



FIG. 23. – **A)** and **B)** Argillaceous dolostones show significant ductile deformation. **C)** and **D)** Pure Dolostones with low clay content do not show ductile deformation. Uneven flexing along stylolites produces brittle fractures. Gravity provides the greatest principal stress, which is vertical compression.

Evolution of a carbonate ramp and unconformity-related microporosity in the Mississippian Pekisko Formation, northern Alberta, Canada

Lauren Eggie*, Nancy Chow, and John Miller

*University of Manitoba, 66 Chancellors Circle, Winnipeg, MB, R3T 2N2. Canada

e-mail: lauren_eggie@hotmail.com

The Lower Mississippian (Tournaisian) Pekisko Formation in the Hawk Hills area of northern Alberta is 25 to 40 m thick and composed of massive skeletal–peloidal limestones with local shale beds. It hosts a large, medium to heavy-gravity oil resource that is presently being evaluated. The formation is interpreted to represent ramp development along the northern margin of the Peace River Embayment, an east-west oriented sub-basin of the pericratonic Prophet Trough that formed through reactivation of pre-existing northeast-southwest trending basement faults. Differential subsidence of strata overlying the fault system resulted in shifting depocenters within the embayment and strongly controlled depositional patterns during Pekisko time.

The Pekisko Formation can be subdivided into four informal units: the lower carbonate, lower shaly, upper carbonate, and upper shaly. These units comprise three lithofacies associations: (1) outer ramp–slope—argillaceous lime mudstones and crinoid wackestones; (2) outer ramp—crinoid–brachiopod wackestones and packstones; and (3) mid ramp—peloidal–skeletal packstones to grainstones. A variety of diagenetic features are present in the Pekisko Formation and are interpreted to have formed during marine, burial, and late meteoric diagenesis. Marine diagenesis was typified by significant micritization and microboring of allochems and limited radial-fibrous calcite cementation. Burial diagenesis resulted in neomorphism of micrite matrix and allochems, dissolution of gastropods and other allochems, syntaxial and coarse mosaic calcite cementation, and limited dolomitization. Late burial to meteoric diagenesis included dedolomitization, precipitation of fluorite, and development of pervasive microvuggy porosity of reservoir quality. Microvuggy porosity formed primarily via selective dissolution of micrite to microspar matrix and micritized allochems; the highest porosities developed in fine-grained peloidal–skeletal packstones of the mid ramp lithofacies association. It is proposed that minor dissolution began during late burial, when hot basinal fluids, introduced by tectonic activity, subsequently cooled and became corrosive. More significant and pervasive porosity development occurred during uplift and erosion of the succession during the formation of the post-Mississippian unconformity, when cool meteoric waters mixed with hot basinal fluids on a regional scale. The most porous intervals of the Pekisko Formation in the study area are located in a broad zone adjacent to the subcrop margin and extend approximately 30 km downdip. Reservoir intervals are 0.1–13.1 m thick, and are typified by 10–20% microvuggy porosity and 0.1–30 mD permeability. Although there are development issues to be addressed, the Pekisko Formation in the Hawk Hills area is an excellent unconventional reservoir, with significant potential for future exploitation.

Porosity in chalk

Ida Lykke Fabricius

Technical University of Denmark, Department of Civil Engineering, Section for Geotechnics and Geology, DTU Brovej, bygning 118, DK-2800 Kongens Lyngby, Denmark

e-mail: ilfa@byg.dtu.dk

Typical chalks from a North Sea Upper Cretaceous or lower Paleogene petroleum reservoir have depositional texture in the range from mudstone to wackestone, only sporadically packstone. The grains of the wackestones and packstones are typically 0.5 to 5 millimeter in size and can be microfossils, fossil debris and intraclasts. The calcitic mud particles are sometimes visibly biogenic, but in many cases recrystallized. They are typically 1 to 5 micrometer in size. In the pore space among these calcitic components, the chalk can contain diagenetically formed clay minerals and silica, both below 0.5 micrometer in size. The particle size distribution in chalk can be rather complicated caused by the mixing at two levels, but from a pore point of view, most chalks have rather narrowly defined pore size distributions with only minor contributions from larger intrafossil pores. Petrographic data, Nuclear Magnetic Resonance data, Mercury Injection Capillary Pressure data, He-porosimetry data and specific surface by Nitrogen adsorption data in combination indicate that on a centimeter scale, chalk pore space is homogeneous and well connected with no pore-throat effects. Permeability is in most cases around 1 milliDarcy and fall in the range 0.01 to 10 milliDarcy. Would we consider such a system microporous?

The diagenetic porosity development of chalk can be inferred, because these pelagic sediments are found in thick sequences on oceanic plateaus, where deposition has occurred continuously from the Cretaceous to Present. In the uppermost 200–300 meter below sea floor we find carbonate ooze, where porosity gradually decreases from around 70% to around 50% due to the load of the sediments, although the particles are in very poor contact in this interval. One reason for this is that the particles repel each other due to adsorbed ions. In order to overcome electrical repulsion a high contact load is required, so when the ooze indurates into chalk, the ooze particles are consequently subjected to an elastic strain of up to 0.5%. This is enough for calcite-contact pressure dissolution to take place and the early pore-stiffening cementation is found. This process leads elastic strain to drop drastically and the porosity remains close to 50% for the next up to 500 meter of burial. Before this depth, clays have dissolved and re-precipitated as stylolite-precursors and elastic strain has built up again to 0.3%. This is enough for pressure dissolution at stylolites which leads to porefilling cementation and marked decrease in porosity.

Micro-pore type controls on hydrocarbon displacement and recovery

Shawn Fullmer*, Stefaan Van Simaey, Benjamin Rendall, PJ Moore, Brian Kelley,
Antonio Buono, and Bo Gao

*Exxonmobil, 22777 Springwoods Village Pkwy, Spring, TX, 77389, USA

e-mail: shawn.m.fullmer@exxonmobil.com

Distinct types of micro-pore space have been well documented from limestones globally in both conventional and challenged carbonate reservoirs. Type I micro-pores are characterized by subhedral crystal textures that result in relatively uniform pore and pore throat size distributions and represent the upper end of porosity and permeability values for micro-pore dominated rocks. Type II/III micro-pores possess partial to fully fitted crystal textures that have pores and pore throat sizes smaller than those found in Type I micro-pores. Smaller pore sizes within Type II/III micro-pores result from increased cementation as evident by slightly larger crystal sizes, greater crystal interpenetration, 120 degree triple junctions where crystals have grown together into pore space. It is not uncommon to encounter the entire spectrum of micro-pore types within a single reservoir. Typically, Type I micro-pores are encountered in a crestal position of the field while Type II micro-pores are commonly more abundant, though not exclusive to, the flanks of the field. Type III micro-pores with fully fitted crystal textures are typically found in non-reservoir intervals or tight gas reservoirs. In large reservoirs with tall hydrocarbon columns micro-pores can contain significant volumes of hydrocarbons. Remaining oil saturation, as measured from centrifuge capillary pressure experiments, decreases as a function of total porosity from Type I to Type III in microporous reservoir rock types. The favorability of displacement within these lower quality microporous reservoirs is somewhat diminished relative to Type I microporous rocks. Stylolitic zones with Type III micro-pores exhibit the most advanced cementation history of the sample set and show the least favorable displacement behavior for micro-pore dominated limestones. In tight gas examples Type I microporous rock types produce higher cumulative gas volumes than Type II or III microporous rock types. These results have implications for asset valuation in challenged carbonate reservoirs and optimizing ultimate recovery in many large conventional reservoirs.

**Pore types and pore system characterization of the Late Devonian
Three Forks Formation, Williston Basin**

Beatriz Garcia-Fresca* and Bob Loucks

*Statoil Gulf Services, Austin, TX 77042, USA

e-mail: BEGAR@statoil.com

The Late Devonian Three Forks Formation of the Williston Basin has been estimated to contain 3.7 billion barrels of recoverable oil, doubling the estimate for the broader Bakken petroleum system. Pore system characterization and distribution is critical for the development of this unconventional resource, as it influences saturations, permeability and mechanical properties.

The Devonian was a predominantly warm and arid period, with the Williston Basin located in an equatorial position and affected by epeiric conditions and times of extensive marine restriction. The Three Forks accumulated during a period of isolation from the ocean, resulting in the accumulation of a mixed carbonate-siliciclastic succession in a playa-lake system. It was sporadically affected by large floods that covered the basin terrigenous sediment, debrite-like deposits with intraclasts, and resulted in widespread erosion. Floods were followed by a drying period when the deposition of the mineral sequence dolomite–anhydrite–halite in ponds distributed across the basin surface. Facies composed of different proportions of penecontemporaneous dolomite, clay, quartz, and anhydrite and a broad range of textures and fabrics. Sediment reworking and authigenic processes have also influenced Three Forks pore systems. Facies configuration resulting from playa-lake depositional system are expected to be relatively circular and concentric.

SEM-EDS characterization of Three Forks pore systems show a strong influence by depositional processes in terms of mineralogy, grain size and shape, and sediment reworking. Porosities range from 1–10% and seem to have a close relationship to facies and clay content. The pores as seen in AR-ion-milled samples show the predominant pore type to be intercrystalline pores between dolomite crystals that are subdivided by clay platelets producing nanopores. Other pores are intraparticle nanopores within clay platelets, formed by the bending and splitting of clay platelets during compaction.

Quantifying the dynamic behavior of multi-porosity systems in carbonates—challenges, perspectives and opportunities

Sebastian Geiger

Heriot-Watt University, Institute of Petroleum Engineering, Edinburgh, EH14 1AY,
United Kingdom

e-mail: s.geiger@hw.ac.uk

Carbonate reservoirs often contain multiple pore systems (e.g., micro-pores, macro-pores, stylolites, vugs, fractures) that span several orders of magnitude in scale, from microns to meters. Key engineering decisions that influence production from carbonate reservoir such as completion schemes, reservoir management strategies and enhanced oil recovery methods, require a rigorous understanding as to how such multi-scale pore systems control the fundamental dynamic behaviors. However, quantifying how multi-scale pore systems impact the dynamic behaviors of carbonate reservoirs, and how the resulting (average) dynamic behavior could be captured best in static and dynamic reservoir models, remains challenging. For example, microporosity can account for significant storage in carbonate reservoirs. Yet, it is difficult to estimate how easily hydrocarbons move from the less permeable micropores to the more permeable macropores from where they can flow towards a well, and how variations in wettability and pore-structure influence the exchange between micro- and macro-pores. Similarly, many carbonate reservoirs contain natural fractures, which cause bypassing of hydrocarbons that are left behind in the less permeable rock matrix. Quantifying the transfer of hydrocarbons from the rock matrix to the fractures while accounting for gravity and capillary forces as well as heterogeneity in matrix permeability and wettability remains challenging. At the log-scale, vugs, cracks, stylolites and other heterogeneities impact flow. But since these features are often larger than the size of a typical plug, it is difficult to quantify their contribution to fluid flow in routine core or special core analysis. This presentation will review some of the recent modelling and experimental approaches that enable us to quantify more robustly how multi-scale pore systems interact with each other, starting at the pore-scale to investigate the links between micro- and macro-porosity, continuing to the log-scale to integrate different macroscopic heterogeneities, and finishing at the gridblock or inter-well scale to incorporate fracture systems. Using different real-life examples, it will be illustrated how these approaches impact oil-in-place estimates and influence our understanding of key dynamic behaviors. This understanding offers new opportunities for reservoir engineers and geoscientists alike to improve our ability to forecast hydrocarbon production from multi-porosity carbonate reservoirs.

Sedimentologic influences on pore evolution and porosity–permeability trends in oolitic grainstones

Hamilton M. Goodner*, Eugene C. Rankey, and Chi Zhang

*Kansas Interdisciplinary Carbonates Consortium, University of Kansas,
Lawrence, KS 66045, USA

e-mail: ham.goodner@ku.edu

Complex carbonate pore networks can arise from variable depositional textures and subsequent diagenetic modifications. Although general trends in porosity-permeability (ϕ - k) relationships within carbonates are well documented, if and how pore evolution and ϕ - k scatter relate to depositional texture (i.e., grain type, size, and sorting) remains poorly constrained. To address this uncertainty, this study compares oolitic grainstones with a spectrum of grain size and sorting, and from a range of diagenetic histories. This approach provides insights into how pore attributes (i.e., size and spatial distributions, geometries) and ϕ - k quantitatively change in response to varied sedimentologic attributes.

NMR T_2 relaxation curves from samples of different geologic ages illustrate relations between sedimentologic attributes and pore networks. For unconsolidated (Holocene, Bahamas) sediment, volumetrically dominant pore size is related to grain size distribution—coarser, better sorted sediment favors larger pores. In addition, relaxation curves are unimodal, reflecting the dominant interparticle pores. In contrast, samples which are sedimentologically similar, but impacted by early diagenesis (Pleistocene, Bahamas), include more complex relaxation curves. Many include multimodal pore-size distributions; macro-porosity modes occur at smaller relaxation times and have smaller amplitudes than unconsolidated samples, and >50% of porosity in some samples is derived from micro- and meso-porosity ($T_2 < 125$ ms, $d_p < 10$ μ m). These results are interpreted to reflect decreased macro-pore size related to early cementation of interparticle pores, and increased abundance of micro- and meso-pores from partial dissolution of ooids, consistent with petrographic observations.

As examples of more advanced diagenesis, Pennsylvanian and Mississippian reservoirs capture potential pore network end-members: Pennsylvanian oolites are dominated by oomoldic pores formed by dissolution of aragonitic ooids, whereas Mississippian oolites are dominated by interparticle pores (grains preserved due to originally calcitic mineralogy). These differences manifest in petrophysical parameters, such as distinct ϕ - k trends: for a given porosity, permeability of Pennsylvanian oolites are commonly 3–4 orders of magnitude lower than those of Mississippian examples. Furthermore, quantitative pore geometries extracted via digital image analysis (DIA) illustrate Pennsylvanian oolites generally exhibit rounder (γ) and simpler (PoA) pores than Mississippian oolites with comparable grain size.

Although these reservoirs differ fundamentally in pore type, geometry, and connectivity, their pore-size distributions (i.e., NMR T_2 curves) can be surprisingly similar, commonly exhibiting high-amplitude peaks within the macro-porosity range and small contributions from micro- and meso-porosity. These observations suggest that pore-size distribution is not a unique control on

permeability. Instead, the geometry and spatial arrangement of pores also are likely important. Patterns of the spatial distribution of pores explored through lacunarity provide a metric to describe the “gappiness” of pores and pore networks. After normalizing to mitigate effects of total porosity, data reveal that Mississippian oolites generally exhibit lower lacunarity (i.e., less clumping) of pores than Pennsylvanian examples, suggesting oolites with evenly distributed pores are likely to have higher connectivity, and thus, greater permeability.

At a larger scale, comparing pore attributes in samples with varied grain size and sorting across diagenesis reveals trends. Independent of diagenetic history, coarser, better sorted sediment or strata include less variable pore-size distributions than finer, poorer sorted samples. Nonetheless, pore type, shape, and connectivity and total porosity clearly can vary, along with permeability, as shaped by both deposition and diagenesis.

This study systematically evaluates sedimentologically similar samples across different diagenetic scenarios (pre-diagenesis, early diagenesis, moldic pores, or interparticle pores), facilitating conceptual models for the potential “evolution” of pore networks in oolitic grainstones. This approach provides insights into how sedimentologic attributes control original pore networks and influence subsequent modifications of those pores. With a knowledge of sedimentologic trends within an oolite, this study facilitates an enhanced understanding and prediction of possible ranges of pore network variability within analogous reservoirs.

Effect of bioturbation on the porosity and permeability of shelf carbonates: Examples from the Middle to Upper Jurassic Tuwaiq Mountain and Hanifa Formations, central Saudi Arabia

Stephen T. Hasiotis*, Hassan Eltom, Eugene Rankey, and Dave Cantrell

*University of Kansas, 1475 Jayhawk Blvd., rm 120 Lindley Hall, Lawrence, KS 66045, USA

e-mail: hasiotis@ku.edu

Shallow to deeply penetrating bioturbation by epibenthic and endobenthic organisms on carbonate shelves can alter the original depositional fabric of carbonate sediments, effectively increasing the overall porosity and permeability in multiple intervals. To explore its impact, this project examines ubiquitous bioturbation throughout outcrops of the Middle and Late Jurassic Hanifa Formation, Saudi Arabia. Specific patterns are evident within high-frequency sequences (HFS) composed of stacks of spiculitic, skeletal–peloidal, coated grainstone, stromatoporoid–coral, and foraminiferal cycles. Ichnodiversity overall is high, including the trace fossils *Asterosoma*, *Chondrites*, *Cylindrichnus*, *Conichnus*, *Diplocraterion*, *Helminthopsis*, *Lockeia*, *Ophiomorpha*, *Palaeophycus*, *Phycosiphon*, *Planolites*, *Schaubcylindrichnus*, *Scolicia*, *Skolithos*, *Teichichnus*, *Thalassinoides*, and *Zoophycos*. Borings in reworked cobble-sized pieces of hardground include *Entobia* and *Gastrochaenolites*. In general, each facies and facies association within the cycles had an ichnofabric index (ii) from nonbioturbated (ii1) to completely bioturbated (ii6). Most important was the occurrence of laterally extensive (>5 km) *Glossifungites* Ichnofacies, which represent firmgrounds with ii4–6 and record discontinuity surfaces that form HFS boundaries. These *Glossifungites* Ichnofacies are composed of complex and deep three-dimensional (3D) burrow networks of *Thalassinoides* in mud-dominated lithofacies filled with peloids, skeletal grains, and coated grains. These 3D burrow networks typically penetrate the entire unit thickness, providing permeability pathways in an otherwise less permeable medium, and interconnects more permeable units above and below firmgrounds. In a few stratigraphic levels, however, the 3D burrow networks of *Thalassinoides* in grain-dominated lithofacies are filled with fine-grained sediment, which reduces permeability. Recent studies on the permeability produced by trace fossils, including those that compose the *Glossifungites* Ichnofacies, have demonstrated a two to four orders of magnitude greater permeability in bioturbated zones vs. nonbioturbated zones, consistent with these interpretations. Research to date on the upper-most units of the underlying Tuwaiq Mountain Formation and the overlying Jubalia Formation show similar ichnodiversity, but trace fossils are larger. The boundary between the Tuwaiq Mountain and Hanifa formations is delineated by rhizoliths and paleosols that overprint marine deposits, evident in both outcrop and core. Boundaries that contain pedogenic modification will likely act as a barrier to flow by reducing permeability. Determining the lithofacies and trace-fossil associations in these underlying and overlying formations can be used to delineate their boundaries in core and used to understand the petrophysical characteristics that result from bioturbated and pedogenically modified carbonate fabrics.

Ichnological, sedimentological, and petrophysical characteristics of bioturbated Pleistocene carbonate shoreface strata: Implications for reservoir quality and development

Stephen T. Hasiotis*, Alexa R. Goers, and Eugene C. Rankey

*University of Kansas, Department of Geology, 1475 Jayhawk Blvd., rm 120, Lindley Hall
Lawrence, KS 66045, USA

e-mail: hasiotis@ku.edu

Ichnologic and sedimentologic variability of Pleistocene and modern shoreface deposits on the leeward margin of Crooked-Acklins Platform, southern Bahamas, illustrate how porosity can be impacted by spatial variability of bioturbation intensity and trace-fossil associations that correspond to regional changes in depositional energy conditions. Foreshore and upper shoreface strata comprise nonbioturbated (ii_1) to thoroughly bioturbated (ii_6) ichnofabrics dominated by deposit-feeding structures with few filter-feeding and dwelling structures. Ichnofabrics have low diversity and limited connectivity. Strata exhibit cryptobioturbation with few discrete burrows. Original depositional textures and physical sedimentary structures appear preserved, yet petrographic analysis reveals textural variations indicative of cryptobioturbation. Burrows include subtle changes in cementation and grain distributions, with fill that is less sorted, with looser grain packing and considerably less cement than the host rock. Primary porosity is occluded partially by meniscus and mosaic clear calcite cement, as well as isopachous and pore-lining fibrous and dogtooth cement, resulting in net porosity of 11–28%. Host-rock cement stratigraphy shows multiple stages of cementation and partial dissolution, resulting in highly variable cement distribution. Upper to lower shoreface strata with or without patch reefs have very high intensity of bioturbation, with diverse vertical, horizontal, and boxwork burrow systems, and cryptobioturbation. Burrows contain poorly sorted, loosely packed peloid fill, surrounded by a halo of interparticle calcite cement. Ichnofabrics exhibit deep tiering and greater burrow connectivity, with cryptobioturbation that destroys primary physical structures, resulting in $ii_{\geq 5}$. Burrows in thin section exhibit drastic differences in cement and preserved porosity compared to the well-cemented host rock, with interparticle porosity partially to completely occluded by blocky calcite cement and micritic cement with net porosity of 3–20%. Porosity and spot-permeability data show that ichnofabric-associated textural variability drives petrophysical heterogeneity, with porosity and permeability varying up to three orders of magnitude. Foreshore strata permeability averages 9089 mD, compared to 6245 mD for cryptobioturbated ichnofabrics. Upper to lower shoreface cryptobioturbated strata permeability averages of only 141 mD. Highly porous and permeable (>5000 md) grainstone units are associated with ichnofabrics with discrete traces. Porosity is highest within burrow interiors, and CT scan data shows that burrow morphology and connectivity influence flow pathways that increase petrophysical heterogeneity. In contrast, facies with cryptobioturbation ichnofabrics ($ii_{\geq 3}$) exhibit a narrower range of porosity and permeability (ϕ - k) than those with $ii_{\leq 3}$. Cryptobioturbated ichnofabrics exhibit $K_{min}:K_{max}$ ratios of 7 and 10, respectively, compared to a value of 92 for ichnofabrics with discrete traces.

Understanding how carbonate micropores affect the Iowa Pore Index method for evaluating crushed carbonates for use as highway aggregate

Franciszek Hasiuk*, Muhammad Firdaus Ahmad Ridzuan, Evelyn K Hussey, and M. Robert Dawson

*Iowa State University, 2237 Osborn Dr, 253 Science I, Ames, IA 50011-1027, USA

e-mail: franek@iastate.edu

The Iowa Pore Index (IPI) test is a method employed by several State Departments of Transportation in the Midwestern US to determine the volume ratio of macropores-to-micropores in a crushed rock by means of water intrusion. IPI has been used in conjunction with x-ray diffraction (to measure purity of dolomite) and x-ray fluorescence (to measure clay content) to predict the durability of carbonate rocks when used in highway pavements. Despite the utility of this method, it has not been established how the IPI compares to more traditional petrophysical methods like helium and mercury porosimetry or how the IPI is affected by specific textural qualities (e.g., pore types, Dunham textures). Paleozoic carbonates from around Iowa were collected that represented end-members of the test parameters (IPI, XRD, XRF). Individual crushed rock pebbles from each sample were characterized quantitatively via helium and mercury porosimetry and qualitatively via thin section. We found that each sample of crushed rock consisted of at least visually distinct three rock types that were also distinct in thin section. When weighted by rock type abundance, helium porosity showed a strong correlation with Total IPI ($R^2 = 0.80$) and Macropore IPI (intrusion volume after 1 minute, $R^2 = 0.76$). Micropore IPI (intrusion volume after 15 minutes) shows a strong positive correlation with rock-type weighted porosity in limestones ($R^2 = 0.73$) and a weak negative correlation with rock-type weighted porosity in dolostones ($R^2 = 0.39$). Limestones with porosity less than 7% correlated with long lasting pavements, as are dolostones with greater than 13% porosity. Micropore IPI is inversely correlated with median pore throat radius and pore performing aggregates are correlated with rock-type weighted incremental mercury intrusion curves with abundant pore throats in the 0.03-0.1 μm range. Grainier limestones tend to have a lower micropore IPI, whereas muddier rocks had higher micropore IPI. Comparing samples from quarry walls with crushed rock showed that crushing had little to no effect on helium porosity, mercury pore throat size distribution, or petrographic texture. This suggests that IPI values can be predicted using the strong correlations identified in this study combined with 1) analyses of core material rather than crushed rock stock piles or 2) literature information for which IPI analyses are not available. This reduces the time it would take to evaluate the quality of a potential resource as well as reducing the need to sample unstable quarry walls.

Dedolomitization of primary dolomicrites in a carbonate–sulphate system and implications for porosity evolution

Tyler E. Hauck*, Hilary J. Corlett, Matthias Grobe, Erin L. Walton, and Pierre Sansjofre

Alberta Geological Survey - Alberta Energy Regulator, 402 Twin Atria Building, 4999 98 Ave.,
Edmonton, Alberta, T6B 2X3, Canada

e-mail: tyler.hauck@aer.ca

The Givetian Prairie Evaporite Formation of northeastern Alberta has experienced extensive dissolution of evaporite minerals at the basin margin along the tapering edge of the Phanerozoic sedimentary succession. Evaporite dissolution has resulted in a prominent halite dissolution scarp within the Prairie Evaporite Formation, followed eastward by a zone of less soluble sulphates, and finally a zone of insoluble residues (brecciated shales and carbonates). Regionally extensive primary dolomicrite beds (marker beds) internal to the Prairie Evaporite succession display evidence for westward down-dip flow of meteoric waters derived from the basin margin that were responsible for the dissolution of evaporite minerals. Meteoric diagenesis has resulted in partial to complete dedolomitization of the marker beds. Elevated $\text{Ca}^{2+}/\text{Mg}^{2+}$ ratios necessary for dedolomitization have been facilitated by dissolution of encasing anhydrites, which also show meteoric influence through gypsification at the margins of the marker beds, especially where dedolomitization has occurred. Along with stratigraphic considerations, stable isotope analysis supports the interpretation of shallow dedolomitization of micritic dolomites driven by meteoric waters derived from the basin margin. Negative $\delta^{18}\text{O}$ and $\delta^{13}\text{C}$ values (averages of -13.6‰ VPDB and 0.5‰ VPDB, respectively) of the dedolomite compared with the primary dolomicrite values (-6.0‰ VPDB and 1.2‰ VPDB) point to isotopically light diagenetic fluids. Reported dedolomite textures from other studies are varied, but the most prevalent are rhombic textures interpreted to result from the partial to complete pseudomorphic replacement of secondary dolomite rhombs that have formed in the burial diagenetic realm. In our study, no prior aggrading neomorphism resulting in secondary rhombic fabrics is recognized in any of the primary crypto- to finely crystalline dolomicrites. However, dedolomitization has resulted in sutured to loosely packed mosaics of calcite that range from subhedral to distinctly euhedral rhombic crystal fabrics. An assessment of porosity in the marker beds reveals a significant decrease in intercrystalline porosity in dedolomite compared to the primary dolomicrite. Whereas good porosity in the primary dolomicrite results from the dissolution of pore-occluding sulphates, porosity reduction in the dedolomite results from a reintroduction of sulphate phases in addition to the larger molar volume of calcite. The low porosity in the dedolomites may be explained by a relatively recent dedolomitization event involving subglacial meltwater recharge.

Pore topology and rock physical properties of microporosity in Lower Cretaceous carbonate sediments: insights from X-ray CT imaging

Cathy Hollis*, Aisha Al Hajri, Nathaly L. Archilha, Marco Ceia, Michael Lacey, Peter Lee, Sam McDonald, and Roseane Missagia

*University of Manchester, Williamson Building, Oxford Road, Manchester M13 9PL, UK

e-mail: cathy.hollis@manchester.ac.uk

Introduction

Micropores (i.e., pores <30 μm diameter) are volumetrically the most important pore type in many Cretaceous sediments, comprising >50%, and often >80%, of the total pore volume. There is considerable uncertainty as to the capacity of microporosity to store and flow hydrocarbon, and little data to assess the importance of pore shape, size and connectivity on recovery efficiency. This partly reflects the limitations of technology to image and characterise micropore topology.

This study focuses upon a large, multiscale dataset of X-ray CT images of 23 samples from Brazil, the Arabian Plate (both Lower Cretaceous) and the North Sea (Upper Cretaceous). The samples include skeletal peloidal pack–grainstones, four of which are pervasively cemented, skeletal wackestones and mudstones/Chalk. This has allowed a unique overview of micropore topology in three dimensions. Interparticle microporosity occurs between grains and/or within grains that have undergone boring and micritisation. Micropores have been diagenetically altered by recrystallization (neomorphism) of primary micrite, which has increased crystal size and decreased micropore volume and connectivity. Conversely, solution enhancement of micrite has enhanced micropore volumes and connectivity.

Methods

Total porosity was determined on core plugs (25 mm diameter) for each sample using helium porosimetry. Permeability was measured on the same plugs by nitrogen gas intrusion. For a subset of samples, mean pore throat radius was calculated from mercury injection capillary pressure. Macroporosity was quantified from thin sections, prepared from core plug offcuts of all samples, by either modal or image analysis. Petrographic analysis also allowed qualitative description of macropore type, genesis and timing.

X-ray CT scanning of 23 samples was conducted using the Custom Bay, XRadia MicroXCT and NanoXCT scanners at the Manchester X-ray Imaging Facility (MXIF) at University of Manchester. A subset of samples underwent high resolution scanning using high energy synchrotron beamlines at the Swiss Light Source, Zurich, and Diamond Light Source, Oxford. Samples were prepared from core plug offcuts as ~ 1 mm diameter sticks of variable length, and imaged areas were selected to be ~ 1 mm³. 3D reconstructed data were filtered, binarised and pore geometry was quantified using Avizo software. Porosity was extracted and quality controlled against core analysis and modal analysis data. Maximum voxel size was ~ 1 μm ,

except for two samples scanned using the NanoXCT scanner, where a 64 nanometer resolution was achieved on two ~65 μm diameter samples. From the extracted pore network, the following parameters were calculated, as per Archilha *et al.* (2016):

- Aspect ratio: the ratio of the minor to major pore lengths
- Specific surface area (SSA): the ratio of total pore surface area to total pore volume. SSA usually increases as pore complexity increases
- Pore shape factor (γ): if $\gamma=1$, then the pore is a sphere, whilst $\gamma > 1$ indicates the pore is flattened. γ is calculated from the SSA of a single pore, normalised to a sphere, i.e.

$$\gamma = \frac{2}{3} \left(\frac{A_s \pi}{V} \right)^{1/3} \sqrt{\frac{6}{9\pi^2 V}}$$

A_s = surface area, V = pore volumes

- Tortuosity (τ): ratio of the length of the fluid path via the pore network compared to the straight line distance between end points
- Dominant pore size: the value of the uppermost pore radius of which 50% of the image is composed (i.e. the dominant pore radius, in μm)
- Co-ordination number: average number of pore throats connected to 1 pore (i.e. the ratio of the total number of pore throats to the number of pores in the sample)

Results

Of the 23 samples analyzed, 9 were oolitic and peloidal grainstone and 2 were mudstone (Chalk). The remainder were skeletal peloidal packstones and wackestones. Helium porosity ranged from 16.3–35.6% (mean = 25.4%) and permeability from 0.24–602 mD (arithmetic mean = 49.6 mD, geometric mean = 7.24 mD). There is no relationship between helium porosity and permeability, or between total microporosity and permeability (Fig. 1A, B).

X-ray CT analysis (excluding the nanoXCT scans) resolved an average of 34.4% of the total pore volume (3.1–100%), with a higher volume of resolved porosity in samples with a larger dominant pore size ($r = 0.44$) and higher permeability ($r = 0.47$; Fig. 1C, D). Although some of these samples might comprise macropores that were not captured by the small size of scanned area, this demonstrates that many samples are dominated by porosity that is $<1 \mu\text{m}$ diameter. Dominant pore size ranges from 1–77 μm (mean = 28.2 μm) and is lowest in samples which have been pervasively cemented (Fig. 1C) and also have a high SSA (Fig. 2A). Samples with largest dominant pore size usually have higher permeability ($r = 0.47$; Fig. 1E). The two samples scanned using the NanoXCT have a dominant pore size of 0.26 μm (pore size range, 0.24–7 μm) and 2.10 μm (pore size range, 0.48–5 μm).

Pores that are $>1 \mu\text{m}$ have a mean aspect ratio of 0.57 (0.53–0.59) and a mean γ of 1.71 (1.18–2.91), consistent with a flattened morphology. The two samples scanned by nanoXCT have a modal aspect ratio of 0.6, slightly flatter than the $>1 \mu\text{m}$ pores measured in the same samples at lower resolution. The average co-ordination number of all pores $>1 \mu\text{m}$ is 2.04 (1.2–3.14), whilst tortuosity averages 4.9 (2.6–10.0). Co-ordination number is higher in samples with a greater volume of resolved porosity (i.e., a higher volume of porosity $>1 \mu\text{m}$; $r = 0.66$), but there is a negative relationship between co-ordination number and dominant pore size ($r = -0.48$).

Tortuosity increases with increasing specific surface area (mean = 259, 46.5–721 mm⁻¹; $r = 0.67$) and decreasing γ ($r = -0.55$). There is no relationship between permeability and co-ordination number ($r = -0.33$; Fig. 1F) or γ ($r = 0.003$), but there is a weak negative regression with tortuosity ($r = -0.40$). The two samples imaged using the nanoXCT have a very low volume of connected pores (2.2 and 7.0% of imaged pores).

Interpretation

Effective porosity

It is not possible from the results of this study to categorically calculate effective porosity, since the fluid type, charge history, hydrocarbon column height, wettability and reservoir pressure could all influence the ability of pores to store and flow hydrocarbon in the subsurface. However, <10% of the pores imaged using the nanoXCT (i.e., <1 μm diameter) were connected which, along with a moderate relationship between permeability and percentage of total resolved porosity and dominant pore size, implies that pores of <1 μm diameter are significantly less effective than porosity >1 μm diameter. Consequently, it is proposed that pores of >1 μm and <30 μm be considered as contributing to fluid flow and are better referred to as mesopores.

Importance of rock texture

Both primary rock fabric and diagenetic modification have a fundamental control on the shape, size and connectivity of porosity. Packstone and grainstone facies have $K_h > \sim 10$ mD and total porosity >20%, with up to 100% of that porosity resolved (i.e., >1 μm). Dominant pore size in these samples is >40 μm , specific surface area <250 mm⁻¹, and tortuosity <4. Lower permeability samples can be divided into two groups. Pervasively cemented packstones and grainstone ($K_h < 2$ mD) have lower volumes of total (<25%) and resolved porosity (<20% of total resolved pore volume), a very low dominant pore size (<20 μm) and high SSA (>500 mm⁻¹) compared to equivalent, less cemented pack/grainstones. Consequently, their ability to store hydrocarbon is limited and flow paths will be extremely tortuous (tortuosity is >6). Conversely, fine grained, muddy wackestones and mudstones have higher total porosity ($\geq 30\%$), although resolved pore volumes remain low (usually <30% of total porosity) and permeability is <5mD. Dominant pore size (<50 μm) and specific surface area (<200 mm⁻¹) are moderate, suggesting that they have some potential to store and flow hydrocarbon. As such tortuosity ($\tau > 4$) is higher than in weakly cemented pack/grainstones but lower than their cemented counterparts.

Controls on permeability

Permeability is not simply controlled by total pore volume or the volume of microporosity (Fig. 1A, B), and therefore pore topology and connectivity are also likely to be important controlling parameters. This was demonstrated by Archilla et al. (2016) who showed that dominant pore size is key parameter to the calculation of permeability, whilst knowledge of co-ordination number, aspect ratio, γ and tortuosity are also important. Average co-ordination number is <3 within pores >1 μm diameter, whilst most pores <1 μm are not connected. The decrease in co-ordination number with increasing dominant pore size, suggests that samples with the largest pore sizes might have fewer interpore connections than samples dominated by smaller pores, which could

create a channelized, fracture-like pore network. Since tortuosity is lower in samples with a lower SSA and higher γ , these shorter flow paths are probably facilitated by a simpler network of larger, flatter pores. The increase in co-ordination number as more pores are resolved (i.e., where there is a greater number of pores $>1 \mu\text{m}$) could reflect an increase in resolvable pore throat diameter or greater connectivity of mesopores (pores = 1–30 μm) compared to macropores (i.e., pores $>30 \mu\text{m}$).

Implications to hydrocarbon recovery

It is not possible from this dataset to unequivocally interpret the implications of the results to hydrocarbon recovery efficiency. Nevertheless, the highest permeability samples may not always have the most efficient recovery efficiency under two phase flow (e.g., Hollis et al. 2010) since gas permeability only measures the fastest flow path within the sample. The data from this study suggests that permeability is highest in samples with the largest dominant pore size, yet these pores appear to have a lower average co-ordination number and flatter pore shape. This lowers tortuosity, resulting in a faster, more direct flow path that will bypass smaller pores. These small pores may be well connected to each other but their small size means that they have a higher SSA which lengthens the flow path, and increases the tortuosity, within the sample.

Conclusions and Implications

Using high resolution X-ray CT analysis it has been possible to extract three-dimensional data pertaining to pore size, shape and connectivity on a range of Cretaceous samples from Brazil, the Arabian Plate and the North Sea. Micropores $>1 \mu\text{m}$ can be resolved, and appear to be well connected and capable of supporting flow. It is recommended that they be referred to as mesopores, and considered as effective porosity. Two nanoXCT scans suggest that micropores $<1 \mu\text{m}$ diameter have a relatively high aspect ratio (i.e., they are flatter than meso- and macropores) and are usually isolated, so are likely to be ineffective. All pores $>1\text{mm}$ have a narrow range of aspect ratio and pore shape factor, but in general the largest macropores are flatter and less well connected than mesopores, which are more rounded and have a higher SSA. Connectivity of these large, flatter pores potentially results in fracture-like behaviour that increases permeability but impedes recovery efficiency.

Acknowledgments

The authors would like to thank Agencia Nacional do Petroleo, Petrobras and Petroleum Development Oman for providing samples. The Manchester X-Ray Imaging Facility and beamtime award MT4017-1 (Diamond Light Source) and Swiss Light Source for access to facilities.

References

Archilha N, Missagia R, Hollis C, de Ceia M, McDonald S, Lima Neto I, Eastwood D, Lee P. 2016. Permeability and acoustic velocity controlling factors determined from X-ray tomography images of carbonate rocks. AAPG Bulletin, 100, 1289-1309.

Hollis C, Vahrenkamp V, Tull S, Mukherji A, Taberner C, Huang Y. 2010. Pore system characterisation in heterogeneous carbonates: an alternative approach to widely used rock-typing methodologies. *Marine and Petroleum Geology*, 27 (4), 772-793.

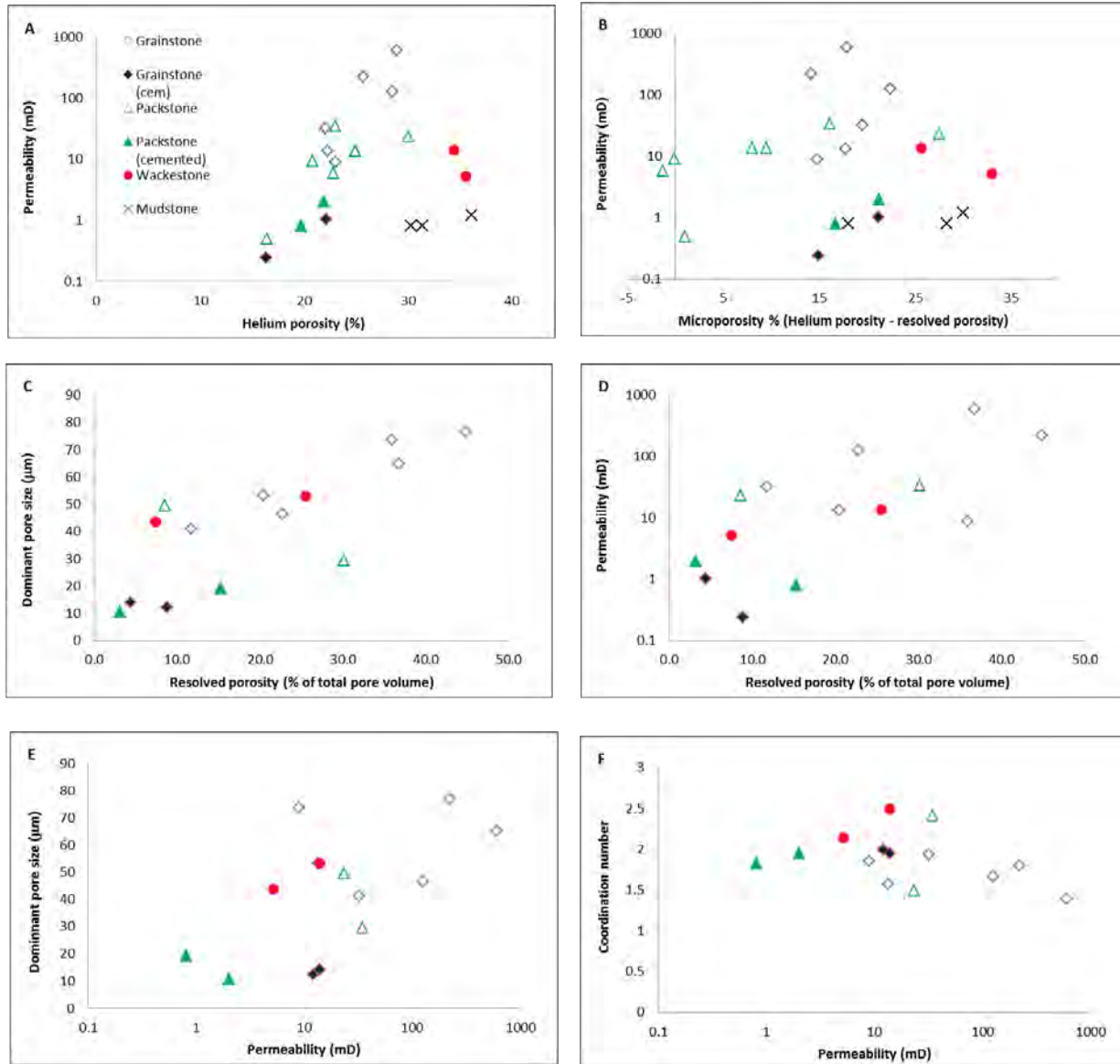


Fig. 1 Relationship between total porosity, resolved porosity (i.e., pores >1 μm diameter), permeability, co-ordination number and dominant pore size

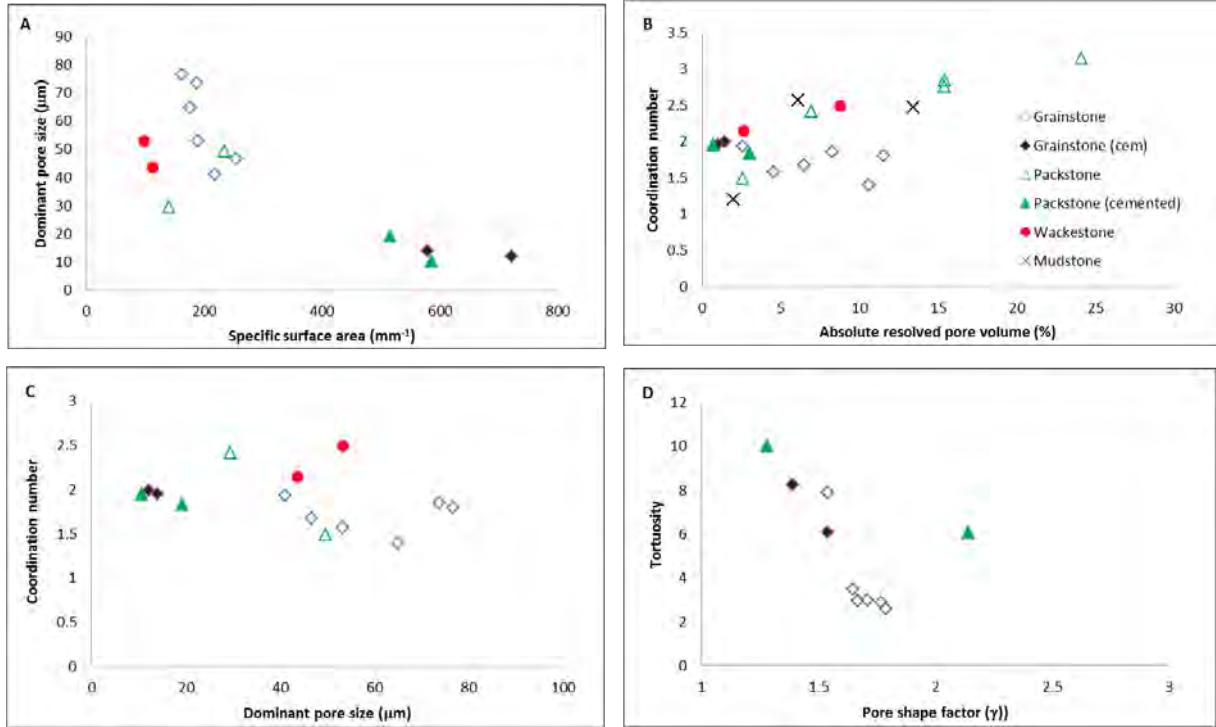


Fig. 2 Relationship between pore size, pore volume and pore topology from micro-XCT data

Upscaling, modelling and predicting porosity and permeability in carbonate systems: how good are we?

Cathy Hollis

University of Manchester, Williamson Building, Oxford Road, Manchester M13 9PL, UK

e-mail: cathy.hollis@manchester.ac.uk

One of the central challenges of carbonate reservoir modelling is the distribution of rock physical properties in 3D space. To be truly predictive of future reservoir performance, porosity, permeability and saturation need to be interpreted in uncored wells, upscaled and distributed in interwell areas. However, the quality and scale-dependency of reservoir data makes this a challenging process. As a result, many flow-simulated reservoir models will only match historical production with significant modification of permeability (K_h , K_v and/or K_v/K_h). This may reflect a number of constraints, including:

- Poor quality seismic data, which often prevents quantitative interpretation of porosity
- Thin (<5 meter thick) baffles, barriers and high permeability layers, sub-seismic scale geobodies and fractures
- Invariant total porosity such that wireline log responses do not adequately differentiate between sedimentary and/or diagenetic facies, inhibiting reservoir quality interpretation in uncored wells
- Multi-modal pore networks with complex shapes, giving a weak correlation between core plug porosity and permeability, inhibiting permeability prediction in uncored wells
- Fracturing, karstification and dolomitization, which can form complex, multiscale (sub-micron to meter-scale) non-stratobound pore networks that are not captured by core datasets
- Porosity distribution can be intimately related to burial history and hydrocarbon charge, inhibiting our ability to unify rules-sets

Numerous approaches have been adopted to manage these uncertainties, including layer-based stochastic modelling, flow zone definition, petrophysical and geological rock typing, near wellbore modelling and object-based modelling of sedimentary and diagenetic geobodies. Each method has its pros and cons, dependent upon known reservoir complexity, data quality and availability and reservoir maturity and development. Often, however, the choice of workflow is governed by other factors, such as personal and team experience, time/cost/resources, software constraints and corporate workflows. Based upon a number of outcrop and subsurface studies, this presentation will assess our current understanding of the spatial and scalar variability in porosity and permeability. It will present data on the shape, size and distribution of rock properties in 2D and 3D space and consider the constraints on determining these parameters. It will then discuss how this knowledge can be best captured during upscaling for geological modelling and reservoir simulation, before addressing areas of uncertainty and future potential research directions.

Distinct growth phases of an Upper Cambrian microbial reef complex (Mason County, Texas): A Core Workshop

Heath Hopson*, André Droxler, Pankaj Khanna, Brian Kubik, Pulkit Singh, Roberto Trotta,
Jacob Proctor, Paul (Mitch) Harris, Dan Lehrmann, and Jeff Dravis

*Rice University, 6100 Main St., Houston, TX 77005, USA

e-mail: hhh1@rice.edu

Interest in microbial deposits has increased following discoveries of hydrocarbon reservoirs in pre-salt deposits of offshore Brazil and Angola. As an analog to these reservoirs, a Rice-Trinity Microbial Research Consortium was established to study a 10–15 meter thick Upper Cambrian microbial reef unit (Point Peak Member, Wilberns Formation) covering as much as 25 km² of southern Mason County, Texas.

Drone based photogrammetry and systematic core drilling of the reef complex along the Llano and James Rivers and Mill Creek reveal three successive microbial shallow marine growth phases. Phase 1 of microbial thrombolitic growth initiated on low-relief sheets of flat rip-up clasts interpreted as transgressive lags and occurred contemporaneous to deposition of bioclastic grainstones. Sufficient accommodation allowed the buildups to develop appreciable synoptic relief; continued cementation and lithification developed the bioherm margin into a well-defined, purely microbial rind. A shallowing event, marked by fine siliciclastics onlapping the uppermost Phase 1 rind, ends Phase 1 growth. The microbial buildups grew contemporaneously in Phase 2 to deposition of inter-reef bioclastic grainstones using Phase 1 as a substrate for growth. Growth was characterized by juxtaposed columnar stromatolites. Incremental pauses in sea level rise periodically constrained vertical growth and induced lateral expansion beyond the margins of Phase 1 growth. These expansions, coupled with low synoptic relief of the bioherm, allowed interaction of the reef margin with inter-reef sediment, creating an interfingering nature between boundstone and surrounding bioclastic grainstones and inhibiting the formation of a well-defined bioherm rind. Termination of phase 2 microbial growth resulted from a deepening event and is marked by the end of bioclastic grainstone deposition. Phase 3 of microbial growth, characterized by a series of juxtaposed, well-defined bioherms, acts as a “capping phase” for the full bioherm unit. Increased accommodation allowed the bioherms to develop significant synoptic relief, once again permitting the formation of a well-defined microbial rind. The influx of fine siliciclastics onlapping the buildups marks the demise of the microbial reef complex.

A total of 195 cores were taken around the three main bodies of water that have exposed the Point Peak Member. The core workshop utilizes a series of transects crossing the buildups both horizontally and vertically to display spatial and temporal variations in growth patterns, respectively. Prime examples of microbial buildups and interbuildup strata of the different growth phases are the focus, as well as examples of transgressive lags representing the initiation of microbial growth within this interval.

Influence of organic matter type and abundance on depositional textures and associated pore attributes of hypersaline lacustrine microbial deposits (Holocene, Bahamas)

Hannah Hubert*, Christopher Omelon, and Eugene C. Rankey

*University of Kansas, 1475 Jayhawk Blvd., Lawrence, KS 66045, USA

e-mail: hannah.hubert@ku.edu

The discovery of hydrocarbon accumulations in carbonate lacustrine microbial reservoirs in the pre-salt of the South Atlantic has motivated the search for analogs that could provide perspective on the nature and origin of initial porosity in these reservoirs. Although previous efforts have mapped spatial patterns and produced facies models of large microbial lacustrine systems, details of their origins and how organic matter type and abundance influence depositional textures, early diagenesis, and associated pore attributes are less well constrained. To address these unknowns, this study tests two hypotheses focused on deposits of a small (<1 km²), shallow (<1 m) lake in the southern Bahamas: 1) the distribution, morphology, and growth fabrics of Holocene microbialites vary within a Bahamian lake as a function of organic matter type and abundance; and 2) textures are related to the pore size, pore distribution, and pore connectivity within these microbialites. This study integrates petrographic and scanning electron microscope observations of rock textures and organic matter, nuclear magnetic resonance imaging, computed tomography (CT) scans, and petrographic characterization of pores, and gas chromatography/mass spectroscopy of organic matter to characterize rock fabrics of Holocene microbialites.

Observations and mapping of the lake reveal systematic distribution of organic-rich surface sediment, unlithified microbial mats, and m-scale microbialites. Macroscopic textures within the microbialites range from stromatolitic (laminated) to thrombotic (clotted) to shrub-like. Porosity (ϕ) varies at several scales and some pore space is filled with microbial biomass (organic matter) and, less commonly, sediment. Buildups include three end-member fabrics: (1) organic matter and fibrous micrite that can be brecciated (mean $\phi = 54 \pm 6\%$); (2) alternating laminations of mm to sub-mm ropy micrite to clear fibrous and botryoidal cement to clotted/brecciated micrite (mean $\phi = 40 \pm 4\%$); and (3) dense laminations of micrite (mean $\phi = 14 \pm 5\%$). The average porosity of entire microbialites, including all pore scales, ranges from 39 to 59% (mean = $47 \pm 5\%$). Organic matter within microbialites is composed of microorganisms similar in size and morphology to those living within unlithified microbial mats in the lake, suggesting that microbial biomass is incorporated into the carbonate framework during growth, and can influence porosity and pore network architecture. Shifts in the macrostructure of microbiota may play an important role in controlling initial texture and subsequent rock fabric. These observations of pore genesis provide a basis for understanding the complex pore evolution evident in ancient carbonates from similar environments.

Characterization and modeling of carbonate pore systems

Neil Hurley

Chevron, 1500 Louisiana St., Houston, TX, 77002, USA

e-mail: nhurley@chevron.com

Carbonate rocks have complex pore systems, ranging in size from caverns to nanopores. Heterogeneity, which is typically high in carbonates, is defined as the variation in rock properties as a function of location within a reservoir or formation. Rock properties include mineralogy, grain type, grain size, depositional environment, porosity, permeability, natural fractures, vugs, faults, and channels. Heterogeneity causes problems in formation evaluation and reservoir simulation because reservoirs occupy large volumes, with limited availability of cores and logs.

Here is a key question: What model size is needed to capture heterogeneity within a given rock type? For certain rock types, heterogeneity can be captured at the pore scale. In most rock types, larger-scale models are needed. Models range in size from pore (nm to micron) to borehole (mm to m) to interwell (tens to hundreds of m) to full-field scale (tens to hundreds of km). In digital rock modeling, resolution is a function of imaging technique. Focused ion-beam scanning electron microscopy (FIB-SEM), petrography, confocal microscopy, and microCTscans are used at the pore scale. At the whole-core to borehole scale, tools include conventional CTscans, gridded minipermeability, and borehole image logs. Karst features, clinoforms, pinchouts, and impedance variations, for example, can be mapped using seismic data at the interwell to full-field scales.

Here is a major problem: Resolution is inversely related to sample size. Because of this, upscaling is commonly needed to do multi-scale characterization. Upscaling is the process of converting rock properties from fine scales to coarser scales. Upscaling algorithms assign suitable values of porosity, permeability, and other flow parameters to coarser grid blocks. Static modeling techniques at the pore-scale include pore-network, process-based, and stochastic models. Models based upon Darcy upscaling and CTscans combined with gridded minipermeability and multi-point statistics can be used at the core-plug and whole-core scales. Dynamic approaches to flow modeling include pore-network models, lattice-Boltzmann, thermodynamic, and conventional reservoir flow simulation.

For each carbonate reservoir rock type, pore-system characterization and modeling requires a series of choices and compromises to address these particular problems: heterogeneity, analytical techniques, required resolution, and upscaling.

Microporosity quantification using confocal microscopy

Neil Hurley

Chevron, 1500 Louisiana St., Houston, TX, 77002, USA

e-mail: nhurley@chevron.com

Confocal microscopy provides high-resolution (0.2-microns/pixel) images of pores in sedimentary rocks. Such features are generally obscure or invisible using conventional petrography. Confocal microscopy, which is relatively new to the earth sciences, provides an innovative way to image pores and quantify pore-body size distributions. This information can be used to define pore types, examine pore connectivity, and better understand diagenesis. In practice, confocal microscopy is applied to thin sections of rocks that are vacuum-pressure impregnated with epoxy. The laser light source interacts with fluorescing dye within the epoxy. Reflected light intensity indicates the physical location of pores. Confocal microscopy uses point-by-point illumination. A pinhole is placed in front of a detector to eliminate out-of-focus light. Because each measurement is a single point, confocal microscopes scan along grids of parallel lines to provide images of sequential planes at specified depths within the sample. Confocal microscopy is used to generate 2D and 3D images of pore bodies and throats. The images can be compared to laboratory-measured petrophysical properties and used to build pore-scale models. From these, we can compute petrophysical properties, such as capillary pressure, relative permeability, and recovery factors. Confocal work, performed within a stratigraphic framework in cyclic carbonates, can be used to improve mapping of pore types. These can be linked to logs to help enable mapping of diagenetic geobodies between wells.

Carbonate Pore Systems Core Workshop: Tengiz Field, Kazakhstan

Neil Hurley, James Bishop, and Greg Hurd

Chevron, 1500 Louisiana Street, Houston, TX, 77002, USA

e-mail: nhurley@chevron.com

Tengiz field, Kazakhstan, is a Devonian-Carboniferous isolated carbonate platform with backstepping, prograding, and aggrading margins. This workshop shows selected cores and petrographic images from: (a) the platform-slope transition, (b) upper slope boundstones, and (c) middle slope breccias and grainstones. Distinctive pore types occur in each depositional environment.

Rock properties versus elastic properties in fine grained tight carbonates

Priyank Jaiswal*, Rohit Raj, Beth Vanden Berg, and G. Michael Grammer

*Oklahoma State University, 105 Noble Research Center, Boone Pickens School of Geology, Stillwater, OK, 74078, USA

e-mail: priyank.jaiswal@okstate.edu

Using a rich database of sonic velocity transit times and microscopy from three cores that sample the Mississippian Limestone reservoir in north-central Oklahoma, we explore the relationship between elastic and rock properties in a low porosity (<10%) and low permeability (meso-to-micro Darcy range) carbonate system to accurately predict porosity and permeability. The transit time measurements include one P-wave, and two S-waves in mutually orthogonal directions. Rock properties utilized in this study include standard laboratory measured porosity, measured pore perimeter and pore aspect ratio from 2D cross-sectional images, standard laboratory measured permeability (air and Klinkenberg adjusted values), bulk composition through X-ray diffraction, and pin-point composition via SEM analysis.

The biggest challenge in identification of a correlation is lack of rock physics models that are applicable to very fine grain low-porosity, low-permeability carbonates. For example, even the Kozeny-Carman-based models, which are fairly advanced models in term of being able to relate porosity and permeability to grain size and tortuosity, appears to be breaking down in the Mississippian Limestone probably because the grain packing is substantially different from that of a conventional carbonate reservoir where this model has been demonstrated successfully by several researchers. Therefore, we have utilized a variety of statistical correlations for testing the sensitivity of elastic velocities to rock properties. Additionally, we explore, for simple pore shapes, how various geometrical aspects are related to each other (e.g., perimeter to surface area, etc.). This is followed by multi-variate non-linear regression and a simple neural-net based model to examine how geometrical aspects of the pore system, such as surface area, perimeter and aspect ratio, might relate to P-wave velocity.

Our initial results suggest the sonic velocities are more sensitive to mean perimeter than porosity. Implications to the interpretation of seismic velocities can be significant: in a low permeability system, the P-wave velocity may be higher when porosity is present as micro-pores rather than meso-pores. On-going work explores the contribution of other geometric factors such as aspect ratio on both P- and S-wave velocities. The goal is to identify if a deterministic rock physics model can be utilized to relate the laboratory measured sonic velocity to mineralogy and pore-geometrical attributes, or whether these systems are best described by statistical correlations and the pores are fractals.

Spectrum of gravity flow deposits on carbonate slopes and basin, Permian Basins, West Texas.

Xavier Janson*, Charles Kerans, Bob Loucks, Seay Nance, and Scott Hamelin

*Bureau of Economic Geology, University Of Texas at Austin, University station Box X, Austin, TX 78713, USA

e-mail: xavier.janson@beg.utexas.edu

The Permian basin of West Texas is one of the few place where conventional oil field producing from slope and basinal carbonate sediments can be found. Most of the slope and toe-of-slope Early Permian reservoirs in West Texas are found on channelized slopes with a variety of confined to semi-confined gravity flow deposits. These type of slope reservoirs can be divided into three categories: (1) coarse grained, concentrated density flow (like Happy field or Powell ranch), (2) dolomitized gravity flows (like Mescalero Escarpe and other northwestern shelf-slope reservoirs), and fractured, tight debris flows (like Bradford K field). Further downslope, thin carbonate hyper- concentrated density flows and turbidites are found intercalated with carbonate and siliciclastic mudrocks that are targeted by unconventional productions. The carbonate gravity flows in this case dilute the organic matter concentration and are non- producing facies. This core presentation will show several example of gravity flow deposits on carbonate slopes from the Permian Basins illustrating a range of facies and potential pore network associated with these carbonate gravity flow deposits.

Diagenesis of the San Andres Formation in the Seminole Unit in the Central Basin Platform, West Texas

Lei Jiang*, Ian Duncan, and Zhaoqi Li

*Bureau of Economic Geology, Jackson School of Geosciences, The University of Texas at Austin, 8524 Burnet Road, Austin, TX 78757, USA

e-mail: lei.jiang@mail.iggcas.ac.cn

The San Andres Formation in the Texas and New Mexico area of the Permian Basin had cumulatively produced more than ten billion bbls of oil by year 2000 (Dutton et al., 2005), and has significant potential for increasing oil production by CO₂ EOR from Residual Oil Zones (ROZs). Previous research on the San Andres Formation is mostly on depositional model and facies analysis, little attention has been given to the diagenesis sequences and the porosity evolution.

We describe a detailed diagenetic study on the San Andres Formation in the Seminole Unit from the Northeast edge of Central Basin Platform. Dolomitization and sulfate cementation were two dominant diagenetic events. Three main dolomitization stages have been identified based on petrological study. The first and dominant phase of early dolomitization occurred early in the rocks history. This dolomite commonly is associated with evaporites, indicating that reflux of brine was the most likely dolomitization model. The second dolomitization phase resulted in spheroidal dolomite cement precipitation, which commonly occurs in the fusulinid-enriched section and filling within fusulinid chambers. Hence, spheroidal dolomite probably reflects an organic or microbe-related dolomitization event. The third dolomitization phase was represented by dolomitic cements that locally fill late stage micro-fractures.

Anhydrite cementation occurred during the earliest dolomitization phase and reoccurred through the entire diagenetic history. Fluid inclusion (FI) study suggests that most of the anhydrite cements only have single phase fluid inclusions. Some two-phase aqueous FI have homogenization temperatures (HTs) ranging from 50–70° C, indicating that most anhydrite cements were precipitated at temperatures lower than 70° C. Most two-phase aqueous FIs in anhydrites are secondary, showing HTs mode at 90–100° C. Although the volume is small, pyrite has been found widely distributed as anhydrite replacement, fracture- and pore-fillings, as well as stylolite-fillings. Bacterial sulfate reduction (BSR) may be responsible for the anhydrite dissolution and pyrite precipitation, as well as the localized calcite replacement of anhydrite nodules in the reservoir. Some anhydrite dissolution enlarged pores, fusulinid moldic pores, micro-fracture-enlarged pores, and dolomite dissolution pores are interpreted probably related to BSR.

A machine learning method for microporosity prediction in carbonate reservoirs

Tiffany Dawn Jobe*, Shuo Zhang, and Susan Agar

*Aramco Research Center–Houston, 16300 Park Row, Houston, TX 77084, USA

e-mail: dawn.jobe@aramcoservices.com

Microporosity can have a significant impact on reservoir quality in carbonate reservoirs. Micropores are commonly invoked to explain high porosity–low permeability intervals, low resistivity pay zones, high water saturations and poor sweep efficiency. Furthermore, petrophysical estimates of porosity cannot differentiate micropores from effective porosity that contributes to reservoir flow. Advances in enhanced oil recovery (EOR) techniques are making production from poorly swept microporous intervals a possibility. Success of any such EOR strategies is dependent on accurate prediction of microporosity and hence reservoir quality.

Here, we present a method using neural network models for micropore prediction in the subsurface. Data for this case study comes from a Jurassic, carbonate reservoir in the Middle East with a bimodal porosity distribution. Hydrocarbon column heights in the area are greater than 1000 ft which is sufficient to overcome capillary entry pressures and charge the micropores (1–10 microns). Key depositional lithofacies include micritic to very fine-grained mudstones; bivalve-coated grain pack- to grainstones; *Cladocoropsis* pack- to grainstones; stromatoporoid coralgall pack- to grainstones; and skeletal–oolitic grainstones. An idealized geo-cellular reservoir model with >200 wells was constructed to visualize lithofacies and reservoir properties. Thin sections representing each of the lithofacies were available for quantitative analysis. Microporosity was quantified by confocal and light microscopy coupled with core plug and laboratory measurements. These data were then used to train and validate a neural network model for microporosity prediction. Descriptors, including measured porosity, texture, lithology and lithofacies are the key input variables in the model. These were chosen as they can easily be attained from core data and/or estimated through petrophysical analysis. The plug-based model was trained with >300 microporosity data points with 30% reserved for testing and validation. The mathematical model was then applied to the subsurface field data set where the spatial distribution of microporosity was estimated and visualized through geo-statistical approaches. Several key uncertainties exist in using mathematical models for micropore prediction. Further research is needed to identify descriptors that best relate available subsurface data to microporosity. Additionally alternative methods for microporosity quantification should be explored.

The fundamentals of limestone microporosity

Stephen Kaczmarek*, Franek J. Hasiuk, and Shawn M. Fullmer

*Western Michigan University, 1903 W. Michigan Ave., Kalamazoo, MI 49008, USA

e-mail: stephen.kaczmarek@wmich.edu

Microporosity is a common attribute of Phanerozoic-age carbonate rocks. A review of the published literature indicates that micropores are ubiquitous in a wide range of depositional facies, grain types, depositional textures, depositional environments, platform types, and burial depths. The vast majority of micropores are hosted within a homogenous framework of diagenetic low-magnesium calcite (LMC) microcrystals measuring 0.5–9.0 μm in diameter with a mode at 2.0 μm . In general, LMC microcrystals exhibit three fundamental textures recognized with scanning electron microscopy (SEM). Granular textures are characterized by a framework of unconsolidated rhombic (euhedral) to polyhedral (subhedral) microcrystals with straight to curvilinear boundaries and intermediate edge densities. Clustered textures are characterized by a framework of irregularly shaped microcrystals exhibiting a high density of discontinuous, curvilinear edges. Fitted textures are characterized by a dense mosaic of slightly larger microcrystals with mostly curvilinear boundaries and relatively low density of edges.

Comparison of SEM and mercury-injection capillary-pressure data shows that in micropore-dominated carbonate rocks, pore throat size distribution, bulk porosity, and permeability correlate with microcrystal texture. Based on these relationships, three micropore-types are distinguished. Type 1, associated with granular subhedral crystal fabrics, typically exhibits relatively large average pore throat radii (~0.7 mm), high porosity (>20%), and permeability (1–20 mD). Type 2, which includes granular euhedral and clustered fabrics, most commonly exhibits intermediate average pore-throat radii (~0.2 mm), porosity (10–20%), and permeability (0.1–1 mD). Type 3, including fitted crystal fabrics, are characterized by smaller average pore-throat radii (~0.06 mm), low porosity (<10%), and low permeability (<0.1 mD). Elemental and stable isotope geochemistry of LMC microcrystals are consistent with a shallow burial diagenetic pathway. In particular, $\delta^{13}\text{C}$ and $\delta^{18}\text{O}$ data plot along a burial trend anchored at the positive end by the composition of age-equivalent marine calcites. More negative $\delta^{18}\text{O}$ values also correlate well with increases in depth and reductions in porosity, which implies progressive growth of LMC microcrystals occurs with depth.

Argillaceous lime Eagle Ford Chalk resource play; Preservation of an original mineral pore network by emplacement of bitumen - Interplay between mineral pores and organic-matter pores

Lucy Tingwei Ko*, Robert G. Loucks, and Stephen C. Ruppel

*University of Texas at Austin, 10100 Burnet Road Bldg 130, Austin, Texas, 78758, USA

e-mail: tingwei.ko@utexas.edu

The Eagle Ford Formation argillaceous lime chalk samples collected from subsurface cores and outcrops (along U.S. Highway 90, west of Del Rio, Texas) are in general composed of more than 55% calcite. The chalk is laminated, nonbioturbated wackestone to packstone with the larger allochems being globigerinids and calcispheres within a finer matrix of coccoliths. Some cephalopods and *Inoceramus* are also present. Early diagenesis is mainly in the form of microscale calcite overgrowths on coccoliths and coccolith plates. The effect of relatively early initial lithification prevented significant porosity loss from compaction and the preservation of abundant primary porosity between the coccolith hash. Other mineral diagenesis during burial was very fine crystalline equant calcite, kaolinite, and quartz cementation in globigerinids and calcispheres body cavities. Quartz cements were also observed within the coccolith hash.

Therefore, the early pore network was composed of primary nanometer (nm)- to micrometer (μm)-sized interparticle pores with nm-sized pore throats. A major change in the pore network started with the thermal maturation of kerogen to bitumen. The bitumen was expelled into the interparticle pore network where it later cracked to oil leaving some solid bitumen behind. The solid bitumen plugged the original primary pores but formed organic-matter (OM) bubble and spongy nanopores. The porosity within the coccolith hash decreases from approximately 38% by volume after compaction to approximately 15% by volume after cementation and bitumen migration. Therefore, approximately 64–84% of porosity loss was caused by bitumen migration whereas the rest of the porosity loss is caused by quartz and kaolinite cement. The induction of bitumen into mineral pores and later OM pore development allowed a continuous bitumen network to develop within the mineral pores setting the stage for a subsequent connected OM pore network. If the bitumen had not occluded the original mineral pore network in this argillaceous chalk, much of the mineral pore network may have been lost to enhanced calcite cementation as it was in similar buried (Eagle Ford was buried to 6000 ft in study area) Buda and Austin Chalks. The bitumen emplacement was a mechanism for providing a connected pore network in what may have become a tight chalk during burial.

**Solution-collapse breccia development and multi-scale protracted pore filling,
Lower Ordovician Knox Group, Tennessee–Kentucky**

J. Richard Kyle*, Raeann Garcia, and Nathan Miller

*University of Texas at Austin, Dept of Geological Sciences, 2275 Speedway, EPS 1.130,
Austin, TX 78712, USA

e-mail: rkyle@jsg.utexas.edu

Diagenetic effects initiated by a ~10-My period of subaerial exposure following deposition of the Lower Ordovician Knox Group carbonates are common features extending throughout the Appalachians and into the continental interior of North America. From the economic perspective, the major features are extensive solution-collapse breccia networks that locally serve as petroleum reservoirs and host strata-bound zinc and related MVT mineralization precipitated from basinal brines generally tied to late Paleozoic orogenic events. Although the breccia bodies are broadly similar over large areas, the cement assemblage, sequence of pore filling, and remaining porosity vary considerably, suggesting spatial and temporal variation in brine systems.

Four mining districts as well as former exploration programs in Tennessee-Kentucky provide regional geologic information and three-dimensional sample suites to assess porosity and cementation histories over a >50,000 km² area. These strata are exposed in the imbricate thrust fault belts in eastern Tennessee (ET), where they dip from 10 to 40°. The essentially horizontal Knox Group carbonates in central Tennessee and southern Kentucky (CTSK) are covered by a minimum of 90 m of younger strata. Local relief on the post-Knox unconformity may be as much as 40 m, and regional beveling is indicated by local preservation of younger Knox strata.

Volume-for-volume dolomitization of upper Knox limestones occurred in many areas providing little opportunity for collapse of overlying strata, and any mineral cements are restricted to vugs and minor fractures. In other areas where solution was the dominant process, the amount of collapse is considerable with either strata-bound breccia zones or local “break-through” breccia bodies that affect a considerable amount of upper Knox strata and may extend into the Middle Ordovician units. Downward displacement of blocks in these breccias is as much as 15 m. The upper part of the late breccia systems had high interblock and fracture porosity that is partially filled with carbonate, sulfide, and related minerals. Only localized areas have commercially significant amounts of sulfide minerals; most late breccias are cemented by carbonate gangue with varying amounts of remaining porosity. Hydrothermal dolomite (\pm quartz) cement predates sulfide mineralization in CTSK, whereas dolomite forms before and after sulfide precipitation in ET. Breccia characterization enhanced by X-ray computed tomography and regional cement microstratigraphy, quantified by LA-ICP-MS geochemistry and stable isotopes, are in progress to constrain the history of breccia formation and cementation, with attendant multi-scale effects on porosity.

Effects of pore size on polymer flooding efficiency in microfluidic pore networks

Mike Lacey*, Cathy Hollis, Mart Oostrom, and Nima Shokri

*University Of Manchester, 4.69 Williamson Building, Oxford Road, Manchester, M13 9PL,
United Kingdom

e-mail: michael.lacey@manchester.ac.uk

The efficiency of enhanced oil recovery is strongly dependent on the pore structure and geometry of porous media, influencing the competition among various forces. Other important factors affecting oil displacement are the properties of the fluids that define the patterns and general dynamics of multiphase flow. In this study, we present a comprehensive series of microfluidic experiments to delineate the effects of pore size distributions on the efficiency of polymer flooding in porous media saturated by oil. To do so, micro-fluidic experiments were conducted on micromodels fabricated based on X-Ray computed tomography images of a sand-pack with varying grain sizes to represent an intergranular pore network. The micromodels were fabricated in a silicon wafer using standard photolithography and inductively coupled plasma–deep reactive ion etching methods. Three micro-models of coarse, medium and fine grain size were initially saturated by Silicone oil. The displacing fluids were aqueous solutions with dissolved xanthan gum whose rheological characteristics were accurately determined by a stress controlled rheometer. The dynamics and patterns of the interface displacement as well as the size distribution of the trapped oil ganglia were visualized using an optical microscope. The results show that the number of trapped oil clusters decrease as pore size increases, although a greater number of oil ganglia are trapped in the largest pores within the coarsest grained model. Addition of a polymer to the displacing fluid created a stable displacement front in all but the finest grained model. Overall, it appears that beneath a critical grain size threshold, the addition of a polymer is less effective at improving recovery, most likely reflecting a change from viscous to capillary dominated flow. The next step will be to extend the experiments to more complex pore network, typical of most carbonate sediments, and to compare the data to in situ fluid flow experiments.

A review on the multiple origins of nano- and micropores in limestones and dolostones

Robert G. Loucks

Bureau of Economic Geology, The University of Texas at Austin, University Station, Box X,
Austin, TX 78713-8924, USA

e-mail: bob.loucks@beg.utexas.edu

Nano- and micropores are common in carbonate reservoirs as either the sole pore type or in combination with macropores and fracture pores. The origin of these fine pores have a variety of processes, some related to depositional processes, but most being related to diagenetic processes. Micropores are defined generally as pores with diameters <10 microns or pore radii <0.5 microns. Nanopores are less than a micron in diameter. These fine pores form in limestones and dolostones. In limestones, the pores occur between crystals that are commonly less than 1 to 6 microns in size, but in dolostones the crystal sizes can be much larger. This size difference is related to multiple contrasting origins of the processes that produce these pores. Limestone nano- and micropores generally originate in three ways. In chalks they are related to the original depositional fabric as interparticle and intraparticle associated with coccoliths and pelagic allochems. In Mg-calcite-rich sediments they form by the transformation of unstable Mg-calcite allochems (e.g., larger forams and red algae) to calcite. The pores are restricted to the distribution of the allochems. In carbonate mud, mixtures of aragonite, Mg-calcite, and calcite, the origin is both depositional and diagenetic as aragonite dissolves and reprecipitates as microrhombic calcite, Mg-calcite transforms to microrhombic calcite, and original calcite allochems form overgrowths decreasing adjacent pores. In dolostones nano- and micropores are associated with extensive dolomitization (competitive crystal growth) and the nearly complete occlusion of pores. In some dolostones the nano- to micropores pores are inherited from the precursor microporous limestone. A very late process (telogenesis) of nano- and micropores formation is subaerial weathering of both limestones and dolostones. Weathering can create extensive micropore formation with porosities above 30 percent. In some cases pulverulite forms (micron-scale calcite or dolomite powder). This is a dissolution process as evidenced by dissolution and corrosion of crystals. This form of micropores could be preserved at unconformities and form enhanced porosity zones. Organic-matter nano- to micropores in solid bitumen in organic-rich argillaceous limestones (e.g., Eagle Ford Group) are very common as well as in cleaner carbonates with solid bitumen filled pores. Only in organic-rich very fine grained limestones do organic-matter pores form an effective pore system. Because nano- and micropores have multiple origins, their lateral and vertical distribution will reflect their origin. Therefore, one must not just describe the nano- to micropores in strata, one must also understand their origin.

Evidence for earlier lower Cretaceous Valanginian shelf margin complexes in the onshore north-central Gulf of Mexico

Robert G. Loucks* and Charles Kerans

*Bureau of Economic Geology, The University of Texas at Austin, Box X, University Station, Austin, TX 78713-8924, USA

e-mail: bob.loucks@beg.utexas.edu

The Lower Cretaceous stratigraphic section around the Gulf of Mexico (GOM) contains several well-documented carbonate systems with prominent shelf margins, which include the Berriasian Knowles ramp, Barremian Sligo shelf, Aptian Pearsall ramp, and Albian Glen Rose/Edwards/Stuart City shelf systems. Two lesser-known but large-scale Lower Cretaceous Valanginian carbonate shelf-to-shelf-margin systems are documented here using core, log, and regional 2D seismic data. The Calvin section (next carbonate unit above the Knowles Limestone) is a complex shelf-margin buildup and may be as thick as 2000 ft (610 m) and internally, it shows back-reef, reef, and fore-reef facies. Major reef-building organisms are *Lithocodium*, stromatoporoids, and corals. The Winn Limestone was deposited just above the Calvin Limestone, and at the shelf margin, it may have been 600 to 800 ft (180 to 245 m) thick and was composed of similar organisms as the Calvin reef complex. Considering the position of the Calvin platform, succeeding the major bypass of Calvin lowstand sands, it is suggested that the Calvin platform records a transgressive and highly aggradational depositional style. The Winn margin did not prograde as far seaward as the Calvin margin. Micropores between calcite microrhombs are the predominant pore type in each limestone. The recognition of these two Lower Cretaceous carbonate systems is important as they further detail the stratigraphic history and architecture of this deeply buried, earliest Lower Cretaceous section in the GOM and these sections are also potential deep-gas, tight-carbonate plays.

Hydrothermal silicification in deeply buried Ordovician carbonate reservoirs in the Shunnan area, Tarim basin, NW China: Insights from fluid inclusion and isotope studies

Ziye Lu*, Hairuo Qing, Honghan Chen, and Siyang Zhang

*China University of Geosciences, 388 Lumo Road, Wuhan, Hubei Province, 430074, China

e-mail: luziyei88@163.com

The Shunnan (SN) area, located in the center of the Tarim basin, NW China, is a newly discovered gas field in deeply buried Ordovician carbonate rocks (current burial >6000 meters and current temperature >190° C). The most important reservoir rocks in the SN area are silicified limestones, characterized by as much as four types of authigenic quartz (Qz1–Qz4) and five types of coarse calcite cement (CC1–CC5). Qz1 is a replacement quartz in both limestone and chert, later than the burial stylolite. Qz2 is the equant quartz cement in fractures or vugs in chert, crosscutting the burial stylolite. Qz3 and Qz4, commonly later than the Qz2, are the core and rim of the bladed quartz in fractures in chert. CC1 is the coarse calcite in the vugs of well SN7. CC2 is the coarse calcite in fractures in limestone, crosscutting the Qz1. CC3, CC4 and CC5 are only identified in chert. CC3 is the coarse calcite in fractures, later than the Qz1 but crosscut by Qz2, Qz3 and Qz4. CC4 is the coarse calcite in intercrystalline pores of the Qz1, later than the Qz1. CC5 is the coarse calcite later than Qz4, filling up rest of the fractures or vugs. CC1 is characterized by $\delta^{18}\text{OVPDB}$ values of -8.31–4.60‰. CC2 is characterized with $\delta^{18}\text{OVPDB}$ values of -13.26–7.76‰, $87\text{Sr}/86\text{Sr}$ ratios of 0.708898–0.709167, homogenization temperatures of 118–131° C, and salinities of 22.9–25.2 wt.% NaCl + CaCl₂. Qz2, Qz3, CC3 and CC4 have similar homogenization temperatures of 143–166° C and salinities of 14.7–23.7 wt.% NaCl + CaCl₂. And CC3 is characterized with $\delta^{18}\text{OVPDB}$ values of -11.09–10.66‰ and $87\text{Sr}/86\text{Sr}$ ratios of 0.709489–0.709721. Qz4 and CC5 are characterized with homogenization temperatures of 125–132 and 86–101° C, and similar salinities of 24.8–26.8 and 22.9–25.2 wt.% NaCl + CaCl₂. CC1 is interpreted to be from seawater or slightly modified seawater. Qz1, Qz2, Qz3, CC3 and CC4 are considered to be from the fluids derived from the Sinian siliciclastic rocks and/or pre-Sinian base. CC2 is interpreted to be precipitated from the fluids derived from the salts bearing Cambrian strata. The change of fluid inclusion homogenization temperatures from Qz2, Qz3, CC3 (at least 143–166° C) to Qz4, CC5 (at most 135° C) indicate that the reservoir rocks experienced a decrease of temperatures, which cannot be explained by an unroofing during burial history. Instead, this can be explained by a hydrothermal fluid cooling after it injecting into the carbonate reservoirs. This hydrothermal activity may not be linked with Permian magmatism because the entrapping temperature of CC5, which is the last mineral phase in chert, is considered to be lower than the ambient temperature during the Permian time, indicating that the hydrothermal activity happened earlier than the Permian time.

Multi-phase dolomitization and recrystallization of Middle Triassic shallow marine–peritidal carbonates of the Mecsek Mountains (SW Hungary)

Georgina Lukoczki*, Jay M. Gregg, and János Haas

*Oklahoma State University, Noble Research Center, Stillwater, OK, 74078, USA

e-mail: gina.lukoczki@okstate.edu

The Middle Triassic Csukma Formation of the Mecsek Mountains in southwest Hungary is comprised of shallow marine–peritidal carbonates. The peritidal inner ramp succession (Kán Dolomite Member) exposed in the western part of the mountains is completely dolomitized, whereas the middle ramp shoal deposits (Kozár Limestone Member), in the Central Mecsek Mountains, are undolomitized in one of the two studied sections, and partially to completely dolomitized in the other. Petrographic features suggest that the fine crystalline peritidal carbonates likely underwent complete dolomitization in a near surface setting due to circulating hypersaline or mesohaline waters. However, the oxygen isotope signature of the dolomite ($\delta^{18}\text{O} = -2.2\text{‰}$ to -4.9‰ PDB) does not reflect precipitation from evaporated seawater. Recrystallization of the dolomite is thus inferred in a shallow to intermediate burial setting.

Meter-scale irregular bodies of coarse crystalline planar- to nonplanar dolomites partially replace previously undolomitized limestones in the lower, shallow marine transitional part of the succession (Zuhány Limestone Formation), and are also associated with the otherwise fine crystalline peritidal dolomites (Kán Dolomite). The low oxygen isotope values of these coarse crystalline dolomites ($\delta^{18}\text{O} = -10.2\text{‰}$ to -12.5‰ PDB) indicate precipitation at elevated temperatures. During the Early Cretaceous, when the succession was deeply buried, rift related igneous activity likely drove circulation of hot fluids that partially recrystallized the peritidal dolomites a second time, further altering their texture and isotope signature. Both phases of dolomitization and recrystallization altered the pore architecture of the rocks. In coeval undolomitized carbonates of the Central Mecsek Mountains (Kozár Limestone) features of various diagenetic stages, from marine diagenesis through shallow to deep burial and then uplift related shallow burial, are preserved. However, five kilometers northwest from the exposed limestone section, partially to completely dolomitized Middle Triassic carbonates are interpreted to be a dolomitized version of the Kozár Limestone. These medium to coarse crystalline, planar- to nonplanar, fabric destructive, replacive dolomites, with low oxygen isotope values ($\delta^{18}\text{O} = -10.2\text{‰}$ to -11.2‰ PDB), and multiple phases of open space filling saddle dolomite are found in the vicinity of Early Cretaceous igneous dykes. Generally, these dolomites have lower porosity than the dolomites in the Western Mecsek. Dolomitization of this succession was likely caused by circulating hot waters, driven by the same Early Cretaceous submarine igneous activity as in the Western Mecsek Mountains. The dolomitizing agent likely was seawater drawn down through rift related fault systems.

Processes and controlling factors of polygenetic dolomite formation in the Transdanubian Range, Hungary

Georgina Lukoczki*, János Haas, Kinga Hips, Tamás Budai, Orsolya Győri, Sándor Kele, Attila Demény, and Zsófia Poros

*Oklahoma State University, Noble Research Center, Stillwater, OK, 74078, USA

e-mail: gina.lukoczki@okstate.edu

In the Transdanubian Range, Hungary, dolostone and dolomitic limestone are present in a number of sedimentary successions, which were formed from the Late Permian to the Late Triassic in various depositional settings, and under various diagenetic conditions. Only a negligible amount of dolomite has been found in the post-Triassic formations. Dolomitization processes of seven dolomite-bearing units representing ramp, small and large carbonate platforms, and intraplatform basin settings are presented in this synopsis. In most cases, multi-stage and polygenetic dolomitization was inferred. The main mass of the dolostones was formed via near-surface diagenetic processes, which were commonly preceded by the formation of syndimentary dolomite. Accordingly, surface conditions that prevailed during sedimentation controlled the dolomite-forming processes and thus the spatial extension, and the time span of dolomitization. The area of episodic subaerial exposure was a critical controlling factor of the lateral extension of the near-surface dolomite genesis, whereas its temporal duration was mostly governed by climate. Burial diagenesis usually resulted in only moderate degree of dolomitization, either related to the expulsion of compactional fluids or to thermal convection. Triassic fault systems provided conduits for fluid flow that led to both replacive dolomitization and dolomite cement precipitation. In the Late Triassic extensional basins, syndimentary fault-controlled dolomitization of basinal deposits was interpreted.

Meso-Proterozoic dolomite reservoir texture within peritidal microbialite successions in northeast China

Ping Luo

Research Institute of Petroleum Exploration and Development, Xueyuan Road 20,
Haidian District, Beijing, 100083, China

e-mail: pluo@petrochina.com.cn

There are three main types of microbial dolostones in the Meso-Proterozoic Wumishan Formation in Northeast China. They are stromatolite, laminite and thrombolite-like or particulate microbialite. The microbialite facies are strongly environmentally associated. Several kinds of stromatolite can be found in the peritidal environments. But mostly plane or wavy stromatolites occur in intertidal and supratidal zones, while dome and conic ones occur in subtidal or lower intertidal zones. The laminite facies mostly deposit in the shallow subtidal zone. In more forceful subtidal zones or tidal channels, microbial grains are formed or deposited, like thrombolite, oncolite, and microbial-coated grains (sandy and gravelly sized). The reservoir rocks are well-related (selected) to lithofacies or their depositional environments. Rocks formed in more energetic water display better reservoir quality, even after diagenesis (ground and burial). The dolomite porosity of plane stromatolites in the suprotidal or intertidal is much worse than that of the particulate microbialite rocks, whether samples from outcrops or drilling cores. The reservoir section in a peritidal microbial cycle is located in its lower part. A peritidal microbial facies succession consists of subtidal particulate microbialite, or laminite in lower part, then intertidal wavy or dome stromatolite in the middle, and finally plane ones in the upper part; representing a cycle of filling depositional accommodation or a parasequence. Reservoir rocks are located in the lower part in a depositional succession of peritidal microbialite dolostones. The thickness of reservoir rocks in microbialite parasequences ranges commonly from 1 to 10 meters, deeply related to depositional cycles or sequence stratigraphy in vertical profile and their areal extent to the paleogeography.

**Complex, extensive karstification of Pleistocene carbonates of Barbados, West Indies—
lessons for karstified petroleum reservoirs elsewhere**

Hans G. Machel

University of Alberta
Department of Earth and Atmospheric Sciences
Edmonton, AB T6G 2E3
Canada

e-mail: hmachel@telus.net

Barbados is located at 13° 10' north latitude, 59° 35' west longitude, and is about 32 x 23 km in size. Overlying tectonically deformed siliciclastic sediments of an accretionary prism, about 80% of the surface of the island is made up of Pleistocene carbonates with ages approximately 800,000 years to recent. These carbonates are a few meters to about 120 m thick and form a series of terraces, which were deposited in response to an interplay of tectonic uplift and eustatic sea level changes, with tectonic uplift ranging episodically from ~7 to 440 m per 100,000 years over the past 800,000 years. Despite their young age the Pleistocene carbonates, and even some underlying Miocene chalks, are riddled with caves and sinkholes, resembling Swiss cheese. Dissolution took and takes place by freshwater forming stream caves; by freshwater-seawater mixing forming flank margin caves; by hypogene water tectonically expelled from the underlying accretionary prism enlarging fracture networks; and by corrasion of freshwater and seawater forming pseudokarstic sea caves. In addition, many caves have a hybrid origin in that they form(ed) by at least two successive karst processes. There also are some artificial caves, dug for drainage of episodic flood waters. Flank margin and hybrid caves are the most abundant cave types. Sinkhole density is extremely high, with an average of 5 sinkholes per square km. However, some areas have a much higher density while others are almost devoid of sinkholes. Another striking karst feature is a network of valleys, locally referred to as gullies, which formed due to at least two phases of subaerial exposure alternating with marine flooding. A number of lessons learned from Barbados can be applied to geologically much older karstified hydrocarbon reservoirs elsewhere. The most striking feature recognized in Barbados is just how extensive, pervasive, and variegated karstic dissolution can be in less than one million years

Impact of diagenesis on reservoir properties of the Upper Jurassic carbonate sediments in the Greater Geneva Basin (Switzerland and France)

Yasin Makhloufi*, Elme Rusillon, Jean-Pierre Sizun, Michel Meyer, and Elias Samankassou

University Of Geneva
Rue des Maraichers 13
CH-1205
Switzerland

e-mail: Yasin.Makhloufi@unige.ch

The Canton of Geneva (Switzerland) is currently exploring the opportunities for geothermal energy exploitation in the Great Geneva Basin (GGB) sub-surface. In this context, a structural analysis of the basin associated with reservoir appraisal and rock-typing of reservoir bodies of potential interest were conducted. The Upper Jurassic carbonate sediments (the *Reef Complex* Unit and the *Calcaires de Tabalcon* Formation) of the GGB represent the best potential reservoirs. However, these units exhibit strong heterogeneities in terms of reservoir quality with the observation of highly porous dolomitic intervals in the western part of the basin that becomes tighter to the south-east.

Diagenesis of carbonate rocks is known to affect the petrophysical properties of the host rock. Assessing the diagenetic history is thus essential when evaluating any reservoir exploitation project. Other geothermal projects elsewhere (e.g., Bavaria, southern Germany; Paris Basin, France) showed that dolomitized carbonate rocks have good reservoir properties and are suitable for geothermal energy production.

Three study sites where the Upper Jurassic carbonates outcrop were selected at the surroundings of the GGB: the Jura Mountains (north-western), the Vuache Mountains (south-western) and Salève Mountains (south-eastern). In addition, one core close to the prospected area was studied (Humilly-2 borehole). Detailed study of each site focused on (1) petrographical analyses in order to assess textures, fabrics, types and locality of pores as well as the diagenetic history and (2) petrophysical analyses to characterize reservoirs properties (Phi, K, MICP).

The reservoir exhibits heterogeneous properties in terms of pore types with abundance of intraparticle porosity and partly interparticle or intercrystalline macroporosity as well as moldic porosity linked to dolomitization. Results from the petrographical analyses display complex diagenetic histories, dependent on the site studied. The paragenesis displays several stages of interparticle calcite cementation as well as different stages of dolomitization and/or dedolomitization. These processes seem to follow constrained path of fluid migrations through burial, faulting or exhumation during the basin's history.

The complex diagenetic history affected the petrophysical and microstructural properties via porogenesis (conservation of initial porosity, moldic porosity) and/or poronecrosis phases. The best reservoir properties appear to be recorded in patch reefs and peri-reefal deposits, commonly linked to porous dolomitized intervals.

The study presented here will help to constrain and quantify reservoir heterogeneities in a complex reservoir and to provide insights into porosity and permeability distribution that will ultimately help in reservoir modeling, a crucial step for further potential exploitation.

High-frequency cyclicity in dolomite stoichiometry in the Upper Glen Rose Formation: Implications for penecontemporaneous dolomitization

Cameron J. Manche and Stephen E. Kaczmarek

Western Michigan University, 1903 W. Michigan Ave., Kalamazoo, MI 49008, USA

e-mail: cameron.j.manche@wmich.edu

Outcrops of the Cretaceous Upper Glen Rose Formation along Highway 360 in Austin, Texas record peritidal carbonate deposition characterized by subtidal mud-dominated milliolid packstones overlain by tidal-flat mudstone caps. The upper ~1.5 meter of each cycle is pervasively dolomitized. Previous work suggests that dolomitization occurred via seepage of hypersaline brines downward through the underlying sediments. To further test this model, 217 samples were collected from six vertical transects positioned across the ~18 meter tall Wild Basin Preserve outcrop. These transects were examined at the centimeter scale using a suite of analytical tools, including powder X-ray diffraction (XRD) and stable isotope geochemistry. Additional analytical tools such as scanning electron microscopy, energy dispersive spectroscopy, energy dispersive X-ray fluorescence, air permeametry, and thin section image analysis were applied at lower resolution. High-resolution XRD data exhibit two fundamental diagenetic trends with respect to dolomite abundance, dolomite stoichiometry, and dolomite cation ordering within individual cycles. Regressive facies successions are associated with systematic increases in dolomite abundance and dolomite stoichiometry, and a decrease in cation ordering up section. In contrast, transgressive facies successions are associated with systematic decreases in dolomite abundance and dolomite stoichiometry, and an increase in cation ordering up section. In one of the regressive cycles, for example, there is a systematic increase in dolomite abundance (20 to 100%), dolomite stoichiometry (45 to 49 mole% MgCO_3), $\delta^{18}\text{O}$ (+1.56 to +2.11‰ VPDB), and a decrease in the degree of cation ordering (0.66 to 0.37). These trends are interpreted to reflect penecontemporaneous dolomitization during temporally changing physicochemical conditions (e.g., Mg/Ca, salinity, temperature, etc.) associated with local sea level fluctuations during deposition, rather than top-down refluxing brines. The high resolution XRD dataset presented here is the first of its kind, and suggests that dolomite stoichiometry and cation ordering may provide valuable proxies for dolomitizing fluids.

Flow unit heterogeneity of a rimmed shelf, Santanyí Limestone, Miocene of Mallorca

Lucy Manifold*, Ahmed el-Bozie, Stefan Schroeder, and Cathy Hollis

*University of Manchester, 4.69 Williamson Building, Oxford Road, Manchester, Lancashire, M13 9PL, United Kingdom

e-mail: lucy.manifold@manchester.ac.uk

Introduction

Carbonate strata deposited in peritidal environments can be important hydrocarbon reservoirs. However, many depositional sub-environments lead to complex facies architecture. Furthermore, diagenetic modification from immediately post-deposition can result in a multitude of pore types and subsequently complex pore networks. Laterally continuous outcrops along the southeast coast of Mallorca provide an excellent opportunity to describe depositional facies and early diagenesis of peritidal environments in detail. The Santanyí Limestone is an Upper Miocene (Messinian, 7.1–5.3 Ma) formation comprising, sub-horizontal limestones and dolomites that onlap thrust and folded Mesozoic to middle Miocene rocks (Arenas and Pomar 2010). These rocks have only undergone slight tilting and flexure, during the late Miocene to middle Pleistocene, and have not experienced significant burial (Arenas and Pomar 2010). This study examines the relationship between the sedimentological and diagenetic evolution of the Santanyí Limestone and its petrophysical rock properties (porosity, permeability, capillary pressure, wettability, and resistivity). The overall aim is to determine the most significant controls on pore network heterogeneity to aid predictability of flow properties in heterogeneous, peritidal limestone formations.

Methods

Field mapping, logging and sampling were used to define lithofacies. From each sample, two plugs of 25 mm diameter were drilled (one perpendicular and one parallel to bedding). The edges were trimmed and used for thin section preparation for microfacies analysis. A ResLab Helium gas porosimeter and nitrogen gas permeameter were used to quantify the pore volume and measure permeability. Resistivity was determined on the same plugs using a CoreLab ARS-250 ambient resistivity core holder. Capillary pressure was determined by desaturation of brine-saturated samples using a porous plate desaturation cell. Wettability was determined by measurement of the contact angle between a flat-sided, dry core plug suspended in a brine, using a high resolution optical camera. All data were measured at ambient conditions.

Lithofacies

Within the study area, six facies and three sub-facies are defined (Table 1) and used to reconstruct the depositional environment (Fig. 1). Back-reef coral rudstones are the most distal outcropping facies, which are dissected by cross-bedded skeletal grainstones deposited within channels up to 50 m wide, which also contain stromatolitic boundstones up to 1.5 m high and 2 m wide. This facies association is pervasively dolomitized. Landward, the grainstones pass into

homogenous mudstones which host oyster-rich rudstone patch-reefs. The fine grain size, abundance of oysters and low faunal diversity all suggest very low energy, wave-protected conditions. Towards the shoreline, molluscan and foraminiferal packstones accumulate and show a high degree of fragmentation. These are interpreted to be subtidal, and to have formed by wave action, and locally by along-shore currents in the west of the study area. Within the peritidal zone, in-situ vertical rhizoliths of mangrove trees are well preserved and calcretes result in partial brecciation. Between mangroves, tidal channels are filled with coquina-type deposits which infill topography and pass landwards by into extensive laminated algal mats that are partially dolomitized.

Diagenesis

The Santanyí Limestone is partially dolomitized. Dolomitization is mostly stratabound, and restricted to stromatolitic boundstone, cross-bedded grainstone, lagoonal mudstone and algal mat facies. The dolomite is finely crystalline and fabric destructive. Where molluscs are abundant, they have commonly been dissolved to form biomoulds, particularly in moldic wack-mudstone. Further dissolution, to create vugs up to 5mm ($\bar{x} = 1$ mm) diameter, has occurred throughout the whole formation. Most limestone facies have undergone calcite cementation in the form of isopachous coating and binding of grains. Karstification is evidenced by a v-shaped collapse structure of phreatic caves, 15 m in length and a 1–2 m deep. Mesopores, several cm in size, are present around the core of collapse structure. Aligned breccia mudstone facies is interpreted to have formed by the collapse structure. It is up to 30 cm thick, occurs infrequently over a lateral distance of 10 to 40 m, between lagoonal mudstone and moldic wack-mudstone, and either thins and grades into dusty marl or pinches out entirely. It comprises partially-cemented plate-like breccia and although it is mud-rich, it is characterized by well-connected vugs.

Porosity and Permeability

Overall, the average porosity is good (4.6% - 41.1%, $\bar{x} = 17.0\%$), whilst permeability ranges between <0.01 mD and 4236 mD ($\bar{x} = 400$ mD). Porosity and permeability show a variable correlation (Fig. 2), which can be subdivided into three groups, A, B and C (Table 1). From this, it can be determined that the best potential flow units are not controlled by facies, but by diagenetic processes. Fabric destructive dolomitization within the algal mat and lagoonal mudstone facies has created a well-connected macroporous pore system. Weakly cemented facies (shell accumulations) have high porosity and permeability. Moldic porosity is the most common pore-type within limestone facies, with the highest permeabilities occurring where densely packed mollusc and gastropods moulds are horizontally aligned, due to along-shore current activity. This characteristic is restricted a sub facies of the moldic wack-mudstones (strata-bound bivalve facies) in the western 600 m of the field area. An increase in micrite and cement (>10%) is associated with decreasing permeability, unless well connected vugs are present. The K_v/K_h ratio from core plugs is <1, demonstrating that permeability is anisotropic throughout.

Core plug resistivity measurements indicate an average Formation Resistivity Factor (FRF) of 1159 (32-5206). The lowest FRF (<100), i.e., the simplest pore system occurs in dolomitized facies (group A) and limestones with high microporosity in Group C (36.8%), whilst the highest

FRF (>1000) occurs in samples with a complex, mixed pore network of moulds and microfractures. The cementation exponent is 2.2. Wettability measurements showed a contact angle of the denser phase (brine) is 26.2° , indicating that the formation is water-wet in an air-brine system, which can be extrapolated to predict oil wettability in a two-phase reservoir.

Conclusions

There is a marked variation in flow properties on multiple scales that demonstrates the complexity of fluid flow prediction in peritidal settings. In most cases, the best potential flow units are controlled by diagenesis (Group A). These samples have experienced fabric-destructive dolomitization (lagoonal mudstone and laminated algal mat facies). Samples of stromatolitic boundstone and cross-bedded grainstone facies could not be obtained but are expected to have similar petrophysical properties due to extensive dolomitization in outcrop. The resultant simple, macropore dominated pore network facilitates high flow rates. A combination of diagenetic and depositional processes, such as alignment of moldic pores by along-shore current activity (strata-bound bivalves, Group A) also enhances permeability (3721 mD) despite moderate porosity (15.2%).

Group B represents samples with the most complex pore networks, indicated by a FRF of >700 (up to >>1000). This group possesses samples which have a range of pore sizes and pore types which are moderately well connected. Vugs are present in all samples which add to this complexity. Some facies in this group have consistently low-moderate permeabilities of <100 mD which are micrite rich (fossil mangroves, brecciated mangroves, moldic wack-mudstone and oyster rich rudstone). The highest permeabilities within Group B are the shell accumulation facies which lack cement and have well-connected macroporosity ($\phi = 15.1\%$, $k = 3271$ mD). This is an unusual observation because the high permeability is controlled by facies type. Diagenesis also degrades permeability, represented by Group C. These samples possess >15% cement, or >10% pore space infilled by cement have low pore connectivity and have low flow potential, despite having high microporosity of up to 36.8%. Over 10% micrite also correlates with low permeability in this group. Partial, fabric-retentive dolomitization in Groups B and C does not improve permeability because it does not form intercrystalline macroporosity as observed in Group A.

Reference

Arenas C, Pomar L. 2010. Microbial deposits in upper Miocene carbonates, Mallorca, Spain: Palaeogeography, Palaeoclimatology, Palaeoecology, v. 297, p. 465-485.

Figure 1: Interpreted reconstruction of the depositional environment of the Santanyí Limestone. In brief, the model portrays a rimmed shelf with five major depositional environments: offshore (not present in outcrop), reef, lagoon, intertidal zone, and tidal flats.

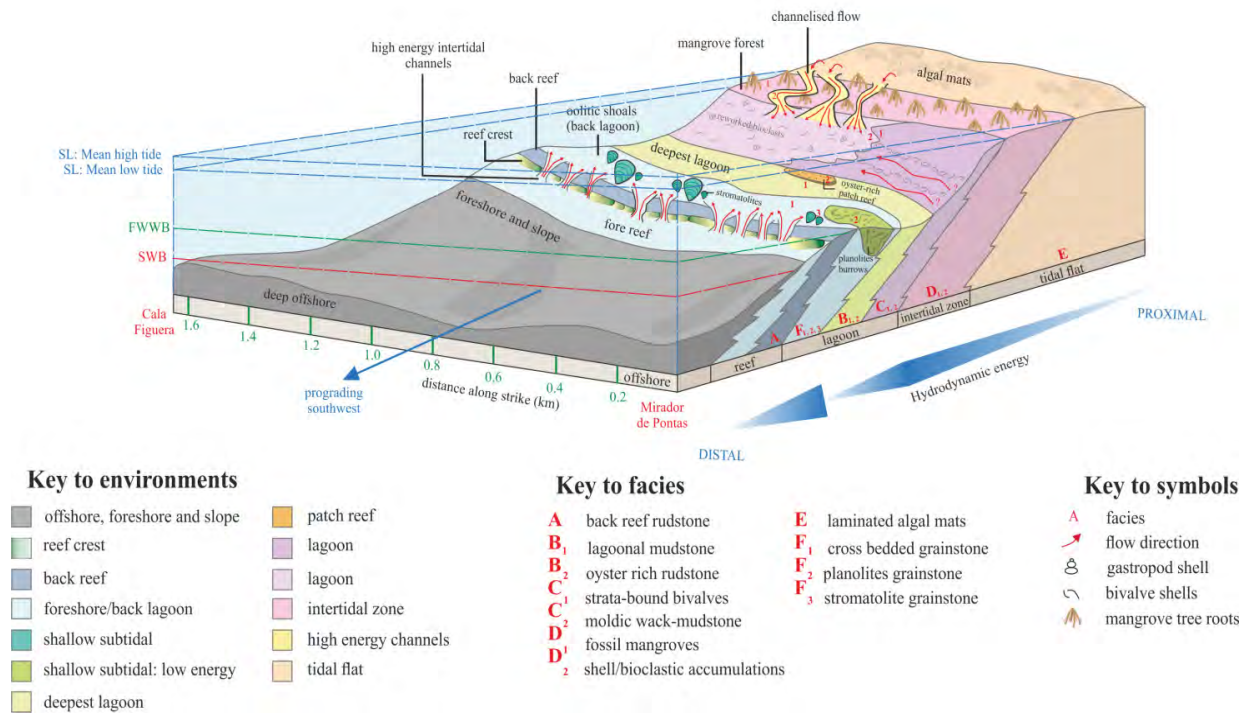


Table 1: Summary of the composition, porosity, permeability and diagenesis of each facies. Letters A-F correspond to the red letters in Figure 1. FD = fabric destructive, FR = fabric retentive.

Lithofacies	Skeletal allochems (listed from most abundant to least)	Coated grains (listed from most abundant to least)	Grain size range	ϕ and k	Pore types	Diagenesis
Back-reef rudstone A	bivalves (0.2 - 2 mm), coralline algae (0.5 - 1.5 mm), miliolids (0.25 mm), gastropods (moulds), bryozoa (0.5 mm), serpulid worm tube, echinoderm	peloids (0.1 mm), grapestone intraclasts (0.3 mm)	0.1 - 3.5 mm \bar{x} = 0.2mm	no data	moldic, interparticle	mechanical compaction, aragonite dissolution, isopachous microsparite
Lagoonal mudstone B₁	miliolids (0.6 mm), gastropods (<2 mm), bivalves - geopetal (0.5 mm), bryozoa (0.9 mm), coral (5 mm), dasycladacean and coralline algae	peloids, elongate (0.01 mm)	0.1 - 5 mm \bar{x} = 0.05 mm	ϕ = 14.2 % (10.5 - 28.6 %) k = 703 mD (6.4 - 1781 mD)	moldic, vuggy, channel (all cemented), + fracture	aragonite dissolution, minor fracturing, FD dolomitization, cementation
Oyster rudstone B₂	bivalves/oysters (0.6 mm), serpulid worm tubes (<0.8 mm), bryozoa (0.8 mm), solitary coral (0.6 mm), miliolids (0.2 mm)	peloids (0.2 mm), ooids (0.2 mm)	0.01 - 1.5 mm \bar{x} = 0.2 mm	ϕ = 15.3 % (7.6 - 23.1 %) k = 9.36 mD (7.5 - 11.2 mD)	moldic, fracture	micrite envelopes, isopachous microsparite, cementation, FR dolomitization
Moldic wack- mudstone C₂	gastropods (2 mm), bivalves (0.8 - 2 mm), miliolids (0.1 mm), fragmented coralline algae (0.1 mm)	peloids, elongate (0.1 - 0.7 mm), ooids (0.1 - 0.7 mm)	0.1 - 2 mm \bar{x} = 0.2 mm	ϕ = 18.3 % (7.0 - 34%) k = 28.5 mD (5.5 - 193 mD)	moldic, fracture, intraparticle	aragonite dissolution, minor fracturing, cementation
Brecciated mangroves and calcrete D₁	miliolids (0.05 - 0.45 mm), bivalves (0.4 mm)	peloids (0.1 mm)	0.01 - 0.45 mm \bar{x} = 0.06 mm	ϕ = 13.1 % (6.9 - 17.4 %) k = 62.8 mD (7.8 - 487 mD)	interparticle, moldic, vuggy	aragonite dissolution, cementation
Mangrove roots D₁	miliolids (0.1 - 0.4 mm), gastropods (0.2 mm), bivalves (0.2 mm), ostracods (0.2 mm), algae?	peloids (0.2 mm), ooids (0.2 mm)	0.01 - 3 mm \bar{x} = highly variable	ϕ = 11.7 % (6.0 - 36.8%) k = 16.77 mD (6.4 - 26.1 mD)	interparticle, moldic, vuggy, channel	aragonite dissolution, cementation, minor fracturing
Skeletal accumulations D₂	gastropods (< 1 mm), miliolids (0.2 mm), fragmented coralline algae, tubular plant, solitary coral	peloids (0.1 - 0.5 mm), ooids (0.3 - 0.5 mm)	0.01 - 12 mm \bar{x} = 0.4 mm	ϕ = 38.5 % (36.0 - 41.1 %) k = 695 mD (223 - 1166 mD)	interparticle, moldic, vuggy	aragonite dissolution, minor cementation
Laminated algal mats E	bivalves (1 - 2 mm), miliolids (0.2 mm), coralline algae (0.5 mm)	peloids (0.05 - 0.4 mm), ooids (0.1 - 0.8 mm), oncoids (0.2 - 1 mm)	0.01 - 0.6 mm \bar{x} = 0.4 mm	ϕ = 29.4 % (28.0 - 30.7 %) k = 2195 mD (12.8 - 5676 mD)	interparticle, moldic, vuggy	FD and FR dolomitization

Figure 2: plot of porosity vs. permeability. There is notable positive correlation between porosity and permeability which can be subdivided in to three groups A, B and C (figure 4). From this, it is clear that a relationship between porosity and permeability is not driven by the facies. Key characteristics which lead to highest permeabilities are fabric destructive dolomitization, alignment of moldic pores (molluscs and gastropods), and lack of cementation (e.q. coquina beds), all of which are evident on outcrop-scale. Minor, fabric retentive dolomitization does not result in enough intercrystalline porosity to produce high permeabilities.

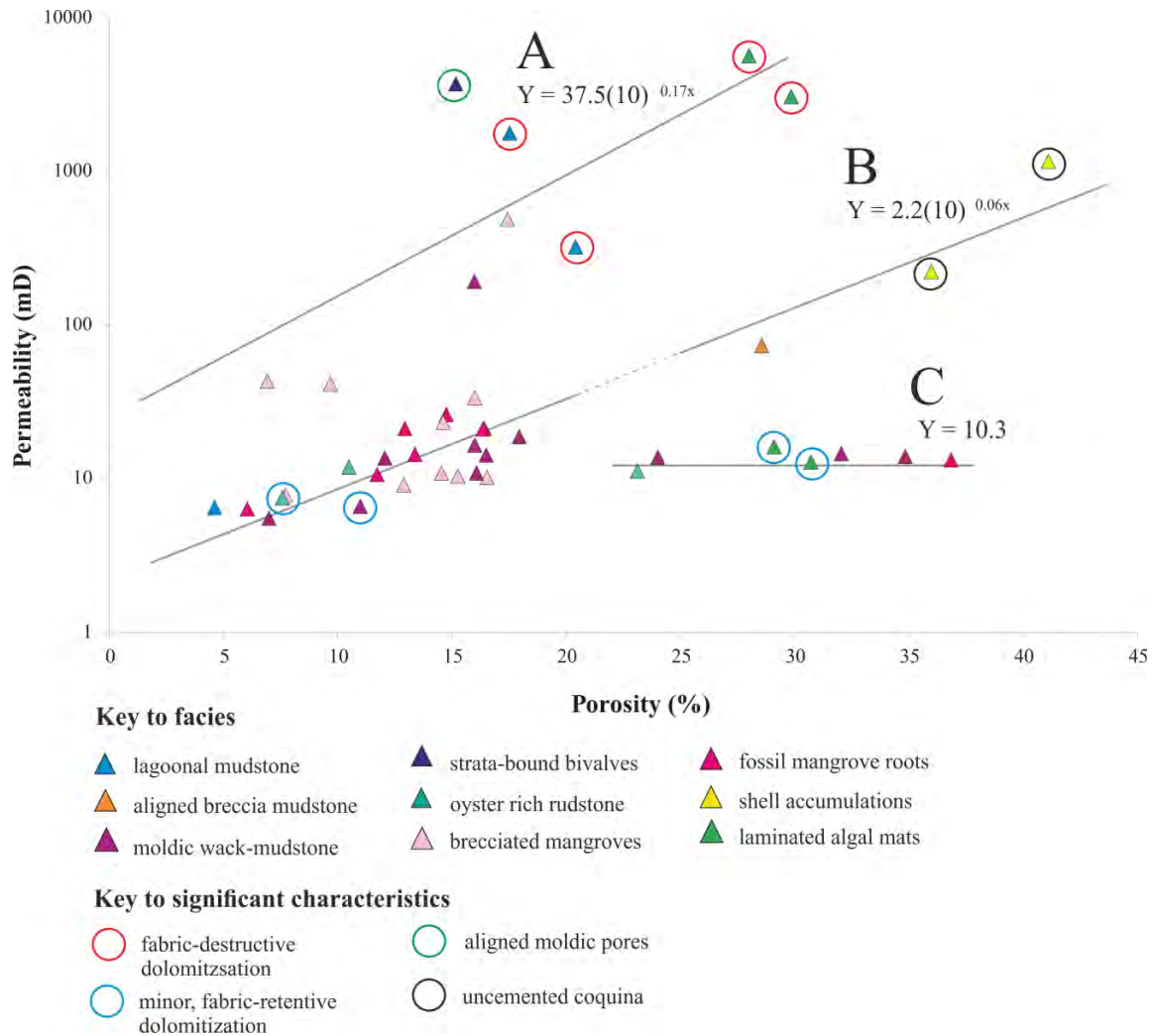


Table 2: key petrophysical and sedimentological characteristics of linear groups defined from plot of porosity vs. permeability

Linear group	Characteristics
A	<ul style="list-style-type: none"> • High k (39.0 - 5677 mD, \bar{x} = 1316 mD), but moderate ϕ (6.9 - 36.0 %, \bar{x} = 20.2 %) • Samples with highest permeabilities are dolomitized, possess aligned moldic pores or • Heterogeneous pore network: moldic (94 % of samples), vuggy (70 %), intercrystalline (47 %, fracture (24 %), and interparticle (12 %) • P_c curves suggest well connected pore network with desaturation of 80 % water at <75 psi • Two samples have FRF, 160 - 180, implying reasonably well connected pore network. • R_o <100 ohm, indicative of conductive fluid path via brine-filled pores
B	<ul style="list-style-type: none"> • Moderate k (65 - 1166 mD, \bar{x} = 192.6 mD), and variable ϕ (4.6 - 41.1 %, \bar{x} = 14.56 %) • Some samples are partially dolomitized but they do not have permeability greater than 7 mD • Lowest permeabilities are associated mostly with mangroves, moldic wack-mudstone, and also non-dolomitized lagoonal mudstone and oyster-rudstone facies • The highest permeabilities are aligned breccia mudstone and shell/bioclastic accumulations. These samples have an aligned pore network or lack cement. • Mixed pore network: vugs (100 % of sample), moldic (75 %), cavern (25 %), channel (25 %) • P_c curves suggest moderately well connected pore network, with desaturation of up to 65 % water at <75 psi • <40 % pore throats are >1 micron • Four of five samples have FRF of >700, with 3 >> 1000 indicating a highly complex pore network. R_o >200 ohm in four of five samples.
C	<ul style="list-style-type: none"> • Invariant k (~10 mD) for a range of ϕ (23.1 - 36.8 %, \bar{x} = 30.1 %) • Limestone, dominated by micrite with cemented moldic pores with few open moldic pores and intergranular space • High porosity suggests high volume of unconnected microporosity • P_c curve (one sample) indicates very poor connectivity of pores (only 16 % water desaturated) • Very low resistivity (11 ohm). Very low FRF suggestive of very simple pore network, perhaps reflecting isolation of porosity.

Unconformity derived controls on the development of porosity and permeability; A case study from the Miocene Cayman Formation, Grand Cayman, British West Indies

Cole Alexander McCormick* and Brian Jones

*University of Alberta, 3415 McKay Lane SW, Edmonton, Alberta, T6W 1L4, Canada

e-mail: camccorm@ualberta.ca

Grand Cayman, the largest of the Cayman Islands, is located in the northwest part of the Caribbean Sea. The Neogene succession is formed of limestones and dolostones that originated on an isolated bank, surrounded by deep oceanic water. This study focuses on the Middle Miocene Cayman Formation, which contains a diverse coral assemblage (domal, platy, branching, free living) as well as bivalves, gastropods, red algae, foraminifera, echinoids, rhodolites, and Halimeda. Most of the formation is composed of fabric-retentive microcrystalline (4–64 μm) dolostones, and varies in thickness from 100 m–120 m. Moldic porosity is high because any allochems originally composed of aragonite have been dissolved. Dissolution fabrics in the Cayman Formation both pre-date and post-date dolomitization. Dolomitization of the Cayman Formation is interpreted to have occurred in two phases: an initial phase of seawater mediated dolomitization, followed by a second phase of mixed meteoric-marine dolomitization. The Cayman Formation exhibits a distinct variation in porosity and permeability between the succession preserved at the base of the formation, and the succession preserved at the top of the formation.

This study outlines the informal division of the lower and upper Cayman Formation as well as the distinct textural differences present across this boundary. The lower Cayman Formation is “soft” with porosities of 34% to 49% (average 42.4%) and K_{max} of 1400 mD to 2810 mD (average 2060 mD). The upper Cayman Formation is “hard” with porosities of 7% to 37% (average 20.2%) and K_{max} of 29.2 mD–2200 mD (average 832.6 mD). There is also a distinct contrast in porosity styles present above and below this unconformity. The lower Cayman Formation is dominated by fabric selective dissolution, resulting in fossil moldic porosity. In contrast, the upper Cayman Formation exhibits fabric non-selective karst features, as well as terra rossa, flowstones, and Caymanite (a laminated cave-filling deposit) that occlude porosity. The contact between the lower and upper Cayman Formation is interpreted as a diagenetic boundary, formed during the Burdigalian–Langhian lowstand. This lowstand, however, is a lower order event than that of the Chattian (Upper Oligocene) and Tortonian to Messinian (Upper Miocene) lowstand events that bound the Cayman Formation. This research provides implications for unconformity derived controls on the development of porosity and permeability in isolated, island settings. These parameters directly affect the styles of porosity exhibited in a given succession; a key feature which can be tied to the magnitude and variability of reservoir quality.

Characterization of carbonate microfacies and reservoir pore types based on formation microimager logging: A case study from the Ordovician in the Tahe Oilfield, Tarim Basin, China

Miaomiao Meng*, Tailiang Fan, and Ian J. Duncan

*China University of Geosciences, No 29 Xueyuan Road, Haidian District, Beijing, 100083, China

e-mail: mmm1988@126.com

Improved reservoir characterization requires a clear understanding of microfacies and pore types. Carbonate microfacies and reservoir pore types are poorly studied in Middle–lower Ordovician of the Tahe Oilfield in Tarim Basin due to the limitation of cores and poor seismic data. Formation MicroImage logging (FMI) provides a bridge to connect the core data and seismic data to study the distribution of microfacies and pore types. However, no research on the identification of carbonate microfacies and few work on the reservoir pore types from FMI have been done in Ordovician of the Tahe Oilfield. Base on the FMI data of 8 wells calibrated with core samples, thin sections and conventional well logs, five FMI microfacies models are established: (1) intershoal sea microfacies (ISMF); (2) low-energy shoal microfacies (LSMF); (3) high-energy shoal microfacies (HSMF); (4) lagoon microfacies (LMF); and (5) tidal flat microfacies (TFMF). The application of FMI microfacies models shows that Yingshan Formation was deposited both in a restricted platform (characterized by the development of LSMF, HSMF, LMF, and TFMF) and an open platform (characterized by development of ISMF, LSMF and HSMF). Three reservoir pore types are identified from FMI: pore (laminated pore and isolated pore), vug and fracture (angle fracture and conjugate fracture). The relationship between microfacies and reservoir pore types indicates that the sedimentary microfacies plays a key role in the reservoir development, among which shoal microfacies (HSMF and LSMF) are the most favorable facies for reservoir development. This study shows that the effectiveness of identifying and mapping carbonate microfacies and reservoir pore types by using FMI logs data in predicting potential reservoirs in subsurface.

Dual pore system in Upper Cretaceous chalk, onshore Denmark

Aurelien Meyer*, Peter Frykman, and Lars Stemmerik

*University of Copenhagen, Øster Voldgade 5-7, 1350, Denmark

e-mail: aurgab@snm.ku.dk

The Upper Cretaceous–Lower Tertiary chalks of Northern Europe contain large volumes of hydrocarbons, estimated around 6 BB of oil and 15 TCF of gas. However, producing oil from chalk reservoirs constitutes a challenge, partly because of the complex distribution of porosity and the low matrix permeability associated with high porosity. Numerous factors control the reservoir quality of chalk both at the micro- and macro-scale, including grain size distribution and mode of deposition, clay and silica content, diagenetic evolution, tectonic fracturing, oil charge and overpressure. Resedimented chalk commonly has higher porosity than pelagic bioturbated chalk. Porosity tends to be higher in clean chalk than in marly or chert-rich limestones. Calcite cementation may be either detrimental or beneficial for porosity preservation, depending on whether it occludes the pore space during burial or produces a solid framework which can inhibit pore compaction. Finally, open fractures do not contribute significantly to the total pore volume but may enhance permeability by several orders of magnitude where they concentrate. Understanding the relationship between the oil-hosting matrix microporosity and oil-draining fracture network is therefore critical but difficult to accomplish on cores from reservoirs. The current research focuses on outcrop analogues in northern and eastern Denmark of the upper Maastrichtian Tor Formation, the most prolific chalk unit in the offshore reservoirs. Its purpose is to investigate the distribution of the dual pore system of deep reservoirs by analysing outcrop analogues at different scales and resolutions. Virtual 3D outcrop models of quarries allow mapping the distribution in microfacies, depositional structures and fracture network at the metre to kilometre scale. A large amount of conventional plugs provide information on the variability of matrix porosity and permeability at the decimetre to metre scale. Finally, SEM analyses of selected samples give an insight into the rock framework, composition as well as the structure of the matrix pore system at the nanno- and micron-scale. This multi-dimensional and—disciplinary study aims to eventually propose an innovative approach to predict the distribution of porosity and permeability of chalk.

Reconstruction of porosity evolution through digital image analysis

Aurelien Meyer* and Cathy Hollis

*University of Copenhagen, Øster Voldgade 5-7, København K, 1350, Denmark

e-mail: aurgab@snm.ku.dk

Porosity distribution in carbonate petroleum reservoirs is commonly controlled by a combination of factors, including depositional texture, geochemical and mechanical processes. Without a clear knowledge of these parameters, the prediction of reservoir properties is speculative. Reservoir models often require the implementation of permeability-modifying coefficients to match the actual reservoir behavior during production. The discrepancy between predicted and actual reservoir behavior is usually poorly understood, arguably in large part because a strong, geological process-driven model is missing. This study provides an innovative methodology to understand what has spatially and temporally controlled the distribution of porosity by back-stripping pore evolution and defining diagenetically-controlled pore fabrics. Importantly, the methodology relies on a sedimentological and structural framework which should be in place prior to such study. First, pore types and cement types should be quantified and the relationship between these parameters, lithofacies and reservoir quality should be analyzed. Second, a pore fabric scheme, which considers the depositional texture, pore types and shapes and the impact of pore-filling cements should be established in order to combine these parameters in a practical manner. Third, mapping the distribution of open and cemented porosity at several key stages of the burial history and the final distribution of pore fabrics should provide the framework in which the diagenetic reconstruction can be implemented. Finally, by combining the diagenetic model and the mapped pore-fabric distribution, petrophysical rock types can be defined that honor those geological process that led to the formation of the final pore network. The methodology is introduced here using a virtual database but was previously tested on a multiscale, multimodal pore network (Lower Cretaceous oil reservoir, Middle East).

The creation of diagenetic facies utilizing core, thin section and MICP data as an input into reservoir rock typing and subsurface modelling studies

William Mills*, Claire Gill, Edward Jarvis, Michael Harrison, Michael Bent, and Ceri Davies

*Robertson/CGG, Tynycoed, Llanrhos, Llandudno, Conwy, LL30 1SA, Wales, United Kingdom

e-mail: William.Mills@CGG.com

Reservoir rock typing (RRT) and subsurface modelling studies often rely on an input linking sedimentological and petrophysical characteristics. When coding routine core analysis (RCA) data points by depositional lithofacies there is often an inadequate link between reservoir quality and depositional lithofacies; this is due to the impact of post depositional diagenetic processes. Using core and thin section observations combined with analysis of RCA and mercury injection capillary pressure (MICP) data, a workflow has been conceived to group facies with similar pore networks. The identification of key controls on reservoir quality created a 'shortlist' of parameters by which the geological data could be coded. However, in order to further qualify the geological inputs it was important to also integrate the MICP data. Although MICP data is primarily used to statistically characterize the petrophysical rock-types, the MICP curves also give important information on pore throat sizes and hence reservoir quality. The curve shape for each sample was reviewed and they were visually grouped, separating out microporous, macroporous and bimodal pore systems. Once the classification of MICP data was completed, these geological MICP groups were plotted in the porosity/permeability domain and showed good discrimination. The groups then formed the preliminary basis for assigning diagenetic facies. The data within each geological MICP group was compared for similarities – i.e. were there any common features within the group? For example high amounts of cementation, close proximity to stylolites or stratigraphic position. Based on these observations, the diagenetic facies were created. It was important to ensure the diagenetic facies were defined by characteristics that would be identifiable across the remaining cored intervals using the core description data. Because depositional facies did not show good discrimination of reservoir quality in the core for these reservoirs, the diagenetic facies are important as they will form the basis of the geological calibration of the log data. In turn, therefore, they are the main link between the rocks and the electrofacies/RRT. The limitation when upscaling the diagenetic facies to the log domain is that they are mainly characterized by permeability variation, therefore the log domain alone cannot capture this variation. However, the process of attempting to integrate geological data allowed a better understanding of the geological background of the petrophysical data set. The best diagenetic facies were linked to the best rock types (in terms of reservoir quality properties).

Cement diagenesis of Mississippian carbonates in the southern midcontinent of the USA

Sahar Mohammadi*, Taylor A. Ewald, and Jay M. Gregg

*Oklahoma State University, 1200 N Perkins Rd., Stillwater, OK, 74075, USA

e-mail: smoham@okstate.edu

Mississippian carbonate rocks on the southern midcontinent of North America comprise an important unconventional as well as conventional petroleum play. This study indicates that the Mississippian carbonates have a very complex diagenetic history, continuing long after early diagenetic cementation. Possibly the most important diagenetic events affecting these rocks occurred during burial and basinal fluid migration through these strata. The area studied extends from the Cherokee–Ozark platform region of southwestern Missouri, northwestern Arkansas, and northeastern Oklahoma to the Nemaha Ridge area of north-central Oklahoma. Mississippian rocks in the Cherokee–Ozark platform region are dominated by cyclic ramp-shelf margin carbonates consisting mainly of wackestones to grainstones that are infrequently dolomitized and in north-central Oklahoma by deeper water carbonates mainly comprised of partially dolomitized argillaceous mudstones interbedded with fine-grained wackestones to grainstones.

Inter-grain, intra-grain, vug, fracture, and breccia open spaces are the most common porosity types encountered in Mississippian carbonate rocks of this study. Early diagenesis primarily involved intra- and inter-grain calcite cementation and minor dolomitization in a seawater environment followed by mixed seawater-freshwater phreatic cementation. Late diagenetic calcite, dolomite, and quartz cements that fill remaining intra- and inter-grain porosity as well as vugs, fractures, and breccia were alternately precipitated by moderately saline and very saline basinal fluids at temperature ranging from $\sim 50^{\circ}$ to 175° C (based on fluid inclusion microanalysis). These fluids also are responsible for the ore deposits of the Tri-State Mississippi Valley-type mineral district, which is a major geological feature of the Cherokee–Ozark platform region. Mississippian rocks in the Cherokee–Ozark platform region retained much of their porosity until late in their diagenetic history. This is indicated by the observation that intra- and inter-grain porosity in the Cherokee–Ozark platform region contain both early diagenetic followed by late diagenetic cements. In contrast, most of the intra- and inter-grain porosity in the Nemaha Ridge region was completely filled by early marine and phreatic cements, with very little open space remaining, and late diagenetic cements in this region are largely confined to later formed fracture and breccia porosity. Late diagenetic saline basinal fluids likely were sourced by underlying Cambrian–Ordovician strata and moved up through faults and fractures into Mississippian strata, displacing less saline resident fluids. This fluid movement likely occurred during the Ouachita Orogeny and coincided with Petroleum migration into the Mississippian rocks. Petroleum is thought to have been sourced from the Devonian Woodford Shale, which immediately underlies the Mississippian section.

**Evaluating multiscale permeability in modern carbonate settings:
implications for flow in carbonate reservoirs**

PJ Moore*, Christine Bachtel, Tony Buono, Shawn Fullmer, Brian Kelley, Jason Gulley, and Charles Kerans

*ExxonMobil Upstream Research, 22777 Springwoods Village Parkway, Spring, TX 77389, USA

e-mail: pj.moore@exxonmobil.com

Permeability in carbonate reservoirs depends on the distribution and interconnectivity of different pore types that range in size from microporous voids at the micron scale to caves at the meter scale. Most measured values of porosity and permeability occur at the core plug and whole core scale (~2–10 cm), which often fails to capture the larger pore space commonly responsible for flow elevated above the contribution expected from the rock matrix. Although pressure build up tests and PLTs may indicate that elevated flow is occurring within a well, linking this flow behavior to a scale dependent pore system often remains elusive. Understanding this connection between flow behavior and the pore system is a critical step required to accurately predict carbonate reservoir performance.

In order to address how different pore systems impact flow, we developed a field-based, dynamically-calibrated approach on San Salvador Island, Bahamas, that combines stratigraphy, pore type characterization, and hydrogeology across a number of features ranging multiple orders of magnitude in scale from micro-pores to caves. Integrating variations in tidal lag and tidal magnitude, otherwise known as hydrogeologic surveillance, observed in wells representing matrix properties and in natural conduits allows us to develop a more holistic understanding of the dynamic behavior of the multi-scale pore system. Porosity and permeability values are derived from standard techniques, such as routine core analysis at the core plug and whole core scale. Permeability is calculated using hydrologic monitoring data within larger scale-dependent pore types, e.g., sinkholes and caves. LIDAR data and detailed feature surveys are used to calculate porosity within these larger scale features. Preliminary estimates of effective permeability across multi-scale pore systems determined from hydrogeologic surveillance agrees with values determined from well test analysis in producing reservoirs with known dual porosity behavior. This work suggests that understanding the controls on permeability across multiple scales in modern carbonate settings may provide key insight on predicting how carbonate reservoirs will flow.

Carbonate pore system characterization and porosity prediction using multi-scale data

Kazumi Nakamura*, Neil F. Hurley, and Tao Sun

*Chevron, 1500 Louisiana St., Houston, TX, 77002, USA

e-mail: kazumi.nakamura@chevron.com

Heterogeneity is a complex characteristic of carbonate rock pore systems, defined by pores of various shapes and sizes across multiple scales. Key questions remaining in reservoir characterization and modeling are (1) at what scale is a system accurately defined, and (2) can measurements taken at the core- and thin section-scale (mm–cm) be used to accurately predict porosity values at the reservoir scale (cell size of 10s~100s meters)? This study examines thin section (mm–cm) and confocal (mm– μ m) photomicrographs from a suite of carbonate rocks with varying depositional and diagenetic histories in order to address this issue. We examine pore size distributions at these different scales and find that the data sets can be modeled by power law functions. Furthermore, these multi-scale data sets can be collapsed to a single power law function if they are normalized to the size of the sample. By using such power laws to model our data, we are able to predict porosities at the scale of interest (up- and down-scale from those observed and measured). This multi-scale method allows us to integrate the measurements at all scales and predict corresponding porosities, taking into account contributions of pores with sizes much greater than that of the sample.

**Integrated reservoir characterization of the Duvernay Play (Alberta, Canada):
Economic sweet spot in unconventional source rock play**

Aurelien Pierre*, Tara Branter, Annie Cox, and Kevin Mageau

*Repsol Oil & Gas Canada Inc., Suite 2000, 888 - 3rd St S.W, Calgary, Canada

e-mail: apierre@repsol.com

The Duvernay Formation has been known for decades as the source rock of the Leduc and Swan Hills oil and gas plays. Today, the Duvernay Formation is also known as an attractive unconventional play because of its ability to produce gas-associated liquids. Duvernay producers want to maximize liquid production in order to improve economics. We believe that diligent reservoir characterization is the key for economic success in this deep unconventional play. However, one has to adapt to the scale of the observation of unconventional resource plays (1 nm to 1 micron) and to use special imagery techniques (e.g., SEM, Ion-milled SEM) to characterize the nature and classes of the pore system. For the Duvernay Formation, porosity typing was conducted on 2D and 3D Focused Ion Beam SEM images. These images showed that between 69% and 85% of the porosity is kerogen porosity with an average of 75% for the studied wells. It is important to recognize that although organic porosity is also developed in the less mature wells, the biggest pores were found in the most mature areas. Careful pore measurement allowed a quantified approach. Liquid yield was plotted against average pore size and a clear trend was seen in the pore size distribution. "Pore size" tends to increase with maturity. The pore volume and/or the number of accessible pores would increase (increase in adsorbed gas and HC in pore volume; and thus, in permeability) following the same trend as the mean pore size. With caution, if additional observations from other wells in the Duvernay play confirm these observations, we can conclude that the porosity and more importantly the permeability are primarily the result of thermal maturation of the kerogen. Some previous studies did not find the same results due to an erroneous estimation of maturity using vitrinite reflectance whereas some other studies did not have the appropriate diversity and quality of sample throughout maturation phase window to obtain statistically representative results. This nanoscale pore system characterization is integrated at the regional scale with subsurface data (wells, seismic), outcrop work from literature and public domain production data.

**Biochemical and stratigraphic controls on pore-network evolution:
The Phosphoria rock complex (Permian), Rocky Mountain region, USA**

Maxwell Pommer* and J. Frederick Sarg

*Colorado School of Mines, 16630 Golden Hills Road, Golden, Colorado, 80401, USA

e-mail: mpommer@mines.edu

Pore systems in the Phosphoria Rock Complex (PRC), Rocky Mountain Region, USA, evolved as a systematic response of biota, sedimentation, and near-surface chemical diagenesis to dynamic paleoenvironmental conditions across the Middle to Late Permian. These environmentally sensitive and interrelated responses coevolved and varied systematically stratigraphically and regionally, resulting in systematic development of prolific reservoir porosity and organic-matter (OM)-rich phosphatic deposits. Near-surface biochemical and shallow-burial processes directly affect the pore network and control diagenetic pathways through burial. This study integrates stratigraphic, geochemical, and petrographic datasets to determine the evolution of this unique sedimentary system deposited during a pivotal climatic shift in Earth history.

Deposition of the PRC occurred over a tectonically influenced second-order transgressive-regressive cycle (~8–14 My duration) overprinted by three (Grandeur, Franson, and Ervay) third-order cycles (~2–5My duration). Biotic, chemical, and porosity trends show pronounced shifts across systems tracts in the Franson and Ervay cycles. This evolution was driven by basin configuration and circulation patterns, global changes in sea-level and sea-water chemistry, and by a major transition from icehouse to greenhouse climatic conditions.

Accumulation and microbial breakdown of sapropelic OM and resulting phosphatization dominated sedimentation in lowstands and early transgressions in distal settings. OM-rich sediments contain small pore volumes (median 4.0% at $R_o \sim 2.0$) comprised of OM-hosted, interparticle, and intraparticle pores. OM-rich sediments were subjected to porosity loss through compaction and incursion of bitumen, as well as generation of small volumes of OM-hosted porosity through burial. Phosphorites contain small pore volumes (median 2.1%) dominated by intraparticle and interparticle pores commonly cemented with authigenic carbonate fluorapatite, silica, calcite, and dolomite.

Spiculitic cherts and calcitic biota (bryozoan, brachiopod, and crinoid) dominate sedimentation through late transgressions and early highstands seaward of bioturbated dolomite muds and peritidal sediments. Calcitic-biota debris are commonly calcite cemented, partially dolomitized, and host pore volumes (median 4.5% in transgression and 15.2% in highstand of the Ervay) dominated by interparticle, and intraparticle porosity. Authigenic silica is abundant in late transgressions and early highstands. Spiculitic cherts contain small pore volumes (median ~3.5%) comprised of intraparticle, interparticle, fracture, and moldic porosity.

Sedimentation in late highstands was dominated by peritidal microbial communities, bioturbated muds and sandstones, ooids, mollusks, and phylloid algae landward of silicisponges and calcitic

biota. Late- highstand carbonates are pervasively dolomitized, partially silicified, and host abundant porosity dominated by intercrystalline, moldic, fenestral, and interparticle pores. Porosity averages ~9.8% and ranges up to 25.3% in samples from the Ervay highstand in the Bighorn basin.

**CT scanning analysis for porosity and development of a permeability log:
Upper Cambrian microbial build-ups, Mason County, Texas**

Jacob Proctor*, Heath Hopson, André Droxler, Naum Derzhi, Jeffrey Dravis, Paul (Mitch) Harris, Pankaj Khanna, and Daniel Lehrmann

*Rice University, 6100 Main St., Houston, TX 77005, USA

e-mail: jmp10@rice.edu

Although rare in the past, major oil and gas discoveries in offshore Brazil and Angola have triggered an increased focus on the petrophysical properties of microbialite carbonates. Due to an extreme heterogeneity of porosity in microbialites, petrophysical studies commonly lack a robust workflow that will take into consideration the many scales of analysis necessary for adequate characterization. Computed tomography (CT) can quantify micro (0.01 mm) to vugular (40 mm) pore sizes, and Dual Energy CT scanning can measure the proportions of calcite, dolomite, clay, and total porosity at every 0.5 mm in the form of a log. The objectives in this study were to define total porosity, permeability, pore type, and pore throat size for three related microbial textures. Data points were then upscaled to dual energy logs calculated from short drill cores, using a new rock typing method—Genetic Rock Typing (GRT).

The field study area encompasses Upper Cambrian microbialite reefs, uniquely cropping out along the James River in Mason County, Texas. Outcrops are cliff and pavement exposures that together offer 3D views of the reefs sufficient to understand their overall evolution. Three primary textures were observed in outcrop: rinds of microbial build-ups, the microbial build-up interiors, and inter build-up sediments. Each texture was uniquely affected by diagenesis and displays unique trends in porosity, permeability, mineralogy, and pore throat size. Three-inch diameter whole cores (126 in total) were collected using a hand held drill to characterize the microbial textures. Thirty plugs, 1 inch in diameter, were extracted from a subset of the cores from which thin sections, helium porosimetry, mercury injection capillary pressure (MICP), and micro CT analyses were performed.

Porosity types observed in the build-up rinds include micro, micro-moldic and vugular porosity associated with sparry calcite cement. The average total porosity measured with helium porosimetry and MICP is 1.5% with the average permeability equaling 0.002 mD. The most frequently occurring pore throat sizes in the rind are 0.01 to 0.024 microns diameter. Porosity types observed in the build-up interiors are micro-pores; vugs, and pressure solution seams and stylolites in calcite cement, and intercrystalline and moldic pores in dolomite. The average total porosity is 2.6% and the average permeability is 0.25 mD. The most frequently occurring pore throat sizes in the build-up interiors are between 0.03 to 0.2 microns diameter. In the inter build-up sediment, porosity types include micro, micro-moldic and vugular pores in calcite cement, and pressure solution seams and stylolites, intercrystalline and moldic pores in dolomite and skeletal grains. The average total is 5.3% with the average permeability equaling 3.03 mD. There are 3 dominant pore throat size ranges: 0.06 to 0.12, 0.2 to 1.6, and 2.4 to 16 microns diameter, respectively.

The GRT method was developed from the dolomite log in order to upscale the geologic and petrophysical properties to the 3 microbial textures observed in whole core. GRTs begin to describe the genesis of pores and minerals, and whether they are primary or secondary in origin. Each texture had two GRTs that were defined with the dolomite log by using the average percent dolomite as a cut off for each texture. Each one of the six GRTs had a unique porosity and permeability trend. Every 0.5mm the porosity log yielded an average porosity value that, when related to the designated GRT's porosity and permeability trend, had an associated permeability value. This resulted in a permeability log. The workflow produced mineralogy, porosity, and permeability logs, but more importantly, it provided a framework to upscale geologic and petrophysical analyses to the whole core in a manner that stays true to the natural geologic and diagenetic variability of the rock.

Characterizing microporosity: a case study from an offshore field in Qatar

Stacy L Reeder*, Austin Boyd, Diana Acero-Allard, Ahmed M Shoman, Ahmed A Fotoh, Sergio L De Almeida Netto, Bovann K George, Omar S. Al-Jaaidi, Deborah Bliefnick, Weishu Zhao, Mohammed Al-Ali, and Emhemed Abousrafa

*Schlumberger, 1 Hampshire Street, Cambridge, MA, 02139, USA

e-mail: sreeder@slb.com

Microporosity is an important aspect of many carbonate reservoirs because the presence of these small pores can influence log responses and flow properties. To properly characterize a reservoir and evaluate the hydrocarbon saturation, it is necessary to identify and quantify different classes of pores and how they influence the petrophysical parameters.

The studied reservoir is almost entirely microporous. Therefore, it provides a good case study for evaluating a new workflow to quantify microporosity using core and log-based analyses. The core analysis includes laser scanning confocal microporosity, mercury injection capillary pressure (MICP), and 3D pore network modeling. MICP signatures assisted in defining rocks of similar petrophysical types, and these rock types were used to propagate results throughout the reservoir. It was possible to quantify the microporosity using confocal microscopy for thin sections from each rock type. This new development is required because traditional 10x microscopy of thin sections has a resolution limit of 10 microns, which is too large to image micropores. Confocal microscopy, however, can resolve pores to 0.250 microns, which is sufficient to image the micropores in the Arab D carbonates. The digital rock modeling assisted in investigating the effect of microporosity on electrical parameters for the different rock types.

The log analysis includes nuclear magnetic resonance (NMR) logs and borehole images to quantify the porosity types and evaluate diagenetic effects on different reservoir facies, along with other standard logs. By combining the core and log measurements, it was possible to quantify the microporosity and compute a continuous log of the microporous fraction within the wells from the spectral decomposition of the NMR response. For this study, it was also possible to estimate the microporosity from the borehole image logs in cases where NMR was not available. Further analysis showed that the microporosity greatly influenced Archie's saturation exponent, n . Properly characterizing the fraction of microporosity and computing a variable n weighted by this fraction, reduced the estimated water saturations by 20%, increasing estimates of original the oil in place.

This case study helped define a multi-disciplinary workflow that can be used to quantify microporosity in carbonate reservoirs. Quantification of microporosity in carbonates can greatly increase the understanding of these reservoirs for more effective development.

**Short-cores from proximal and distal positions in the prograding
Vaca Muerta Formation, Neuquén Basin, Argentina**

Laura E. Rueda-Sánchez*, Gregor P. Eberli, Donald F. McNeill, Ralf J. Weger, Max Tenaglia,
Leticia Rodriguez Blanco, and Peter K. Swart

*RSMAS–University of Miami, 4600 Rickenbacker Causeway, Key Biscayne, FL, 33149, USA

e-mail: lrueda@rsmas.miami.edu

Eighty 1 m short cores of the early Tithonian–Valanginian Vaca Muerta Formation display the sedimentary characteristics of calcareous and siliciclastic mudstones in the Neuquén Basin and also display the different mixing motifs in the proximal and distal portions of the basin. Although bioturbation is ubiquitous, laminations and foresets indicate bottom currents and repeated low-oxygen conditions throughout the deposition of the Vaca Muerta Formation (VM). Most porosity in the formation is microporosity ranging from 0 to 32% but are skewed towards the single digit values.

Representative lithofacies and their porosity and permeability values will be presented in this core display. Twelve main lithofacies are identified within the VM. The collected cores represent the mixed calcareous-siliciclastic nature of the VM depositional system; sandstones and calcareous facies dominate the proximal position, while siliciclastic to partially calcareous facies control the center of the basin. The cut and polished cores display with great detail the sedimentary structures of the fine-grained facies that include, in addition to bioturbation, layering (microbial lamination) and fine laminations from bottom currents that are rarely evident or well preserved in outcrop. In cores drilled in a proximal position (Sierra de la Vaca Muerta), the sedimentary structures include cross-bedding, faint and fine-plane and inclined parallel-lamination, and small-scale ripples. Cores from the distal-basin center (Puerta Curaco and Yesera del Tromen) display predominantly fine plane-parallel lamination and few small-scale ripples. The fossils content in the cores consist of ammonites, oysters, gastropods, shells, bivalves, fish scales. Microfossils are mainly benthic foraminifera, radiolarian, and sponge spicules. The XRD analyses show that calcite, quartz, pyrite, montmorillonite and plagioclase feldspar are the dominant minerals, while dolomite and albite are less abundant. Cores drilled through concretions display preservation of sedimentary structures and uncompact skeletal grains and peloids. Overall, both proximal and distal cores show varying degrees of bioturbation. Some intervals lack bioturbation but instead contain fine plane laminations. Most lamination is parallel but low-angle foreset bedding is also observed. The current induced laminations indicate that benthic currents were present in the basin during the time of deposition of the VM Formation.

A classification of chalk microtexture to better understand petrophysical properties

Jessica Saiag*, Pierre-Yves Collin, Jean-Pierre Sizun, Bruno Caline, and Éric Lasseur

*University Bourgogne Franche-Comté, 6 boulevard Gabriel, 21000 Dijon, France

e-mail: saiag.jessica@gmail.com

Chalk is defined as a microporous reservoir rock, a prolific hydrocarbon-bearing reservoir in the North Sea, and also one of the main aquifers in the Paris Basin (France). In the study area (Normandy cliffs, France), taken as an outcrop analogue, 114 samples (Cenomanian–Santonian) were collected. As in the North Sea fields, these samples show great petrophysical heterogeneity: total porosity from 6.1 to 46.5%, very low permeability (0.002 mD) to atypical high permeability (477 mD; without fractures), and P-wave velocity on water-saturated samples ranging from 1.8 to 5.5 km.s⁻¹. The origin of this great variation in petrophysical parameters is, as yet, poorly understood.

The classification of chalk microtexture proposed here should contribute to better explain this petrophysical variability. Microtexture describes the type of particles and their arrangement in matrix samples at Scanning Electron Microscopy scale. Four groups of criteria are proposed to characterize chalk microtexture: mineralogical content, biogenic fraction (<10 μm), micritic fraction (<10 μm), and cement fraction (>10 μm). From these criteria, two major groups are defined: Pure Chalk Microtexture (Microtextures 1 to 7); and Impure Chalk Microtexture, which is subdivided into two subgroups - Argillaceous Microtexture (dispersed clays, unoriented clays, oriented clays, and draped clays) and Siliceous Microtexture (spherulitic opal-CT and draped opal-CT). The Pure Chalk Microtexture group reflects the intensity of modification during diagenesis (rate of diagenesis, whether early stage or not). The transition from Microtexture 1 (initial microtexture) to Microtexture 7 results from increasing diagenetic intensity. Diagenetic transformation induces a decrease in pore size, with better grain contact, but not a decrease in pore-throat size. These transformations explain the decrease in porosity, the improved propagation of acoustic P-wave velocity and the absence of any specific variation of permeability with increasing diagenetic intensity. For the Impure Chalk Microtexture group, the percentage of carbonate content is not linked with porosity, but the type of non-carbonate particles can affect porosity (e.g., fibrous clays). Non-carbonate particles reduce pore-throat size (Mercury Injection Capillary Pressure data), thus explaining lower permeability than for Pure Chalk Microtexture at a given porosity. Microtexture variability and the resulting petrophysical heterogeneity are therefore related to initial sedimentation and diagenesis.

Diagenetic influences on the Pennsylvanian platform-top karstic system of Valdorria, northern Spain

Nabil A. Shawwa*, Valentin Chesnel, Branimir Šegvić, Óscar Merino-Tomé,
Luis Pedro Fernández, and Elias Samankassou

*University of Geneva, Rue des Maraîchers 13, Geneva, 1205, Switzerland

e-mail: Nabil.Shawwa@etu.unige.ch

Repetitive and short-lived glacial events linked to high-amplitude glacio–eustasy during the Late Paleozoic Ice Age subaerially exposed platform tops during sea-level lowstands. Such phenomena have led to (i) karstification, (ii) paleosol profile accumulation, and (iii) precipitation of meteoric cements. The isolated carbonate platform of Valdorria, presently exposed in the Cantabrian Mountains of Northern Spain as part of the Valdeteja Formation, represents a good opportunity to study the impact of such sea-level fluctuations on the development and evolution of pore systems. The platform developed during the Bashkirian (Pennsylvanian) in the Variscan foreland basin, which is nowadays known as the Cantabrian Zone of the Iberian Massif. Variscan tectonism eventually deformed the foreland basin causing the platforms dip to be nearly 90° exposing a complete lateral and vertical transect of its stratal patterns.

The top of the platform is of particular interest because it exhibits an extensive paleokarstic system related to a major emersion event as a result of a significant sea-level drop. The paleokarstic system can be presently observed to reach stratigraphic depths of at least 150 meters extending from the top of the platform. Extensive dissolution of the limestone parent rock is most likely a product of significant weathering during subaerial exposure, which is characteristic of a wet climate. Voids of the ancient cavern system were predominantly filled with fine-grained calcite reminiscent of a collapsed system and sucrosic dolomite that occurs locally as laminated features. Among clay minerals present in the carbonate-dominated voids is kaolinite, which supports the interpretation that the karstic system developed in a wet climate. Furthermore, other platform top cavities have been cemented by blocky sparite and rarely by blocky dolomite indicating that some pores were not fully infilled or cemented until deeper burial conditions. Cathodoluminescence combined with geochemistry confirms this interpretation. The Valdorria platform, along with its pore system, is exposed at the surface making it of interest as an analogue to buried Carboniferous hydrocarbon-bearing reservoirs such as those of the Caspian Basin. The stratigraphy of Valdorria shows that diagenesis is the major process controlling the pore development and sealing during platform growth and burying activity.

Lithofacies and diagenetic controls on dolostone reservoir quality for the Lower Cambrian Longwangmiao Formation in central Sichuan Basin, SW China

Shuyuan Shi*, Hu Suyun, Fu Qilong, Liu Wei, and Huang Qingyu

*Research institution of petroleum exploration & development, Petro china, NO.20 Xueyuan Road, Haidian District, Beijing, 100083, China

e-mail: shishuyuan25@petrochina.com.cn

A large gas reservoir was discovered in previously unproductive dolostone in the Longwangmiao Formation, of the central Sichuan Basin, SW China. Most of the reservoir porosity is developed in dolograins and dolopackstone. However, it is difficult to identify dolomite grain types since internal grain fabrics were mostly destroyed during diagenesis, especially dolomitization. Therefore, grain types can only be distinguished based on outline/ghost of grains. In some cases, it is difficult to differentiate ooids from peloids as dolomitization has altered the preexisting mudstone, wackestones, packstones, and grainstones.

This study documents the quality of dolostone reservoirs using a combination of petrology, cathodoluminescence (CL) microscopy, SEM, fluid-inclusion microthermometry, and stable isotopes of core samples. Eight lithofacies are differentiated: (1) Peloid/ooid grain-dominated packstone and grainstone; (2) Intraclast grain-dominated packstone and grainstone; (3) Peloid/ooid wackestone and mud-dominated packstone; (4) intraclast wackestone and mud-dominated packstone; (5) bioclast wackestone; (6) Oncoid packstone; (7) mudstone; and (8) sand-bearing or sandy wackestone and mudstone. Pore spaces can be divided into six types: inter-granular pore, inter-crystalline pore, intra-granular pore, vug, micropore and fracture. Vugs mainly occur in dolomitized peloid/ooid grainstone, and intraclast grain-dominated packstone and grainstone. Micropores are abundant in all dolomite lithofacies and bitumen.

Three 3-order sequences are identified. The lower sequence is characterized by meter-scale cycles dominated by mudstone and wackestone, with a thin layer of ooid packstone and grainstone occurring at the top of each individual cycles. The middle sequence displays thicker cycles than the first sequence, dominated by packstone and grainstone. And the upper sequence exhibits cycles thicker than the second sequence, and lithofacies are dominated by wackestone and mudstone with packstone at the top of cycles. Most of the reservoirs occur in the middle sequence of the cycle with lithofacies dominated by dolograins and intraclast dolopackstone.

Petrographic observations and geochemical data also show that five types of diagenesis can be identified: dolomitization, cementation, dissolution, pyritization and stylolization. Early dolomitization and dissolution mainly contribute to reservoir genesis. The degree of dolomitization of original lithofacies also controls the quality of reservoir. Cementation, pyritization and stylolization reduce reservoir porosity.

Diagenetic controls on the spatial variability of carbonate pore systems within the Niobrara chalk-marl reservoirs of the Denver–Julesberg Basin, Colorado

Rebekah Simon* and David Budd

*University of Colorado, Boulder, Dept of Geosciences UCB 399, Boulder, CO 80309, USA

e-mail: rebekah.simon@colorado.edu

The Cretaceous Niobrara Formation constitutes a significant unconventional resource in the Denver-Julesberg Basin of eastern Colorado, USA. The producing section consists of nested multi-scale alternations of chalk and marl, which results in a high amount of lithological complexity over short vertical distances. The finest alterations are millimeter to centimeter-scale laminations, which are embedded throughout decimeter-scale couplets dominated by chalk or marl. The decimeter-scale packages in turn stack into decameter-scale stratigraphic units dominated by one lithology or the other. Within these lithological packages, intercrystalline micro to nano-scale porosity is most abundant. These pores occur between crystals of calcite and exhibit angular shapes as well-defined crystal terminations protrude into the pores. In all lithologies, these pores occur within calcitic peloids, and they also occur in the matrix of the chinks and marly chinks. In 3D, FIB-SEM imagery, these intercrystalline pores form an intricate web of branching and interconnected intercrystalline flow paths that serve as the dominant source of pore connectivity.

Compaction and calcite cementation both contributed to gross progressive porosity loss during Niobrara burial, as noted in compilations of borehole data (Scholle 1977) and supported by $\delta^{18}\text{O}$ -depth curves (Scholle 1977, Pollastro and Scholle 1986, Humphrey et al. 2016). However, establishing the spatial scale(s) of this mass transfer, and the distribution of diagenetic products at the pore scale is difficult, so the scale-dependent link between calcite cementation and porosity loss remains unknown. We approached this problem by taking tightly-spaced samples from a thermally mature (wet gas) well over the same decimeters-thick chalk-marl couplets as crushed shale porosity and permeability measurements. Bulk stable isotope analyses and cathodoluminescence (CL) petrography coupled to scanning electron microscopy were used to document calcite mass transfer. Dissolution and limited CL response are dominant in centimeter-scale marl laminations within the marly portions of couplets, while cementation and bright CL response occur in the adjacent centimeter-scale chalk laminations, suggesting mobilization of calcite from the former to the latter. Oxygen isotopes appear to confirm that calcite mobilizes from marl laminations to local chalk laminations, while the chalky portions of couplets are less affected. A model of roughly closed-system alteration involving lithology-dependent differences in diagenesis that leads to lamination-scale diagenetic un-mixing is suggested. The process produces significant heterogeneity in pore systems and porosity in marl-rich stratigraphic units. In chalk-dominated couplets and stratigraphic units, less heterogeneity in mass transfer, pore systems, and porosity occurs.

Carbonate pore types—from pore scale to the reservoir model

Mark Skalinski*, Robert Mallan, Paul Theologou, Rafael Salazar, and Mason Edwards

*Chevron, 1500 Louisiana St., Houston, TX, 77002, USA

e-mail: mtsk@chevron.com

Carbonate petrophysical heterogeneity is generally the result of complex and multi-modal pore systems. This complexity is due to a combination of complex depositional rock fabric textures and diagenetic modification of the rocks. Pore types are a critical element of rock types since they exert a dominant control over petrophysical properties and fluid flow. Conventional pore typing methods use petrographic observations, including image analysis, to determine pore types, qualitatively or quantitatively, in an attempt to relate the pore system, at least in part, to flow and textural pore types. However, such techniques more than often do not resolve the complexity and multi-modality of the pore system and subsequently result in a misrepresentation of dynamic properties as documented by examples. Pore typing based on mercury porosimetry (MICP) draws on the modality of pore throats accessed by specific pore volumes, which is a strong factor controlling fluid flow in reservoirs. One of the primary parameters in pore typing definitions is the pore system modality. The number of modes is associated with petrophysical properties and depositional or diagenetic processes. However, a more comprehensive link to the recovery factor needs examination of the whole pore system including the pore size distribution.

We have developed a method of automatic modal detection from MICP data using Gaussian decomposition. It allows an objective estimation of the modality of the pore system. We are also investigating the whole pore system defined by both pore throats (from MICP) and pore size distributions (from NMR and image analysis). Integration of MICP, NMR measurements, BSEM images and digital core modeling on the same core plugs enable us to describe the modality of the whole pore system in a more comprehensive way and gain better understanding of pore system. Pore types are defined by unsupervised clustering of capillary pressure data or its Gaussian inversion parameters describing pore modes. Initial clusters are then lumped honoring petrophysical and geological data and extrapolated to all plugs available in the field. Core-scale pore types are transferred to log domain using KNN (Nearest Neighbor method) and integrated with pore types in larger scale (molds, vugs) which are usually not detected from plug measurements. Vuggy porosity is quantified using core-calibrated NMR and FMI logs.

In this presentation, we will describe the integrated pore typing workflow with examples from several carbonate reservoirs. The pore typing workflow is core to the Chevron Petrophysical Rock Typing (PRT) workflow.

Tight chalk: Applying digital rock physics to unravel the 3D pore network and its fluid pathways

Jeroen Soete*, Ophelie Fay-Gomord, Catherine Davy, Nick Janssens, David Troadec, Bruno Caline, and Rudy Swennen

*KU Leuven, Celestijnenlaan 200E, Heverlee, 3001, Belgium

e-mail: jeroen.soete@kuleuven.be

Low-permeability tight chalk intervals play a major role in North-Sea hydrocarbon fields and aquifers, since they control fluid pathways of hydrocarbons and water. Recent studies reveal that their permeability depends essentially on clay content and cementation. Therefore, three characteristic samples were selected for this investigation: (a) a porous micritic reservoir chalk, (b) a cemented chalk and (c) an argillaceous chalk, the two latter being tight chalk. Micrometric pore volumes are provided by applying Focused Ion Beam-Scanning Electron Microscopy (FIB-SEM), because no percolating pore network is obtained at larger scales. Voxel sizes range from $12 \times 15 \times 20 \text{ nm}^3$ to $25 \times 31 \times 30 \text{ nm}^3$ and resulting volumes range between $1071 \mu\text{m}^3$ and $10542 \mu\text{m}^3$. Segmentation in Matlab and 3D rendering in Avizo allowed extracting digital pore data, including porosity, tortuosity, pore volume and pore dimensions.

Digital rock porosity is consistent with He-porosity and MICP pore-throat diameters match calculated pore widths. These correlations relate to the complexity of chalk porous media which possess interconnected capillary networks. The narrowest pathways of the capillaries, captured during MICP analyses (which provides pore entries), correspond to the pore's shortest principal axes or pore width. Average pore length is twice the size of the width. These preliminary findings confirm the potential of FIB-SEM in characterizing tight chalk microporous media. Results also show how average pore length is reduced in tight chalk, with values as low as 140 nm in argillaceous chalk and 533 nm in cemented chalk, compared to 1091 nm in micritic reservoir chalk.

Pore shape analyses demonstrate that clay flakes control morphologies. Argillaceous chalk yields 35 vol% of flattened pores, while they represent only 15 and 18 vol% in micritic and cemented chalk respectively. Cements also induce pore size reductions, but will not significantly alter their shape. Pore size reductions and clogging of fluid pathways result in more tortuous paths in samples with clay or diagenetic cements. Pore network models were prepared to perform permeability simulations. Single-phase flow was simulated using the Lattice Boltzmann method, which visualizes fluid pathways and calculates permeabilities. Absolute permeabilities are in the same order of magnitude as N₂-permeabilities.

Agreement between virtual lab and measured properties shows that (1) FIB-SEM volumes qualify as representative elementary volume for tight chalks and (2) the pore network was imaged at fine enough spatial resolution to resolve its components. The impact of clay content and cementation on porosity and pore morphology in chalk is a key finding, with many possible implications such as in microscale fluid flow modeling.

The characteristics and controlling factors of the microbial carbonate pore systems in the Middle Triassic Leikoupo Formation (Anisian) in the west Sichuan Basin, China

Jinmin Song*, Shugen Liu, Ping Luo, Hairuo Qing, Di Yang, and Zhiwu Li

*Chengdu University of Technology, No.1, Erxianqiao, Dongsan Road, Chenghua District, Chengdu, Sichuan Province, 610059, China

e-mail: songjinmin@sohu.com

Microbial carbonate reservoirs have become a new type of hydrocarbon exploration target all over the world since breakthroughs being achieved in the past few years in the Jurassic of North America (Mancini et al. 2000, 2004, 2008; Wright et al. 2009; Ahr et al. 2011) and the lower Cretaceous of Brazil offshore area (Muniz et al. 2012, Rezende and Pope 2015), as well as in the upper Neoproterozoic of Sichuan Basin, SW China (Wei et al. 2008, Luo et al. 2013, Liu et al. 2016). Recently, a new producing strata has been discovered by Sinopec in the west Sichuan Basin, SW China, where the microbial carbonates of the Middle Triassic Leikoupo Formation (Anisian), have gas production up to 1,150,000 m³/d (Xu et al. 2013). The production numbers indicate good exploration prospect and suggest microbial carbonates both in the Sichuan basin and the paleotethys tectonic region need to be closely evaluated.

The Sichuan Basin lies in the east margin of the Tibetan Plateau in China. During the Anisian stage in the middle Triassic, the Luzhou–Kaijiang submarine high formed from the Jiangnan palaeoland and Xuefeng palaeoland rapidly uplifting and compressing to the northwest induced by the early stage of the Indosinian Movement. Consequently, the topography changed from low low-lying West-East to otherwise (Li et al. 2012, Tang et al. 2013). A series of northeast-striking upheaval and depressions have emerged during this process including the west Sichuan depression. Confined by the surrounding palaeoland and Longmenshan submarine high, the Anisian stage hydrodynamic conditions of Sichuan basin are peaceful, shallow and well restricted, influenced by both tide and wave energy, but building a restricted carbonate platform including lagoon, tidal flat, interior and marginal shoal depositional settings (Zeng et al. 2007, Wang et al. 2009, Qin et al. 2012, Li et al. 2012).

The Leikoupo Formation (Anisian) could be subdivided into four members and nine submembers according to the lithology characteristics, that is, Member T₂l₁ (including two submembers) in the lower part, Member T₂l₂, Member T₂l₃ (including three submembers) and Member T₂l₄ (including three submembers). The hydromica claystone occurs as a marked layer at the bottom of the submember T₂l₁¹, the top of which is gypsum or dolostone. The submember T₂l₁², lying on the submember T₂l₁¹, is dominated by gray to deep gray muddy micrite dolostone interbedded with gypsum. As to the Member T₂l₂, they are mostly light gray gypsum, dolomitic gypsum interbedded with gray dolostone, gypsum-bearing dolostone. And the bioclastic-bearing mudstone, bearing light gray gypsum, grainstone dolostone and limestone develop in the submember T₂l₃¹; when it comes to the member T₂l₃², they are mostly gypsum, salt rock and micrite dolostone interbedded with micrite limestone. The petrologic characteristics of the submember T₂l₃³, lying at top the Member T₂l₃, are different in different part of Sichuan basin; and they are mostly massive lime mudstone interbedded with thin layered dolostone in central

part; But to the Northwest part, they are needle-like pores developing grainstone dolostone and thrombolite dolostone with marlstone, micrite limestone or dolostone at the bottom. There are three submembers in the Member T₂l₄; the micrite dolostone and limestone develop in the submember T₂l₄¹, with thin layered gypsum, while the thick layered gypsum, micrite dolostone, and lime mudstone dominate in the submember T₂l₄². The submember T₂l₄³ are the producing layers, with clot-stromatolite, stromatolite and thrombolites in the Western Sichuan basin and breccia dolostone related with palaeokarst in Longgang to Yuanba in the Central to North Sichuan basin.

The microbes of Leikoupo Formation (Anisian) have been identified including *Renalcis*, *Girvanella*, *Rivularia lissaviensis*, *Entophysalis*, *Tortofimria* and *Gloeorrh*, forming stromatolite, laminite, thrombolite, spongiostromata, dendrolite and oncolite morphologies. The microbial carbonate reservoirs lie in the T₂l₃³ submember in Zhongba area and T₂l₄³ submember in the middle to north segment of the west Sichuan Basin (Fig.1).

The pores have been analyzed by different methods. Under core description, the pores are irregular, condensed, needle-like, ~1mm × 0.4mm in size and mostly along the lamination. Under microscope, the pores are mostly develop in microbe coelomo, framework pore, fenestral structure and inter- and intra-clot (Fig.2). Under FESEM, the pores are mostly intercrystalline pores among the microbial framework and coelom dolomite, with size of 0.5 mm × (0.2-0.3) mm; And the pores are connected by the small throats with size of (20-50) μm between clots or among the framework; although the pores in nano scale are abundant, they are not composed of the main reservoir spaces. It is suggested that different pore spaces may develop in different microbialite, for example, the fenestral pores are mostly in the clot-stromatolite and stromatolite and the microbial framework pores and inter-clot dissolved pores in the thrombolite or laminated thrombolites. The microbial carbonates are of low porosity and permeability according to petrophysical experiments. The porosity in clot-stromatolite mostly ranges from 0.4% to 11%, with permeability being (0.003-85) × 10⁻³ μm² while in stromatolite, the porosity is form 0.6% to 13% and the permeability is (0.003-710) × 10⁻³um². In the thrombolite, the porosity changes from 0.2% to 7%, with permeability among the range of (0.0016-186) × 10⁻³ um², however, oncolites are (0.28%-0.52%) in porosity and (0.0028–0.034) × 10⁻³um² in permeability. In comparison, the reservoir quality may be better in clot-stromatolite, stromatolite and thrombolite.

It is proposed that the extreme palaeogeological conditions, dolomitization and burial dissolution together decide the formation and distribution of the microbial carbonate pore systems. Elevated sea-surface temperature, hypersaline and anoxic in paleocean environments, arid climate under the mega monsoon, external compression and internal tension in tectonic settings as well as the restricted paleographic conditions by the subaqueous uplift, all influence the development and distribution of the microbialites. And the dolomitization in the contemporaneous to penecontemporaneous stage is of great importance to the formation of the microbial carbonate reservoirs, and also the following burial dissolution does favor to the improvement and preservation of the microbial carbonate reservoirs.

References

Ahr WM, Mancini EA, Parcell WC. 2011. Pore characteristics in microbial carbonate reservoirs. Houston: AAPG Annual Convention and Exhibition.

Liu SG, Song JM, Luo P, Qing HR, Lin T, Sun W, Li ZW, Wang H, Peng HL, Yu YQ, Long Y and Wan YB. 2016. Characteristics of microbial carbonate reservoir and its hydrocarbon exploring outlook in the Sichuan Basin, China. *Journal of Chengdu University of Technology, (Science & Technology Edition)*,43(2): 129-152

Luo P, Wang S, Li PW, Song JM, Jing TF, Wang GQ and Yang SS. 2013. Review and perspectives of microbial carbonate reservoirs. *Acta Sedimentologica Sinica*, 31(5): 807-823 (in Chinese with English abstract)

Mancini EA, Parcell WC, Ahr WM, et al. 2008. Upper Jurassic updip stratigraphic trap and associated Smackover microbial and nearshore carbonate facies, Eastern Gulf Coastal Plain. *AAPG Bulletin*, 92(4): 417-442.

Mancini EA, Benson DJ, Hart BS, et al. 2000. Appleton field case study (eastern Gulf coastal plain): Field development model for Upper Jurassic microbial reef reservoirs associated with paleotopographic basement structures. *AAPG Bulletin*, 84(11): 1699-1717.

Mancini EA, Llinás JC, Parcell WC, et al. 2004. Upper Jurassic thrombolite reservoir play, northeastern Gulf of Mexico. *AAPG Bulletin*, 88(11): 1573-1602.

Muniz M C, Bosence D. 2012. Carbonate platforms in non-marine rift system in the Early Cretaceous(Pre-salt) of the Campos Basin, Brazil. Long Beach: AAPG Annual Convention and Exhibition.

Rezende MF and Pope MC. 2015. Importance of depositional texture in pore characterization of subsalt microbialite carbonates, offshore Brazil. In Bosence, D. W. J., Gibbons, K. A., Le Heron, et al, (eds) , *Microbial Carbonates in Space and Time: Implications for Global Exploration and Production*. Geological Society, London, Special Publications, 418: 193–207

Wei GQ, Chen GS, Du SM, Zhang L and Yang W. 2008. Petroleum systems of the oldest gas field in China: Neoproterozoic gas pools in the Weiyuan gas field, Sichuan Basin: *Marine and Petroleum Geology*, 25: 371-386

Wright PV, Racey A. 2009. Pre-salt microbial carbonate reservoirs of the Santos Basin, offshore Brazil. Denver: AAPG Annual Convention and Exhibition.

Xu GM, Song XB, Feng X, Long K, Wang QX, Shi GS and Zhu L. 2013. Gas potential of the Middle Triassic Leikoupo Formation in the western Sichuan Basin. *Natural Gas Industry*, 33(8): 8-14

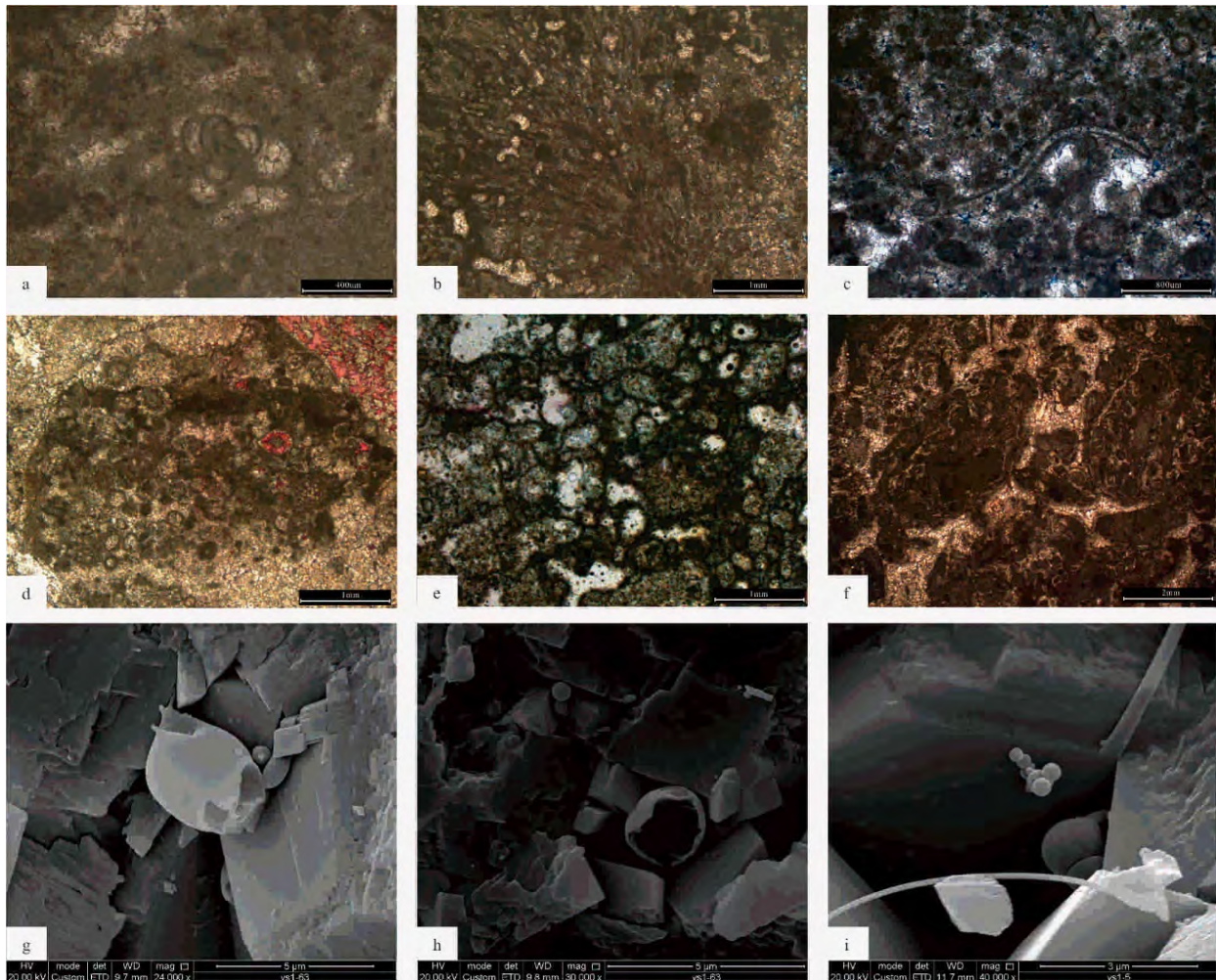


Fig.1 The type and morphology of the microbes in the Middle Triassic Leikoupo Formation in the western Sichuan Basin:

- (a) *Renalcis*, 5767.28m, T_2l^4 , well YaS1, plane polarized light;
 (b) *Epiphyton*, 5766.70m, T_2l^4 , well YaS1, plane polarized light;
 (c) *Girvanella*, 5784.27m, T_2l^4 , well T1, plane polarized light;
 (d) *Entophysalis*, 6189.77m, T_2l^4 , well T2, plane polarized light;
 (e) *Tortofimria*, 5826.9m, T_2l^4 , well T3, plane polarized light;
 (f) *Gloeorrh*, 6235m, T_2l^4 , well T2, plane polarized light;
 (g) sub rounded microbial dolomite, 6200m, T_2l^4 , well YS1, FESEM, $\times 24000$;
 (h) hemispherical microbial dolomite, 6200m, T_2l^4 , well YS1, FESEM, $\times 30000$; and
 (i) globular chain microbial dolomite, 6242m, T_2l^4 , well YS1, FESEM, $\times 40000$.

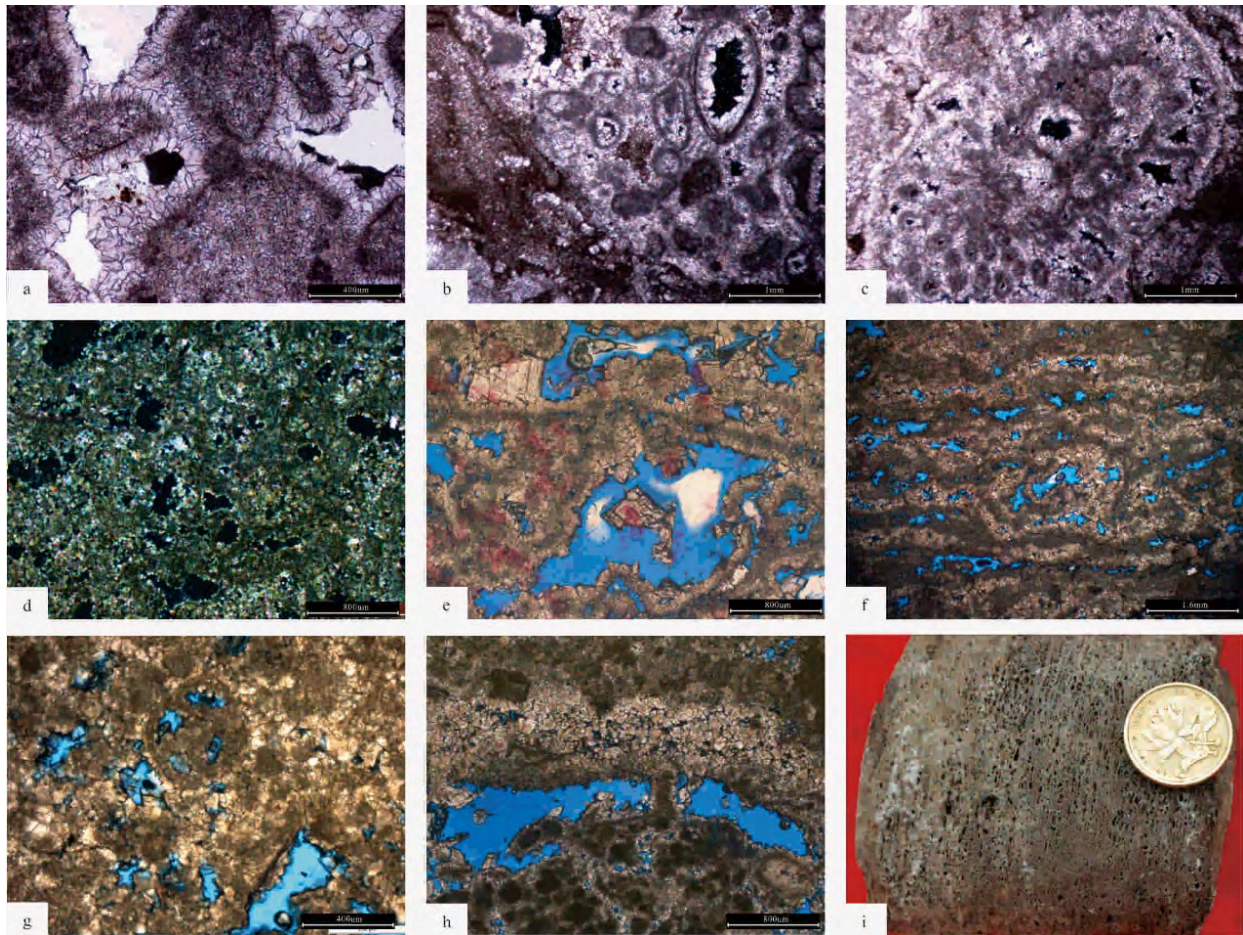


Fig.2 The microbialite reservoir spaces of the Middle Triassic Leikoupo Formation in the western Sichuan Basin:

(a) thrombolite dolomite, with dissolved pores interclot partially occluded by dog-teeth like dolomite and bitumen, 3135.77m, T_2l^3 , borehole T4, plane polarized light;

(b) bioclast bearing thrombolite dolomite, with intragranular dissolved pores, 3107.16m, T_2l^3 , borehole T4, orthogonal light;

(c) microbial framestone, with frame porosity, 3107.31m, T_2l^3 , borehole T4, orthogonal light;

(d) spongiostromata dolomite, developing microbial coelomopore, 5819.88m, T_2l^4 , borehole T3, orthogonal light;

(e) microbial framestone, with frame porosity, partially occluded by saddle dolomite, 6219.96m, T_2l^4 , borehole T2, casting thin section, plane polarized light;

(f) stromatolite dolomite, fenestral pores along lamination, 5791.92m, T_2l^4 , borehole T1, casting thin section, plane polarized light;

(g) thrombolite dolomite, dissolved pores inter and intra clots, 6213.68m, T_2l^4 , borehole T2, casting thin section, plane polarized light;

(h) thrombolite-stromatolite dolomite, dissolved pores along lamination, 5397.47m, T_2l^4 , borehole T1, casting thin section, plane polarized light; and

(i) laminite-stromatolite dolomite, needle-like dissolved pores densely developed along lamination, 6219.8m, T_2l^4 , borehole T2.

Micro-porosity creation in a Lower Cretaceous carbonate sequence of the Arabian Plate—initiated during early and finalized during burial diagenesis driven by tectonically driven regional subsurface flow

Volker Vahrenkamp*, Joao Barata, Pierre Van Laer, Peter Swart, and Sean Murray

*KAUST (King Abdullah University of Science & Technology), Thuwal, 23955-6900, Saudi Arabia

e-mail: vol_vkamp@hotmail.com

Micro porosity associated with micro-rhombic calcite provides volumetrically the largest pore volume in Middle Eastern Cretaceous carbonate reservoirs. With progressing reservoir development and depletion of macro-pore systems, the low permeability micro pores have ever-increasing importance as host to remaining hydrocarbons and for reservoir performance. Results are presented that suggest for the micro-rhombic calcite an early diagenetic near-surface origin through micritization and a final maturation through recrystallization driven by tectonically driven regional subsurface flow in a burial setting.

Modern lagoons of the Arabian Peninsula are the site of carbonate deposition similar in many aspects to the giant lagoons of the Cretaceous carbonate platforms with deposition often characterized by grainy sediments with packstone fabrics. However, within a few thousand years most grains are micritized to the extent that grain textures have often become obliterated. The process of micritization is considered the first step towards generating micropores of the character found in Cretaceous reservoir sequences.

The genesis of micro-rhombic calcite has previously been placed into the shallow burial realm under the influence of meteoric or marine pore waters (Budd 1989, Moshier 1989) using oxygen stable isotopes and petrographic observations. However, the interpretation of oxygen isotope data was limited by the fact that the isotopic composition of calcite minerals is determined by two independent factors: the isotopic composition and the temperature of the precipitating water. The new analytical technique of clumped isotopes has established a way to independently determine one of the variables (temperature) thus allowing the other (water composition) to be fixed. A total of 38 samples were analyzed from the Barremian Upper Kharaib Fm from 8 different locations from onshore Abu Dhabi. Carbon and oxygen stable isotope values are in line with existing values for this subsurface layer (-9.17 to -5.27 $\delta^{18}\text{O}$; 2.99 to 4.10 for $\delta^{13}\text{C}$). Clumped isotopes indicate precipitating temperatures of 47°C to 110°C , and a relatively heavy isotopic composition of diagenetic water of 0.2‰ to 5.6‰ $\delta^{18}\text{O}$. Thin sections were created of the 38 samples for a semi-quantitative petrographic analysis to provide further insight on temperature variations. Samples with a higher volume of intraclasts have lower temperature of precipitation while samples with higher volume of diagenetic cement show higher temperatures of precipitation. Cutoffs were applied to filter out these early and late diagenetic overprints. Using the existing basin model and results from the most pristine micro-rhombic samples, temperatures translate into an Upper Cretaceous age and a depth for diagenesis in the eight structures of between 610 and 1370 m. The difference in burial is linked to differential subsidence of the structures during the Late Cretaceous caused by plate collision and ophiolite

opduction on the eastern plate margin. The heavy oxygen isotopic signatures point towards an evolved basinal brine as the diagenetic fluid. This suggests that the genesis of micro-rhombic calcite and hence the micro-pore system was finalized in a burial setting characterized by a tectonically driven regional flow system. An understanding of the large scale fluid-flow system is important in resolving issues related to the regional distribution of reservoir properties.

Microporous nodular beddings in the carbonate reservoirs of the Cretaceous in the Middle East: A review

Benoit Vincent*, Andrew Horbury, Joanna Garland, Peter Gutteridge, Christoph Lehmann, and Omran Al-Zankawi

*Cambridge Carbonates Ltd., 4 th The Courtyard, 707 Warwick Road, Solihull, West Midlands, B91 3DA, UK

e-mail: benoit@cambridgecarbonates.co.uk

Nodular bedding is a very common fabric in the Cretaceous carbonates of the Middle East, and possibly even more so during the Albian to Turonian period. This style of bedding is mostly considered to be a result of bioturbation, involving *Thalassinoides* ichnotraces, and can be developed in open marine carbonates, as well as shallow marine lagoonal to restricted platform top carbonates. The pervasive bioturbation creates several meter-thick monotonous successions where original depositional fabrics are often difficult to identify properly (Hollis 2011). Our data also suggest that other original genetic processes, such as karstification or hardgrounds/omission surfaces, are capable of creating very similar fabrics. All kinds of nodular bedding display inherent microporosity. This is heterogeneously distributed within the bedding (edges of nodules vs. core of nodules, inter-nodule zones), depending on (1) the original composition of the sediments, and (2) the diagenesis affecting the sediments. Bioturbated open marine micritic facies display microporous nodule cores (burrows), and tight nodule edges towards compacted inter-burrow areas, which shows stylolites and dolomitisation of variable intensity. There, stylolitised zones served as a source for carbonate cementation of the edges of the nodules, while cores preserved microporosity. Conversely, shallow marine lagoonal micritic facies show tight “cemented” nodule cores, and microporous nodule edges but similarly compacted inter-burrow areas. There, aragonite dissolution served as a local source for cementation of the nodule cores, while edges remained microporous. In both cases microporosity was sometimes later enhanced prior/during hydrocarbon emplacement. The nodular bedding associated with karstification implies different processes, but the final fabric is very similar to the more classical nodular bedding in shallow marine carbonates. Understanding the processes responsible for these nodular bedded fabrics is of importance since the thick homogeneous successions formed by the above mentioned processes, although often associated with baffle zones in oil reservoirs, display significant storage capacity. These intervals may additionally impact the distribution of flow capacity for gas reservoirs.

Reference

Hollis C. 2011. Diagenetic controls on reservoir properties of carbonate successions within the Albian–Turonian of the Arabian plate: *Petroleum Geosciences*, v. 17, pp. 223-241.

Characterizing and predicting natural fractures in the “Mississippian Limestone” play, U.S. southern mid-continent

Yulun Wang*, Taylor Thompson, and G. Michael Grammer

*Boone Pickens School of Geology, Oklahoma State University, 105 Noble Research Ctr
Stillwater, OK 74078, USA

e-mail: marcowang1989@hotmail.com

Natural Fractures are common in several unconventional carbonate reservoirs around the world, including the “Mississippian Limestone” of the U.S. Southern Mid-Continent region. Although many of the fractures have been occluded with cement, they may assist in the propagation of induced fractures during hydraulic fracturing, and are thus an important component to include in the overall reservoir characterization workflow. This study is focused on correlating fracture types and intensity to petrophysically-significant facies and to an established sequence stratigraphic framework in these Carboniferous unconventional carbonate reservoirs.

Four types of natural fracture are observed: ptigmatic, vertical extension, shear, and mixed types of fractures, with the highly folded ptigmatic fractures being the most common type. Fractured zones are vertically heterogeneous at various scales, indicating the variability in rock mechanical properties. At the millimeter scale, fractures are commonly discontinuous and exhibit variable width in both petrographic analysis and micro-CT imaging. At the centimeter scale, ptigmatic fractures exhibit variable termination modes in relation to bedding planes, suggesting a mineralogical control on rock mechanical properties. At the meter scale, the highest fracture abundance corresponds to the petrophysically significant facies type with the highest calcite content. Such mineralogical control of fracture distribution is also represented by the higher fracture intensity within the regressive phases of “third-order” sequences, indicating the value of incorporating a sequence stratigraphic approach in characterizing and predicting fracture distribution. Co-existence of the highly folded, “early” ptigmatic fractures and “late” vertical extension fractures in the same facies suggests a temporal variation in rock mechanical properties related to varying amounts of calcite cementation and a complex structural history, illustrating the necessity of incorporating structural diagenesis when inferring mechanical stratigraphy at the time of fracturing from present-day fracture stratigraphy. Fracture abundance varies among individual cores, likely attributed to variations in the proportion of petrophysically significant facies, variations in structural settings throughout the region, variable patterns in the evolution of rock mechanics, and clustering of the fractures. Constraining relationships between fractures and bedding structures, such as fracture height vs. spacing vs. bed thickness, are poorly recognized because of the poorly defined bedding structures, complex termination patterns of fractures in cores, and narrow core width of around 85 mm.

Although revealing the fracture distribution with vertical continuity, subsurface cores poorly resolve the lateral fracture distribution due to the narrow width. In order to overcome this limitation, a highly fractured Mississippian outcrop in northwestern Arkansas is being examined. In the lower part of the outcrop, the Reeds Spring Formation contains well defined and laterally continuous, planar and lenticular/nodular chert and lime mudstone beds, both of which

commonly contain natural fractures. Similar to observations in cores, fractures in the outcrop, which are present in both chert and mudstone beds, are commonly vertical to sub-vertical in orientation and are filled with calcite and microcrystalline quartz cement. These fractures also exhibit variable width and a variety of termination styles. Fracture types present in cores, such as ptigmatic, vertical extension, and shear fractures, are observed in both the chert and mudstone beds, suggesting the presence of structurally originated fractures similar to what is observed in cores. Fractures are mostly constrained within beds, and fractures in the chert beds seem to be more closely spaced than fractures in the more ductile mudstone beds, suggesting the impact of mineralogical variations in rock mechanical properties and fractures propagation. Therefore, the fractures in outcrop may serve as a valuable analog for better understanding the lateral distribution of fractures in the subsurface and the constraining relationship among various fracture attributes and bedding structures, although different structural histories between the outcrop and subsurface should be considered. In particular, many of the fractures in the outcrop are chaotically arranged and dissolution enhanced, seemingly hydrothermal brecciated zones. In contrast, fractures in the cores examined in this study rarely show these features, suggesting that different structural setting in different parts of the depositional system may have disconnected part of the outcrop fracture system from its subsurface counterpart in terms of origin and diagenetic history. In this sense, it would be necessary to treat these hydrothermal fractures as a separate system when applying the spatial distribution of fractures and constraining relationships among fractures and bedding structures in the outcrop into the subsurface. Despite such a potential mismatch between the present-day fracture stratigraphy and mechanical stratigraphy at time of fracturing and various origins of fractures, the sequence stratigraphic framework, which governs the distribution of petrophysically significant facies and impacts diagenetic patterns and rock mechanics, may provide insight that may enhance the prediction of natural fractures (e.g., attributes and distribution) in these Mississippian and other unconventional carbonate reservoirs.

Multi-scale characterization of pore systems and natural fractures of the “Mississippian Limestone”, southern mid-continent, USA

Yulun Wang*, Ibukun Bode, Beth Vanden Berg, and Michael Grammer

*Boone Pickens School of Geology, Oklahoma State University, 105 Noble Research Ctr
Stillwater, OK 74078, USA

e-mail: marcowang1989@hotmail.com

The unconventional ‘Mississippian Limestone’ of the U.S. Southern Mid-Continent, which consists of calcareous siltstones and silty mudstones to packstone-grainstones, is characterized by porosities of 9 percent or less and permeability in fractions of millidarcies. Complex facies distribution, diagenetic trends, and structural settings result in variable reservoir quality, petrophysical properties, natural fracture patterns, and rock mechanics. This heterogeneity necessitates an integrated reservoir model that incorporates multiple datasets—from core to pore scale—to predict the distribution of naturally fractured and reservoir intervals. Pore sizes varying over three orders of magnitude, have been defined by optical microscopy, SEM, and micro-CT imaging. The majority of the pores identified are within the nano- to micropore size range, and therefore not observable when doing routine core description. Due to the highly irregular pore network in these unconventional carbonates, expected relationships between pore geometry and laboratory-measured sonic velocity, which are well-defined in conventional carbonate reservoirs, are not readily apparent. These insights emphasize the need to develop other proxies through various analytical techniques, such as nuclear magnetic resonance (NMR), by which these pore systems can be better characterized petrophysically. Preliminary assessment indicates a relationship exists between NMR transverse relaxation time (T₂) distribution and the different petrophysically-significant facies groups. The T₂ curves exhibit up to 3 modes: varying by facies and pore size distribution. These results highlight the multi-modal nature of micro-nanopore dominated pore systems in some carbonates. Natural fractures are observed in both core and outcrop exposures of these units. Although mostly mineralized and do not contribute significantly to primary reservoir performance, different types of fractures and distribution patterns observed through micro-CT imaging, petrography, core, and outcrop reveal the spatial and temporal variations of rock mechanics and may assist in identifying optimal zones for hydraulic fracturing. In core, the highest fracture abundance corresponds to facies with the highest calcite content and the regressive phases of “third-order” sequences. This indicates the value of sequence stratigraphic approach in characterizing and predicting the natural fracture distribution in these unconventional reservoirs. In outcrop, highly fractured beds with varying lateral continuity help better understand the spatial organization (e.g., spacing) of the fractures, resolving the inherent limitation of core-based dataset due to the narrow core width. Because the outcrop has experienced a different burial history, these units may exhibit different rock mechanics, revealed by the fracture patterns, facilitating a relationship between present-day fracture stratigraphy and mechanical stratigraphy at the time of fracturing.

Sedimentary characteristics of intra-platform microbial mounds and their controlling effects on the development of reservoirs: A case study of the Lower Cambrian in Tarim Basin, China

Liu Wei*, Huang Qingyu, and Hu Suyun

*PetroChina Research Institute of Petroleum Exploration & Development, No.20 Xueyuan Road, Haidian District, Beijing, China

e-mail: liuwei086@petrochina.com.cn

A succession of microbial carbonate rocks is widely developed in the Lower Cambrian Xiaerbulake Fm in the Keping-Bachu area, Tarim Basin. Previous studies focused on the sedimentary and reservoir characteristics of the platform margin microbial reefs. However, the intra-platform microbial mounds were less investigated. In this paper, therefore, the sedimentary evolution and reservoir characteristics of intra-platform microbial mounds in the Xiaerbulake Fm were analyzed systematically by means of field outcrop measurement, thin section analysis, cathodoluminescence examination and physical property test.

Based on the integrated studies, the following results are obtained. Firstly, intra-platform microbial mounds are mainly developed in the zones of open platform facies and hummocky highs are obviously presented in the macroscopic scale. Thrombolite dolostone and very fine to fine crystalline dolomite with residual grain texture → stromatolite dolomite → foam spongy dolomite → cyanobacteria dolo-grainstone are developed successively from bottom to top and a complete sedimentary assemblage of mound base-core-cap is constituted. Secondly, the reservoir quality of the microbial mound in the upper part of the formation is much better than that of laminated microbial carbonate in the lower part. The pore types of the microbial mound mainly include foam spongy framework pores, interclot pores, intergranular pores, pin-point dissolution vugs and bedded dissolution vugs. Thirdly, the origin of the porosity is interpreted as the short-term subaerial exposure and meteoric dissolution based on the petrographic analysis of thin sections, cathodoluminescence detection, as well as carbon and oxygen isotope analyses of cements. The evidence of the meteoric dissolution includes the partially absent of fibrous cements representing marine environment, clotted medium bright red luminescence and slightly depleted oxygen isotope values. Besides diagenesis, sedimentation plays a vital role in the development of microbial mound reservoirs. Porosity of the mound core (average 5.47%) is much better than that of mound cap (average 3.51%) and mound base (average 2.01%). The intra-platform microbial mound reservoir, as an important type of reservoir in the Xiaerbulake Fm, is significant to the extension of the Cambrian subsalt oil and gas exploration in the Tarim Basin from the platform margin to the internal platform.

Episodic, energetic event beds and their relationship to brittle, carbonate intervals in the Triassic Shublik Formation, North Slope, Alaska.

Katherine J Whidden* and Adam Boehlke

*USGS, P.O. Box 25046, MS 939 DFC, Denver, CO 80225, USA

e-mail: kwhidden@usgs.gov

The Shublik Formation is a Triassic, organic-rich, calcareous mudstone to micritic limestone which has been identified as a major source of oil in Prudhoe Bay and other accumulations in northern Alaska. The Shublik is also currently being evaluated by industry as a self-sourced resource play. Ongoing USGS studies are focusing on characterizing the depositional and early diagenetic mineralogy associated with organic-rich intervals within the Shublik. This work will yield a better understanding of the controls on the production and preservation of organic matter, as well as determining intervals that may serve as target zones for future production.

Core samples from two wells in the National Petroleum Reserve in Alaska have been described using optical and scanning electron microscopy, and analyzed for total organic carbon (TOC) and mineralogy. Two end-member microfacies have been recognized: (1) a bivalve-rich packstone-grainstone to marl, and (2) a bioclastic calcareous mudstone to wackestone-packstone. The bivalve packstone-grainstone is an organic-rich facies, with measured TOC values up to 4 percent. This microfacies comprises mm-thick layers of flat-clam shells in a mud matrix. It is interpreted as having been deposited during quiescent depositional conditions. In contrast, the bioclastic calcareous mudstone has a chaotic texture, with broken and abraded fossil fragments, and authigenic calcite cement. TOC values are less than 1 percent in these samples. This microfacies is interpreted to represent episodic, energetic event beds. A continuum of microfacies exists between these end-members, characterized by gradations in texture, mineralogy, TOC, and bioclast composition. This transitional microfacies is interpreted to represent varying degrees of energetic disruption along the sediment-water interface. Semi-quantitative X-ray diffraction data show that the end-member facies are composed of 65–75 percent calcite. Microscopic observations reveal that the calcite in the bivalve packstone-grainstone is primarily biogenic, whereas predominantly authigenic calcite cement occurs in the bioclastic calcareous mudstone. Quartz, dolomite, pyrite and apatite concentrations are highest in the transitional facies.

A model is proposed whereby the sequence of diagenetic mineral precipitation depended on the amount of reactive particles, particularly organic matter and clays. The episodic, energetic events mixed the uppermost sediment column, allowing solutes in the pore waters to escape back to the water column, thus favoring authigenic calcite precipitation over other cements. The strength of the episodic, energetic events may have played a key role in the development of brittle carbonate intervals within an organic-rich sequence.

Variations in karsted and fractured outcrop porosity analysed in Lower Cretaceous shelf carbonates, Gargano Peninsular, Apulia, Italy

Francis Witkowski*, Peter Gutteridge, Ivar Grunnaleite, Niels Bo Jensen, and Gunnar Sælen

*Cambridge Carbonates Ltd., 4 the Courtyard, 707 Warwick Road, Solihull, West Midlands, B91 3DA, UK

e-mail: francis@cambridgecarbonates.co.uk

A series of wire-cut quarry faces were digitally captured using multiple colour images to construct detailed mosaics of the outcrop surface. These calibrated images were enhanced to remove noise/extraneous vegetation/boost details. They were then thresholded with image analysis software to generate macropore maps at various scales (dependent upon the individual quarry face). This process was undertaken for (i) entire faces and (ii) multiple Areas of Interest (AOIs) in various orientations acting as “pseudo wells” or well analogues. Comparisons were made between the different faces to establish the degree of lateral variation throughout the quarry. Analyses were also undertaken on individual whole face porosity maps and the AOIs to determine the AOI accuracy at capturing the pore system exposed in individual faces. Further assessments were made between different AOI (pseudo well) trajectories to judge the effect of orientation on fracture/karst porosity interception and characterisation. These provide an analogue to how subsurface wells characterise macropore/fractures systems in target horizons.

Modelling the evolution of permeability in carbonates

Rachel Wood* and Aleksandra Hosa

*University of Edinburgh, James Hutton Road, Edinburgh, EH9 3FE, UK

e-mail: Rachel.Wood@ed.ac.uk

Carbonate pore structure and therefore permeability is controlled in large part by unique diagenetic events and products, and a complex wettability structure that is often dominantly weakly-oil wet. This produces a highly diverse array of pore types and size, styles of connectivity and tortuosity, and in turn flow behaviours. While changes in porosity can be directly related to diagenetic petrographic characteristics such as cement distribution and dissolution features, quantifying how these textures control attendant changes in permeability is more challenging. The impact of individual diagenetic events and their products on flow properties can, however, be isolated and modelled using 3D pore architecture models. Porosity and permeability evolution through many diagenetic scenarios often display several ‘diagenetic tipping points’ where the decrease in permeability is dramatically larger than expected for the associated decrease in porosity. The effects of diagenesis also alters the capillary entry pressures and relative permeabilities, so providing trends that can be applied to real rocks. In turn, such diagenetic pathway models can be used to provide constraints on predicted flow behaviour during burial and/or uplift scenarios using ‘diagenetic back stripping’ of carbonate rocks. In dominantly microporous carbonates, average pore radius controls single-phase permeability, but has minimal effect on multiphase flow. When moldic mesopores are added to a microporous matrix, they only impact flow when directly connected: micropores control the magnitude of single-phase permeability. Recovery, however, is dependent on both wetting scenario and pore-network homogeneity: under water-wet imbibition, increasing proportions of microporosity yield lower residual oil saturations. Process-based models of early cementation (isopachous and syntaxial) show that isopachous cement is effective in closing pore throats and limiting permeability, but permeability changes due to syntaxial cement growth (preferentially on monocrystalline grains) is highly dependent on monocrystalline grain location and direction of the grain crystal axis, as this can create a highly ‘patchy’ distribution of cement. This highlights the importance of diagenesis in creating pore-scale heterogeneity.

Hydrothermal chert reservoir in Middle–Lower Ordovician carbonate in the Shunnan Area, Tarim Basin, NW China

Ning Ye*, Shaonan Zhang, Yingtao Li, Siyang Zhang, and Ziyu Lu

*State Key Laboratory of Oil and Gas Reservoir Geology and Exploitation and College of Energy Resource, Chengdu University of Technology, No.1. Dongsan Road, Erxianqiao, Chengdu, Sichuan, 610059, China

e-mail: 235576991@qq.com

The Shunnan area is a newly discovered hydrocarbon field in the Shuntuoguole lower uplift with the host rocks of Ordovician Yingshan Formation carbonates. The carbonate reservoirs are well affected by hydrothermal silicification with well-preserved dissolution pores, intercrystalline pore of replacement quartz and megaquartz cements. Based on the petrography and geochemistry studies, this research evaluated the reservoir quality and re-constructed porosity evolution in different diagenetic stages.

Samples are collected from 3-cored wells distributed along NNE- or NEE- trending sinistral strike-slip faults. Five types of host rocks were identified in study area, including micrite, pack-grainstone, slightly silicified limestone (silica less than 25%), strongly silicified limestone (silica around 50%) and chert. Strongly silicified limestone and chert have the better porosity (average 9.8%) and permeability (average 19.34 mD) than others. The main reservoir porosities are fractures and intercrystalline of replacement quartz. According to the fluid inclusions, rare-earth elements and trace element analysis studies, the result of homogenization temperature and positive Eu-anomalies point out the strongly silicified limestone and chert associated with hydrothermal fluids. Meanwhile both of Th/U-Y/Ho correlation and freezing point temperature display the hydrothermal fluids with medium-low temperature and high salinity which seem to be derived from the mixing of Yingshan formation waters and magmatic fluids. Magmatism is considered to provide heat and silica for the silicification. The Permian volcanic activities are interpreted to be related with the hydrothermal chert reservoirs in the Shunnan area.

Porosity and diagenetic evolution of the Upper Cretaceous–Tertiary slope carbonates, northern Arabian carbonate platform, SE Turkey

Ismail Omer Yilmaz* and Oguz Mulayim

*Middle East Technical University, Department of Geological Engineering, Ankara, 06800, Turkey

e-mail: ioy6841@gmail.com

The studied succession crops out in the Mardin city, SE Turkey and lies on the northern Arabian Platform. The microfacies, facies, and diagenetic evolution along the measured sections have been studied by field and petrographic analysis. Alternations of bioclastic packstones including mixed fauna including benthic foraminifera, red algae, planktonic foraminifera, echinoidea, bryozoan, coral, brachiopoda, with dolomitic bioclastic wackestone/packstone including planktonic foraminifera, echinoidea, bivalves take place at the bottom and middle part of the section. Alternation of dolostones with dolomitic bioclastic wackestone/packstone including planktonic foraminifera, echinoidea, bivalves takes place at the top of the section. Fining upward features at the bottom of the beds of the bioclastic packstones lying at the lower part of the section are interpreted as related to turbiditic flow deposits. This facies is interpreted as calciturbidite flux within pelagic carbonate slope. Calciturbidite facies also includes quartz/chert silt content, but it disappears towards the middle part of the sequence, where the facies gets muddier. Stratigraphically, bioclastic dolomitic packstone/wackestone facies take place towards middle to top. Calciturbidite facies displays various types of secondary porosity like matrix dissolution, interparticle, intraparticle and molding porosity with different sizes. Dissolution porosities can also be seen on the poikilotopic calcite and syntaxial overgrowth of calcite on echinoidea fragments. Bioclastic dolomitic packstone/wackestone facies displays disseminated fine grained idiomorphic dolomite crystals in the matrix in around 20–40%. Oil staining can be seen between the dolomite crystals and high to middle amplitude stylolites are developed in the matrix. Dolostones cover the rest of the section. Coarse and fine grained dolostones display idiomorphic or hypidiomorphic textures and present two different dolomite crystals as clear and dirty. Zonning is also observed in some of the crystals. Dolomitization takes place in two stages during burial and in late burial diagenesis. Preserved poikilotopic calcite cement partially observed but both dolomites and calcites are subjected to dissolution. Secondary porosity is observed as selective and intra and intercrystalline porosity. Silicification took place after secondary porosity development following oil staining in the secondary pore spaces. So, it seems that burial and late burial diagenesis are followed by uplift or hydrothermal alteration after oil migration.

The importance of touching and non-touching vuggy pores in carbonate flow characterization—An example from the Cretaceous Pipe Creek, Texas

Chris Zahm*, Charles Kerans, Xavier Janson, Jim Jennings, and F. Jerry Lucia

*Bureau of Economic Geology, University Of Texas at Austin, University station Box X, Austin, TX 78713, USA

e-mail: chris.zahm@beg.utexas.edu

Touching and connected vuggy pores within carbonates can create a flow system that can have more than a darcy of permeability and significant porosity at some scales of observation. However, measurements of permeability over different scales of investigation reveal the importance of characterization of the representative elemental volume (REV) at the reservoir scale. Significant variability between intact reef facies compared to flank debris rudist rudstones reveals the challenge of characterizing vuggy pore systems. The Cretaceous Pipe Creek pinnacle reef outcrop of central Texas has been the subject of many geology reports from its discovery in the 1950s up through current time. Five research cores were collected by the RCRL group of the Bureau of Economic Geology at the University of Texas at Austin as part of an industry and NSF funded study of touching and non-touching vuggy pores and the resultant permeability. The cored wells were also used for gas and water flow tests along with outcrop facies mapping using standard aerial photos, UAV-acquired photographs, terrestrial lidar, and ground-penetrating radar. In addition to the collected cores, a large hand specimen (0.75 m) was collected and analyzed for pore structure architecture using micro-CT scanning. Numerous NSF, BEG, UT-PE and RCRL studies have been conducted from the Pipe Creek site. Highlights from the five cores are presented here along with a summary of the findings from this research.

Lithofacies, diagenesis and reservoir development of the pre-salt Mississippian carbonate rocks in the Rozhkovsky structure, Fedorovsky Block, northern Pre-Caspian Basin, Kazakhstan

Siyang Zhang*, Hairuo Qing, Shaonan Zhang, Qiang Zheng, Ning Ye, and Ziyu Lu

*Department of Geology, University of Regina, 3737 Wascana Parkway, Regina, Saskatchewan, S4S 0A2, Canada

e-mail: siyang2z@uregina.ca

Recent exploration in pre-salt carbonate rocks in the northern Pre-Caspian Basin has identified a number of oil/gas fields. The Rozhkovsky structure is an anticline structure trap located in the north part of Fedorovsky block near northern margin of Pre-Caspian Basin. During the Permian time, salts deposits were pervasively distributed in this basin, and divided the thick successions of sediments into three units: pre-salt, salt, and post-salt. The pre-salt Mississippian carbonates were developed in the inner and mid ramp environments in the study area. However, there is limited understanding of petrology, sequence stratigraphy, sedimentary facies, diagenesis, and reservoir characteristics of these carbonate rocks. Samples are collected from 6-cored wells, four are along the hinge line of the anticline and other two in the limbs. Based on analysis of petrography, stratigraphy, SEM, EPMA and reservoir property, this study identified the pore-system and interpreted its evolution in different lithofacies and depositional environment. Ten major carbonate ramp lithofacies and one siliciclastic rock type were identified in the Rozhkovsky structure, however, only four types of lithofacies, including grainstone, pack/grainstone, dolomitic limestone, and dolostone, have developed good porosity (average 6.8%) and permeability (average 7.12 mD). Four types of pores were recognized such as interparticle/residual interparticle pore, intraparticle pore associated with foraminifera, dissolution pore (including moldic pore) and intercrystalline pore contributed by dolomitization. With over 2000 meters thick of salt strata serving as a regional seal overlying the carbonate rocks, the pre-salt carbonate reservoirs are in a relatively close diagenetic system, therefore, the near-surface and penecontemporaneous diagenesis such as marine cementation, early dolomitization, and dissolution, had major impact on the pore system. Our preliminary study suggests that porosity in the inner to mid ramp facies follows the lithofacies pattern. Sea level fluctuation resulted in the marine cementation and dissolution that modified primary porosity. The burial diagenesis, represented by minor calcite cementation and rare fracture, did not significantly alter the porosity in different lithofacies.